660499

111-p #2.50

U. S. ARMY
TRANSPORTATION RESEARCH COMMAND
FORT EUSTIS, VIRGINIA

TRECOM TECHNICAL REPORT 64-11

VISCOUS MIXING OF TWO-DIMENSIONAL JETS WITH PARTICULAR REFERENCE TO JETS IN GROUND PROXIMITY

Task 1D021701A04814
(Formerly Task 9R99-01-005-14)
Contract DA 44-177-AMC-71(T)

April 1964

prepared by:

FROST ENGINEERING DEVELOPMENT CORPORATION
Englewood, Colorado

DDC
JUN 3 1964

DISCLAIMER NOTICE

When Government drawings, specifications, or other data are used for any purpose other than in connection with a definitely related Government procurement operation, the United States Government thereby incurs no responsibility nor any obligation whatsoever; and the fact that the Government may have formulated, furnished, or in any way supplied the said drawings, specifications, or other data is not to be regarded by implication or otherwise as in any manner licensing the holder or any other person or corporation, or conveying any rights or permission, to manufacture, use, or sell any patented invention that may in any way be related thereto.

DDC AVAILABILITY NOTICE

Qualified requesters may obtain copies of this report from

Defense Documentation Center
Cameron Station
Alexandria, Virginia 22314

This report has been released to the Office of Technical Services, U. S. Department of Commerce, Washington 25, D.C., for sale to the general public.

The findings and recommendations contained in this report are those of the contractor and do not necessarily reflect the views of the U. S. Army Mobility Command, the U. S. Army Materiel Command, or the Department of the Army.

HEADQUARTERS
U S ARMY TRANSPORTATION RESEARCH COMMAND
FORT EUSTIS, VIRGINIA

Knowledge of the mechanics of an air jet in unsymmetrical pressure fields while subjected to considerable analysis and experimentation in recent years is somewhat limited. Simplifying assumptions, of which inviscid flow is the most common, have been made to facilitate analysis, yielding results which, although generally in agreement with experimental data, have produced unexplained discrepancies with experimental results.

The approach taken in this investigation provides a better understanding of the flow patterns of annular jet and recirculation flow fields and of their influence on performance and stability characteristics of air cushion vehicles.

W. E. Sickles

WILLIAM E. SICKLES
Leader
Ground Effect Research Group

APPROVED.

FOR THE COMMANDER:

Larry M. Hewin

LARRY M. HEWIN
Technical Director

CONTENTS

	Page
LIST OF ILLUSTRATIONS	v
LIST OF SYMBOLS	ix
SUMMARY	1
SECTION ONE - INTRODUCTION	2
SECTION TWO - INDUCED FORCES DUE TO FREE-AIR ENTRAINMENT	23
SECTION THREE - MIXING LOSSES IN AN ANNULAR JET	54
SECTION FOUR - MIXING LOSSES IN A RECIRCULATING JET	64
SECTION FIVE - SOME EXPERIMENTAL MEASUREMENTS OF STATIC PRESSURE NEAR A NOZZLE	74
BIBLIOGRAPHY	86
APPENDIX I - AN ANNULAR JET VERY CLOSE TO THE GROUND	89
APPENDIX II - EFFECTIVE PERIPHERY OF A CIRCULAR ANNULAR JET	90
APPENDIX III - AN EXACT SOLUTION FOR A LAMINAR JET	95
DISTRIBUTION	99

ILLUSTRATIONS

Figure		Page
1	Static Pressure Distribution Over Rear of Jet Engine Nacelle Caused by Free-Air Entrainment.	2
2	Illustration of the Effect of Nozzle Geometry Upon Negative Lift due to Jet Entrainment.	4
3	Fluid Element Geometry Used in Deriving Equations of Motion.	6
4	Typical Laminar Flow Jets	7
5	Periodic Jet Structure in the "Transition" Reynold's Number Region	8
6	Approximate Flow Picture for a Turbulent Jet.	9
7	Ordinates for a Two-Dimensional Jet	10
8	Effect of Nozzle Shape on Entrainment Pattern	13
9	Variation of Entrainment Ratio n With x/t	14
10	Variation of Entrainment Function Derivative $dn/d(x/t)$ With x/t.	15
11	Ratio of Dynamic Pressure q in Jet to Initial Value q_0 As A Function of Jet Length.	19
12	Half-Line of Sinks.	23
13	Simulation of a Thick Jet	23
14	Two-Dimensional Jet Issuing From a Plane Wall	24
15	Two-Dimensional Jet From a Wedge in a Free-Stream Flow of Velocity.	25
16	Flow Off a Wedge When No Jet Mixing Occurs.	26
17	Flow in an Obtuse Angle	27
18	Definition of Geometry and Sketch of Velocity Ratio Function.	31

Figure		Page

19 Two-Dimensional Static Jet Issuing From a Wedge 32

20 Thrust Loss For h/t = 1.0. (At Other Values, $\Delta F/J_1$ is A Linear Function of h/t .) 35

21 External Induced Air-Flow 36

22 Geometry of Primary Cushion Vortex. 37

23 Geometry of Vortex Entrainment. 38

24 Geometry of Inner Jet Boundary. 38

25 Effective Jet Mixing Length in Cushion. 40

26 Ratio of Momentum Flux in the Primary Cushion Vortex to That of the Jet 41

27 Geometry of Secondary Cushion Vortex. 42

28 Static Pressure in Cushion Vortices As A Ratio of Basic Cushion Pressure (No Momentum Loss) 43

29 Theoretical Static Pressure Distribution Under a GEM. . . . 44

30 Idealization of Actual Cushion Pressure Distribution. . . . 44

31 Calculated Vortex Pressure Compared With Experiments Reported in Reference 10. 45

32 Measured Cushion Pressure From Reference 11 Compared With Theory θ = 0. 47

33 Reference 11 Vortex Pressure Data Corrected For Test Rig Leakage θ = 0 48

34 Increased Cushion Volume. 49

35 Rectangular Cushion Planform. 49

36 Loss of Cushion Lift Due to Primary Vortex - Circular Planform θ = 30°. 51

37 Model Data for Total Lift Compared With Theory. 53

38 Basic Geometry. 54

Figure		Page

39 Plot of $\xi(\theta) = (\pi/2 + \theta)/(1 + \sin\theta)$ Against θ 56

40 Mean Mixing Length Ratio S_m/h To Point Where Jet Static Pressure is Ambient. 56

41 Comparison of Cushion Pressure Theories For $\theta = 60°$. . . . 60

42 Effect of Allowing for Jet Expansion to Ambient Without Mixing $\theta = 60°$ 63

43 Partially Recirculating Jet. 65

44 Free-Air Entrainment Periphery for Recirculating Jet . . . 66

45 Geometry of Jet External Surface 67

46 Theoretical Cushion and Cavity Pressure For a Recirculation Test Rig. $\theta_1 = \theta_2 = 30°$. 72

47 Predicted and Measured Total Head Loss for Martin Model No. 1. 73

48 Location of Pressure Taps. 75

49 Static Pressure Measurement, Series D, Group II, Run No. 9. (1000 RPM, h = 22.75") 76

50 Series D, Group II, Run No. 10. (1400 RPM, h = 22.75"). . 77

51 Series D, Group II, Run No. 11. (1000 RPM, h = 13.75"). . 78

52 Series D, Group II, Run No. 12. (1400 RPM, h = 13.75"). . 79

53 Series D, Group II, Run No. 13. (1000 RPM, h = 9.25") . . 80

54 Series D, Group II, Run No. 14. (1400 RPM, h = 9.25") . . 81

55 Series D, Group II, Run No. 15. (1000 RPM, h = 4.5"). . . 82

56 Series D, Group II, Run No. 16. (1400 RPM, h = 4.5"). . . 83

57 Nozzle Static Pressure Decrement On Internal and External Surface. (Corrected to 1000 RPM). 84

58 Effective Entrainment Angles For Frost Fan Test Rig. . . . 95

Figure		Page
59	Annular Jet Very Close to the Ground	88
60	Assumed Jet Geometry	89
61	Effective Jet Circumference For $\theta = 0$, $t/D = 0.1125$. . . .	94
62	Laminar Jet From a Slot.	95

SYMBOLS

a	empirical constant in potential flow theory
or	length of rectangular planform GEM
or	substitution used in equation 116
A_c	cushion area
b	width of rectangular planform GEM
or	substitution used in equation 116
c	substitution used in equation 116
C	empirical constant in potential flow theory
$C_{\Delta F}$	jet force drag coefficient
C_p	pressure coefficient
$C_{\Delta p}$	pressure coefficient
C_D	drag coefficient
C'	outer periphery of plenum chamber
D	diameter of circular planform GEM
or	diameter of outside edge of nozzle
E_j	power of jet
$f(x)$	function of x
F	force
h	hover height of GEM
i	$\sqrt{-1}$
J_1	momentum flux within primary cushion vortex
J_3	momentum flux within secondary cushion vortex
J_j	momentum flux in jet

J_{jo}	momentum flux in jet leaving cushion
k	effective jet mixing length in cushion of GEM
K	coefficient, $K = {}^{.08}/_{\pi} + \theta$
ℓ	characteristic length, used in definition of Reynold's number
ℓ_v	distance between jets entering and leaving cushion
ℓ_{vo}	effective length of vortex
L_c	cushion lift
$\dot{m}$	mass flow
$\dot{m}_j$	mass flow of basic jet
$\dot{m}_{jo}$	mass flow of jet leaving cushion
$\dot{m}_{jN}$	mass flow of jet measured at nozzle
M	magnitude of sink
M_o	momentum of laminar jet
n	entrainment function
p	pressure
or	numerical index in dimensional analysis
P	total pressure in jet
q	dynamic pressure
or	numerical index in dimensional analysis
q_{jo}	dynamic pressure in jet leaving cushion
q_{jN}	dynamic pressure in jet measured at nozzle
r	magnitude of radius vector (r, φ) in Figure 17
or	radius of inner surface of jet impinging on ground
or	substitution for $\partial v/\partial x - \partial u/\partial y$

r_{10}	outer radius of jet entering cushion
r_{20}	outer radius of jet leaving cushion
r_{11}	inner radius of jet entering cushion
r_{21}	inner radius of jet leaving cushion
R	particular value of r (first definition)
Re	Reynold's number
S	effective mixing length of outside of jet
S_1	circumference of upper half of jet boundary
S_2	circumference of lower half of jet boundary
S_c	periphery of cushion
S_f	free-air entrainment periphery for recirculating jet
S_m	mean mixing length
S_v	periphery of entrainment zone
t	time
or	diameter of orifice
or	thickness of jet
t_1	thickness of jet entering cushion
t_2	thickness of jet leaving cushion
t_{vo}	thickness of jet passing under jet
T_j	jet thrust
u	velocity in direction of x axis
$\bar{u}$	radial component of velocity
u_o	axial free-stream velocity
u_R	velocity at radius R, in x direction

v	velocity in direction of y axis
$\bar{v}$	circumferential component of velocity
v_j	jet velocity
v_0	velocity of entrained air immediately prior to entering jet
V	resultant velocity, $V^2 = \bar{u}^2 + \bar{v}^2$
or	free-stream velocity
x	distance along jet, downstream from jet
x_0	length of potential wedge or cone
y	transverse distance across jet
z	complex quantity, $z = x + iy$
or	radius to jet center-line, measured from cushion center
Z	radius to nozzle center-line, measured from cushion center
ΔA_{v1}	total vertical area of upper half of jet
ΔA_c	effective cushion area
ΔF	jet force drag
ΔL	negative lift due to proximity of jet to ground
Δn	incremental increase in n
Δp	pressure difference between jet and ambient
Δp_1, Δp_2, Δp_3, Δp_4	cushion static pressures as shown in Figure 27
Δp_c	basic cushion pressure
Δp_{vo}	static pressure with vortex
ΔP_{jo}	total pressure in jet leaving cushion

ΔP_{JN} total pressure in cushion, measured at jet nozzle

Δx incremental increase in x

α $\arcsin\left(\frac{\text{exhausted momentum}}{\text{total nozzle momentum}}\right)$

ϵ eddy viscosity

θ inclination of peripheral jet

θ_1 inclination of incoming jet

θ_2 inclination of jet leaving cushion

μ coefficient of viscosity

ν kinematic viscosity

ξ distance from jet center-line to nozzle center-line

ρ density of fluid

φ $\arcsin U/V$

ϕ real part of potential flow function

ψ imaginary part of potential flow function

w complex potential flow function, $w = \phi + i\psi$

∇^2 the Laplacian operator,

$$\nabla^2 = \frac{\partial^2}{\partial x^2} + \frac{\partial^2}{\partial y^2}$$

Subscripts:

a denotes ambient conditions

C denotes conditions within cushion

$crit$ denotes critical condition

J denotes conditions within jet

JN	denotes conditions at jet nozzle
0	denotes conditions in jet leaving cushion
or	denotes initial or datum condition
1	denotes conditions after entrainment occurs

SUMMARY

This report reviews the existing jet mixing theory and the best available experimental results. Simple mixing equations are developed and applied to the following problems.

The average total pressure variation is determined as a function of distance along a two-dimensional jet from the nozzle.

The momentum flux change due to a static pressure change at some arbitrary distance from the nozzle is calculated.

The theory of induced pressure forces due to free-air entrainment is developed, and potential flow solutions are given for the case of a static jet issuing from a plane wall, a jet issuing into a free stream from the trailing edge of an aerofoil (jet-flap propulsion) and a static jet issuing from a wedge.

The generation of vortices in the cushion region of a GEM is shown to be due to viscous mixing, and a method of calculating the lift loss due to this effect is shown to give reasonably good agreement with experiment. Altogether, these entrainment effects can result in the actual lift of an annular jet GEM being as much as 20 per cent lower than the lift which would be calculated using presently available theoretical methods, so that it is important, obviously, to take account of them in performance calculations.

The effect of jet mixing on the central cushion pressure is also investigated, using both "thin jet" and "layered jet" approaches. The traditional assumption of constant jet momentum flux is also examined in this section of the report, and it is shown to be considerably in error. Fortunately, the effect of this assumption is to underestimate cushion pressure, while the omission of mixing effects gives an overestimate. Since both have been neglected in most earlier treatments, the two errors tend to cancel out and the equations thus give roughly the right value for cushion pressure.

The mixing equations are used to estimate the total head loss in a recirculating jet, and good agreement with experiment is obtained. This means that it is now possible to calculate the power requirements of a recirculating jet GEM and to optimize its geometry for minimum power loss.

The report concludes with some experimental observations of the static pressure distribution in the vicinity of a two-dimensional nozzle of complex shape.

SECTION ONE

INTRODUCTION

1.1 The General Problem.

Because of viscosity, a true velocity discontinuity can never exist between two streams of air. As soon as an air jet emerges from a nozzle, it starts to carry along with it some of the previously stationary atmospheric air, and in the process of accelerating this "entrained" air, gives up some of its own momentum. For this reason the velocity profile of a jet changes rapidly as it travels downstream from its nozzle, and accelerates progressively more and more of the free air around it, until it soon loses all resemblance to a discrete jet.

Also, since the free air in the immediate vicinity is accelerating to move with the jet, the pressure distribution over any solid bodies near the jet will be modified by the secondary airflow, the results of which may be beneficial or adverse, depending on the nature of the problem.

The best known example of this effect is the "mixing drag" experienced by a jet engine in an aircraft, the mechanism of which is illustrated in Figure 1. Since the free air is accelerated by the jet, an area of suction is generated over the rear portions of the nacelle.

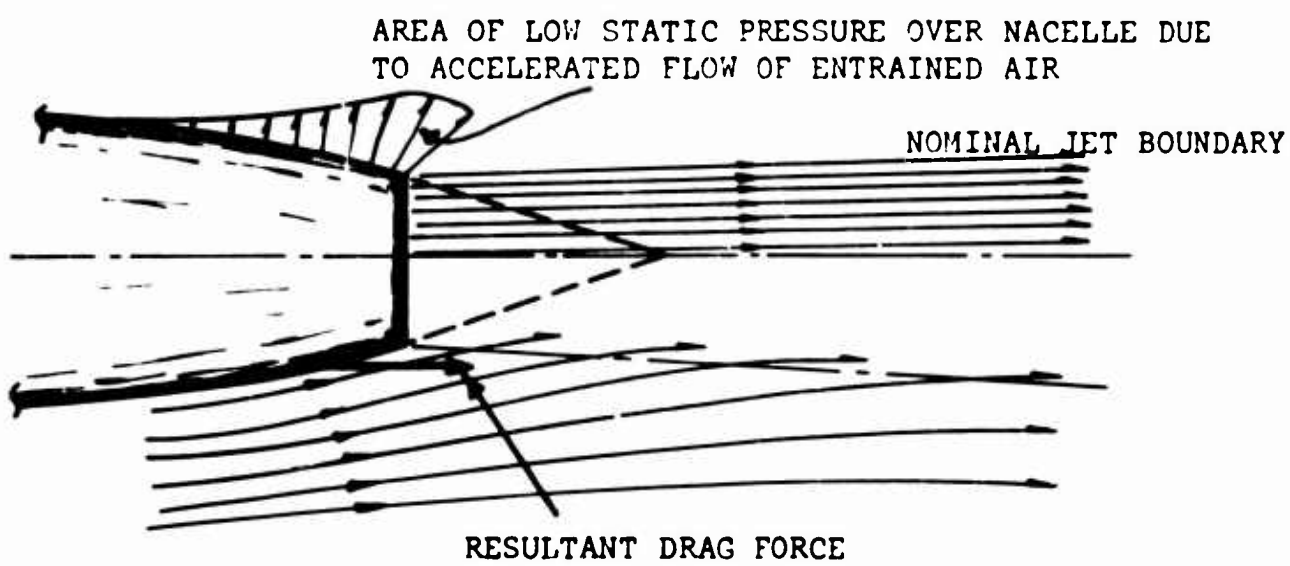

Figure 1. Static Pressure Distribution Over Rear of Jet Engine Nacelle Caused by Free-Air Entrainment.

Since the forces caused by this suction are inclined backwards, due to the shape of the nacelle, their horizontal component constitutes a drag which reduces the total thrust of the engine-nacelle combination. In this case the mixing drag forces are usually quite small, amounting to perhaps 1 or 2 per cent of the engine thrust. However, it is easy to see that in the case of a long two-dimensional jet whose periphery might be ten times the periphery of the equivalent circular jet, the jet drag could amount to from 10 to 20 per cent of the total jet momentum flux under the same free-stream conditions. Obviously, this would have a large effect upon the determination of optimum jet thickness, and a significant effect upon the calculated performance.

Kuchemann (Reference 1) has observed that the pressure velocity ratio in the region of the nozzle exit is given roughly by the empirical equation

$$C_p = \frac{\Delta p}{\frac{1}{2}\rho V^2} = -0.01\left(\frac{v_j}{V} - 1\right) \tag{1}$$

where V is the free-stream velocity and v_j is the jet velocity.

This result is based upon experimental observations made with a finite free-stream velocity, V, and cannot, of course, be applied to the static case of $V = 0$.

A second effect of mixing, and in many ways the most important, is the effect which it has on the jet. Until the advent of jet flaps and ground effect machines, aerodynamics was primarily concerned with the reaction force obtained from a jet, or its momentum flux, neither of which was significantly influenced by mixing. In fact, one of the fundamental theorems of mixing is that momentum is conserved if the process takes place at constant pressure. Total pressure is not concerned, however, so that when we are concerned with jet characteristics some way downstream of its nozzle, the picture bears little relationship to the same problem in inviscid flow.

Finally, we have the problem that if mixing takes place at a pressure less than ambient, an increase in momentum will be effected when expansion to ambient occurs. The reverse is true if the mixing pressure is greater than ambient, and herein lies one explanation of the jet engine pod mixing drag illustrated in Figure 1.

These, then, are the problems to be investigated. We can obviously do little to prevent air being entrained in a jet and little to modify the suction pressure distribution which it induces over the outer surfaces of the nozzle structure. As indicated in Figure 2, our target must lie in obtaining an adequate quantitative understanding of the losses due

to free-air entrainment, so that the geometry of the nozzle can be optimized to give maximum total lift.

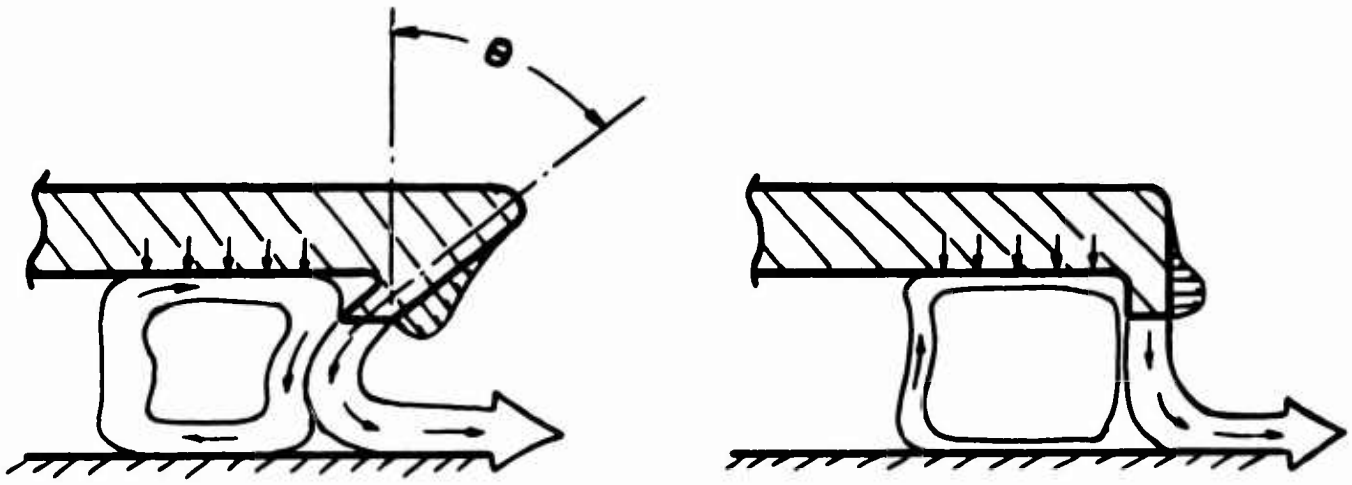

(a) Large Negative Lift, High Cushion Pressure

(b) Zero Negative Lift, Lower Cushion Pressure

Figure 2. Illustration of the Effect of Nozzle Geometry Upon Negative Lift Due to Jet Entrainment.

The example in Figure 2 illustrates a possible trade-off in negative lift acting on a GEM with one other variable which influences total lift; namely, the angle θ at which the peripheral jets are inclined inwards. Increasing θ increases the cushion pressure, all other factors being constant, but may also increase the negative lift component on the exterior of the nozzle and the lift loss due to the primary cushion vortex.

Since the total jet momentum flux must be equal to the total reaction force associated with it, it follows that "negative lift" forces will reduce the momentum flux of the jet in case (a) (in other words, the "negative lift" suction gives rise to pressure forces which tend to inhibit the free acceleration of the entrained air), resulting in a reduction of the cushion pressure relative to the calculated value. In general, this indirect reduction of cushion pressure is more important than the actual negative lift forces induced around the nozzle structure.

1.2 Types of Jet Flow.

As an initial generalization, jet flow may be divided roughly into four separate categories, the Reynold's number (Re) of a jet determining which category best describes its behavior.

Reynold's number is defined as

$$Re = \frac{u\ell}{\nu}$$

where

u = the jet velocity

ν = the kinematic viscosity μ/ρ.

μ = the viscosity of the fluid

ρ = the density of the fluid

ℓ = a characteristic length, usually the minimum dimension across the jet nozzle.

At very low velocities the flow of a jet is laminar and is described by the Navier-Stokes equations, which are, for two-dimensional flow,

$$\left.\begin{aligned} \frac{\partial u}{\partial t} + u\frac{\partial u}{\partial x} + v\frac{\partial u}{\partial y} &= -\frac{1}{\rho}\frac{\partial p}{\partial x} + \frac{\mu}{\rho}\nabla^2 u \\ \frac{\partial v}{\partial t} + v\frac{\partial v}{\partial x} + v\frac{\partial v}{\partial y} &= -\frac{1}{\rho}\frac{\partial p}{\partial x} + \frac{\mu}{\rho}\nabla^2 v \end{aligned}\right\} \qquad (2)$$

where $\nabla^2 = \frac{\partial^2}{\partial x^2} + \frac{\partial^2}{\partial y^2}$

- the velocities and ordinates being as defined in Figure 3.

The pressure term in p can be eliminated by cross-differentiation, giving

$$\frac{\partial r}{\partial t} + u\frac{\partial r}{\partial x} + v\frac{\partial r}{\partial y} = \frac{\mu}{\rho}\nabla^2 r$$

$$r \equiv \frac{\partial v}{\partial x} - \frac{\partial u}{\partial y} \qquad (3)$$

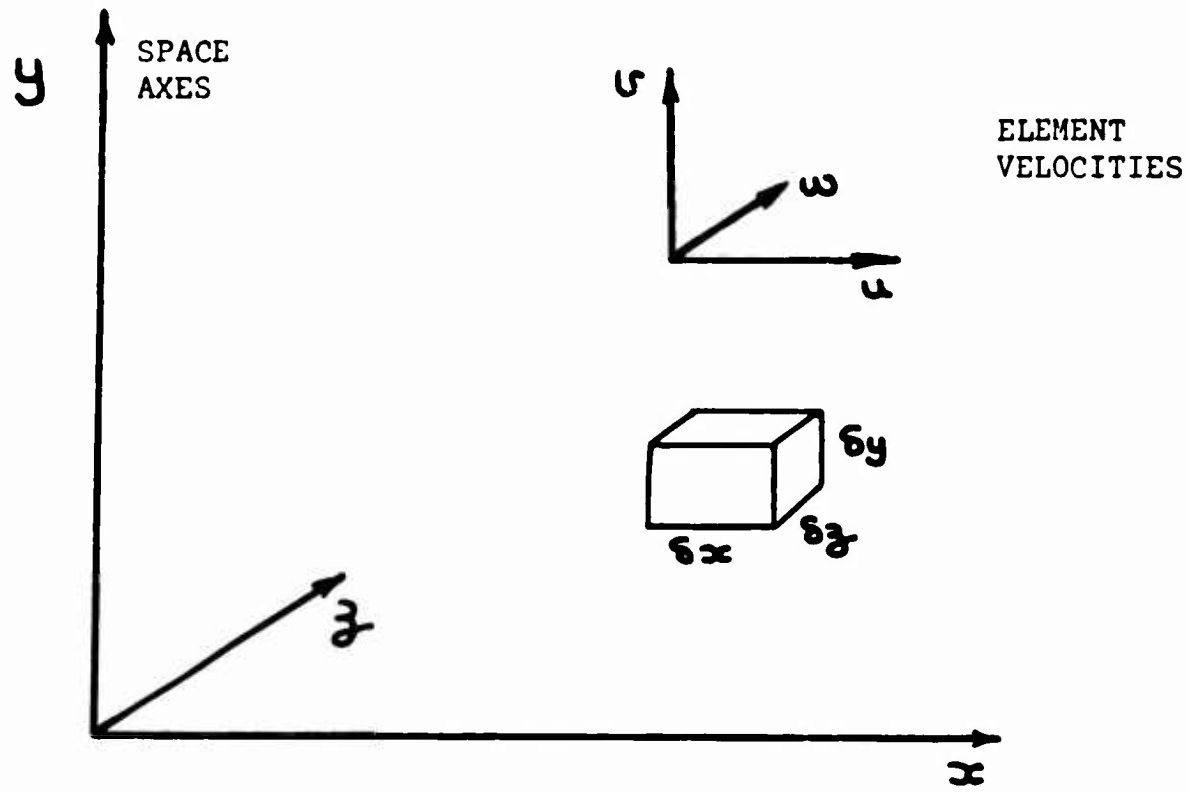

Figure 3. Fluid Element Geometry
Used in Deriving Equations of Motion.

For Re $\ll$ 1 we can neglect the inertial terms on the left-hand side of equation (2), and the resulting equations describe "creeping flow", giving good agreement with experimental observations. Needless to say, this is not a flow condition which has much practical application.

Below Reynold's numbers in the range 25 - 1000, the flow pattern of a jet is characteristically laminar and of the type illustrated in Figure 4.

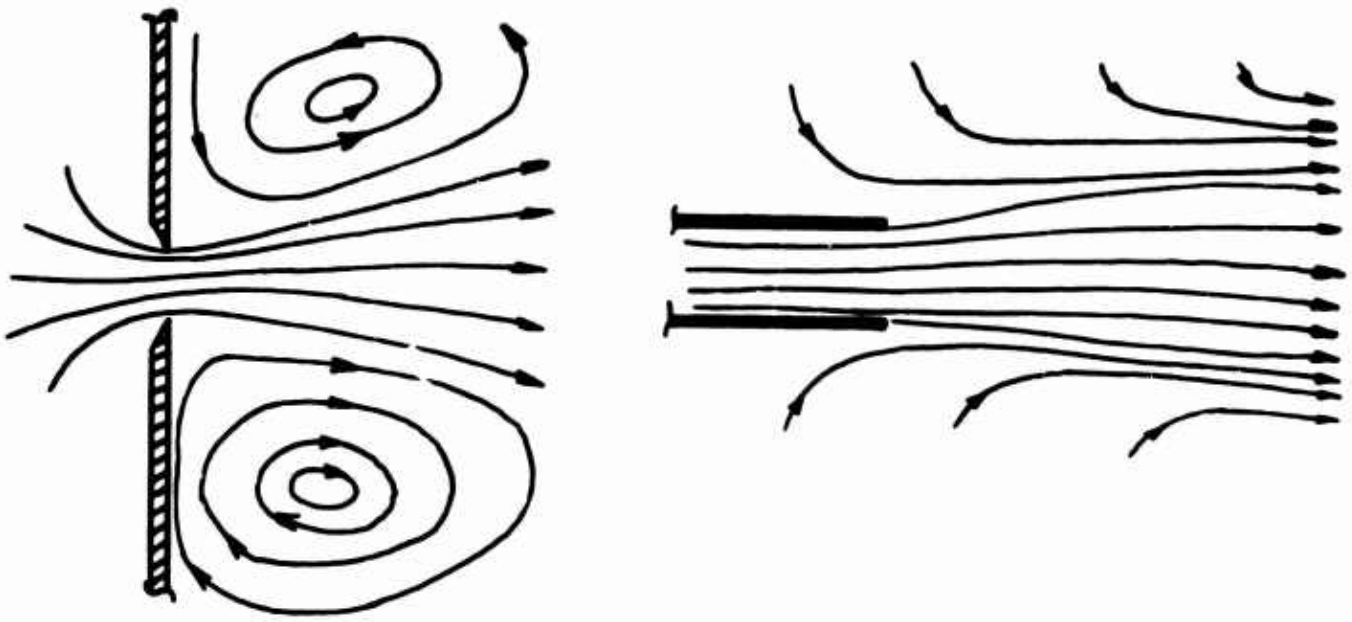

(a) Laminar Jet From an Orifice (b) Laminar Jet From a Thin Tube

Figure 4. Typical Laminar Flow Jets.

A few solutions exist for idealized laminar jets, but again the Reynold's number is so low that the results could only be applied to extremely small and light model GEM's, since Re = 25 - 1000 implies $u\ell$ = .004 - 0.16 ft.^{2}/sec. at sea level. The usefulness of laminar solutions is extended by three considerations, however. At high Reynold's numbers, when the jet is turbulent, it is surrounded by a laminar "sheath" in the region where the local velocity is less than half the maximum jet velocity. Secondly, it is (theoretically) possible to assume an effective "eddy-viscosity" coefficient which permits turbulent flow to be represented by the Navier-Stokes equations. The "eddy-viscosity" has a much larger value than the true (laminar flow) viscosity and is not a linear function of shear velocity gradient, so that its usefulness is very limited.

Finally, it is found that the mixing process in a basically turbulent jet may be laminar for a short distance downstream of its nozzle, so that laminar theory may be applied in this area.

Returning to our description of jet characteristics as a function of Reynold's number, we have seen that the creeping flow which occurs at very low values of Re becomes laminar as Re increases. A further increase to the region $100 < Re < 6000$ causes the jet to become "ragged" and periodic, as illustrated in Figure 5.

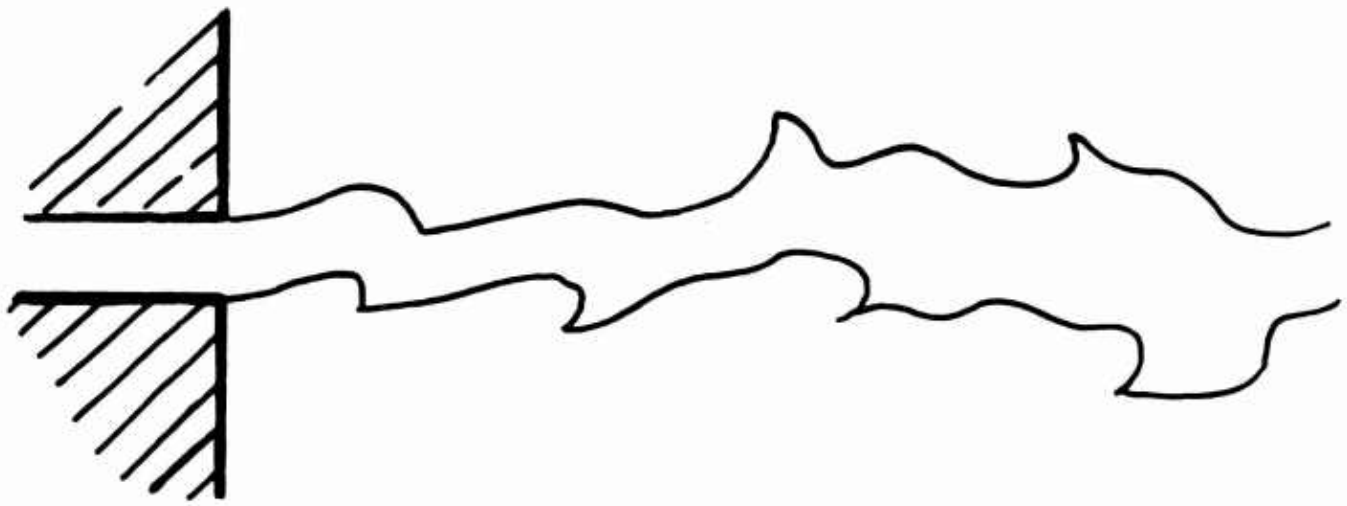

Figure 5. Periodic Jet Structure in the "Transition" Reynold's Number Region.

Since the transition Reynold's number region corresponds to the range $.016 < u\ell < 0.375$, it is easy to see that small models could experience this phenomenon. If the exit of a peripheral jet were 1/8 of an inch wide, for example, the jet velocity would have to be about 36.0 ft./sec. to insure that periodic jet flow did not occur, which would correspond to a cushion pressure of 1.0 - 1.5 lb./ft.^{2} Thus, very lightly loaded models could experience scale effects which would make their performance quite different than that of geometrically similar but larger models.

The "super-critical" Reynold's number region starts at $Re \approx 6000$ and is of course the region of interest in most practical applications. For a two-dimensional jet, the flow picture is roughly as indicated in Figure 6.

It should be noted that there are two distinct flow regimes and that the theoretical analysis is quite different in each regime. It should also be noted, as mentioned previously, that laminar entrainment may occur in the immediate vicinity of the nozzle exit plane, as indicated in Figure 6.

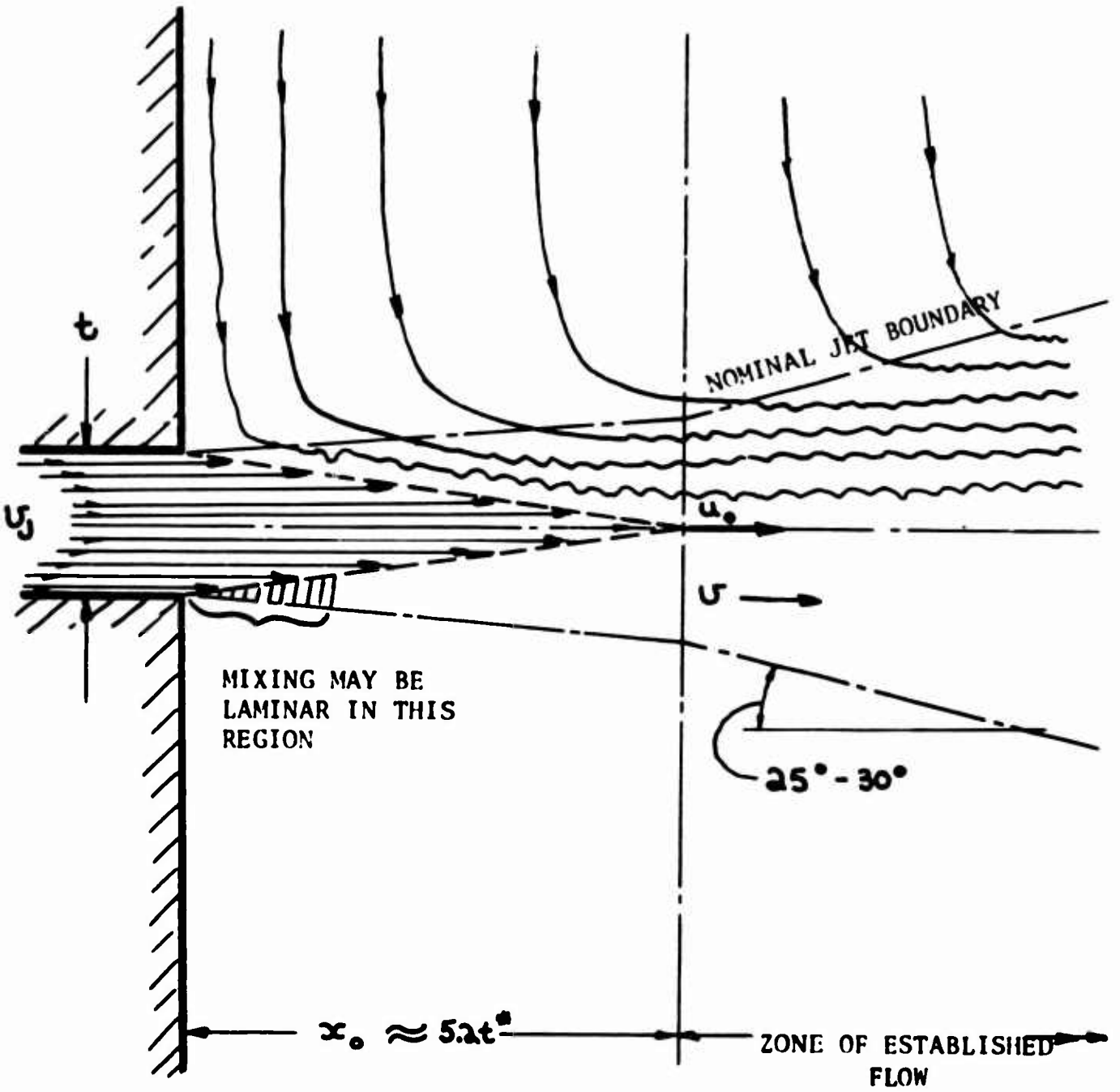

(*The length of the potential wedge [or cone, for a circular jet] varies with Reynold's number and the turbulence in the initial jet.)

Figure 6. Approximate Flow Picture for a Turbulent Jet.

1.3 Dimensional Properties of Two-Dimensional Jets.

For flows nearly parallel to the x-axis (v an order of magnitude less than u , say) we can simplify the Navier-Stokes equations (2) to Prandtl's approximate boundary layer equations:

$$\left.\begin{aligned} u\frac{\partial u}{\partial x} + v\frac{\partial u}{\partial y} &= -\frac{1}{\rho}\frac{\partial p}{\partial x} + \frac{\mu}{\rho}\frac{\partial^2 u}{\partial x^2} \\ \frac{\partial u}{\partial x} + \frac{\partial v}{\partial y} &= 0 \end{aligned}\right\} \qquad (4)$$

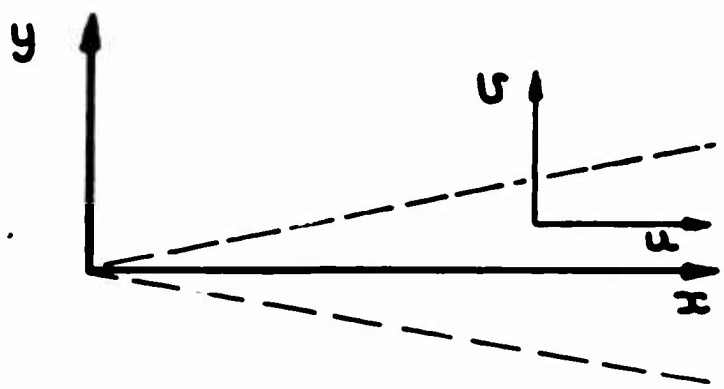

Figure 7. Ordinates for a Two-Dimensional Jet.

The pressure p is a function of the external flow field and is therefore assumed to be known. If p is constant, it may be shown that the momentum integral

$$\int_{-\infty}^{+\infty} u^2 dy = \text{constant} \qquad (5)$$

- for any value of x.

We also have to assume that the velocity profile in a jet is geometrically everywhere the same (the similarity hypothesis) for any value of x. Thus, we can write the following equality, using the methods of dimensional analysis, for a jet from an infinitely thin slot:

$$u(x, y) = x^{-p} f(y, x^{-q}) \qquad (6)$$

In order for this solution to satisfy equation (5), $2p = q$. In order to satisfy equation (4), $2q - p = 1$. Thus, equation (6) can be written more explicitely as

$$u = x^{-\frac{1}{3}} f(y/x^{2/3}) \tag{7}$$

- for a laminar jet. Substituting this result into equation (4),

$$u = \frac{2a^2}{3x^{1/3}} \operatorname{sech}^2 \frac{ay}{x^{2/3}} \tag{8}$$

- where a is indeterminate, corresponding to the angle of spread of the jet. By adjusting (a) to fit experimental results and by putting the origin of the coordinates upstream of the jet exit plane, equation (8) is found to give good agreement with practice.

For a turbulent plane jet from an infinitely thin slot, equations (4) and (5) are still applicable if for μ/ρ we substitute the fictitious scalar "eddy viscosity" ϵ in equation (4). It can be shown that $2p = q$, as before, for constant momentum, and $q = 1$ for the conventional postulation of eddy viscosity. Thus

$$u = x^{-\frac{1}{3}} f(y/x) \tag{9}$$

- for a turbulent jet, the "angle of spread" again being indeterminate. Note that the mass flow varies as $\sqrt{x}$ for a turbulent jet, so that the fluid around it is entrained into the jet as if by a nonuniform line of half-sinks.

Equation (9) applies to the flow from an "infinitely thin" slot, so that it obviously relates to the zone of established flow in Figure 6.

It is possible to calculate the velocity distribution within the jet, for both zones of Figure 6, in terms of the eddy viscosity ϵ or Prandtl's "mixing length" concept (References 7 and 8) and then to determine the value which gives best agreement with experimental observations. Such a procedure results in a velocity distribution, with respect to y, which closely approximates a normal (Gaussian) probability density function, so that it is often more convenient to use the latter. It should be emphasized that whatever the methods used to attack the problem of turbulent jets theoretically, we always end up with a constant which must be determined by comparison with experiment. Thus for practical engineering results we may as well confine our theoretical analysis to those steps necessary to determine the important variables.

such as equation (9), and then determine the appropriate coefficients from experiment.

If this procedure is followed with the assumption of a Gaussian velocity distribution, we obtain the results

$$\frac{u}{U_J} = e^{-\left[1+\frac{1}{2}C_1\sqrt{\pi}\,\frac{x}{y}-\frac{1}{2}\frac{t}{y}\right]^2\Big/\left[2C_1^2\left(\frac{x}{y}\right)^2\right]} \qquad (x < x_0) \tag{10}$$

$$= \sqrt{\frac{t}{x}\,\frac{1}{C_1\sqrt{\pi}}}\; e^{-\frac{1}{2C_1^2}\left(\frac{y}{x}\right)^2} \qquad (x > x_0) \tag{11}$$

- where C_1 is the arbitrary constant which must be determined from experiment. In Reference 6, the value

$$C_1 = 0.109 \tag{12}$$

has been determined, based upon $x_0/t = 5.2$, a result which will vary somewhat with both Reynold's number and the turbulence of the initial jet. Using this value, Reference 6 gives

$$\log_{10}\frac{u}{U_J} = -18.4\left[0.096 + \frac{1-\frac{1}{2}\frac{t}{y}}{x/y}\right]^2 \qquad (x < x_0) \tag{13}$$

$$= 0.36 - 1.84\,(y/x)^2 \qquad (x > x_0) \tag{14}$$

These results are shown in Reference 6 to be in good agreement with experiment, and for our present purposes there is hardly any point in attempting to derive more sophisticated expressions or in attempting to predict the variations with Reynold's number and initial turbulence.

However, the excellence of the experiments reported in Reference 6 should not be allowed to blind us to the fact that they are very incomplete, even for the static case.

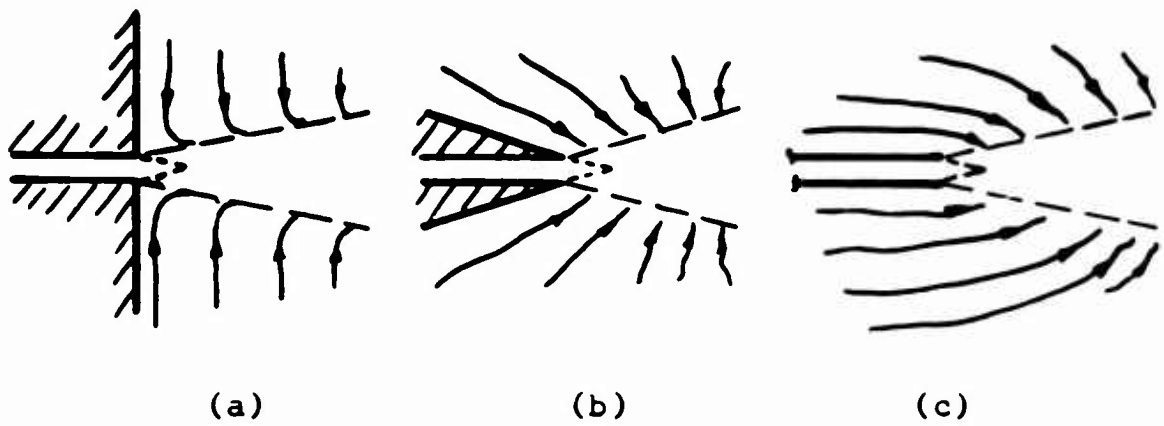

Figure 8. Effect of Nozzle Shape on Entrainment Pattern.

Referring to Figure 8, the Reference 6 measurements correspond to case (a) and for a limited range of Reynold's numbers only. It is known that the entrainment details are influenced by both the Reynold's number and the initial jet turbulence. In addition, it is reasonable to suppose that nozzle profiles of the types sketched in Figure 8 (b) and (c) will significantly influence the entrainment pattern. Indeed, the tests reported in Section Five of this report show that the apparent entrainment close to the nozzle is an order of magnitude greater than the values given in Reference 6.

In addition to this, the experiments are confined to the static case. Although we can postulate corrections for motion of the ambient air, there is a great need for experimental investigations in this area.

1.4 Entrainment in a Two-Dimensional Static Jet.

By integrating equations (10) and (11) with respect to y and substituting equation (12) for C_1, we find that the mass flow at any position x is, in relation to the mass flow of the basic jet,

$$\frac{\dot{m}}{\dot{m}_j} = 1 + 0.08\,\frac{x}{t} \qquad (x < x_0) \tag{15}$$

$$= 0.62\sqrt{\frac{x}{t}} \qquad (x > x_0) \tag{16}$$

We define the mass of entrained air as $\dot{m}_1 = n\dot{m}_j$, so that

$$\frac{\dot{m}}{\dot{m}_j} = (n+1) \qquad \text{or} \qquad n = \left(\frac{\dot{m}}{\dot{m}_j} - 1\right)$$

$$\left.\begin{aligned} \text{Thus, } n &= .08\,\frac{x}{t} && (x < x_0) \\ &= 0.62\sqrt{\frac{x}{t} - 1} && (x > x_0) \end{aligned}\right\} \tag{17}$$

and the entrainment per unit (x/t)

$$\left.\begin{aligned} \frac{dn}{d(x/t)} &= .08 && (x < x_0) \\ &= \frac{0.31}{\sqrt{x/t}} && (x > x_0) \end{aligned}\right\} \tag{18}$$

These results are plotted in Figures 9 and 10. It is interesting to note that the value of $dn/d(x/t)$ is constant for $x <$ 5.2, which is the region of greatest interest for most GEM applications.

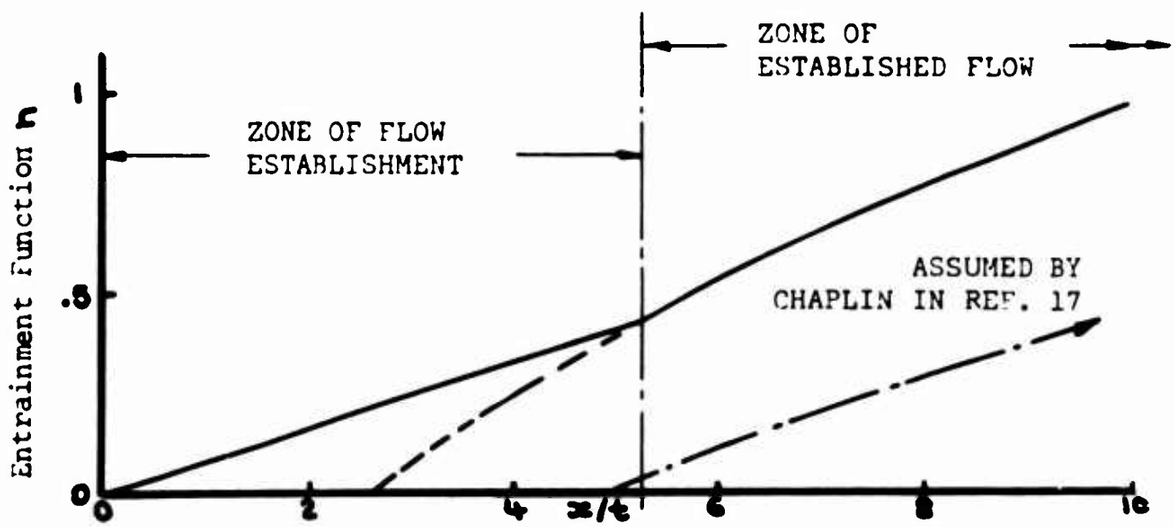

Figure 9. Variation of Entrainment Ratio n With $\frac{x}{t}$.

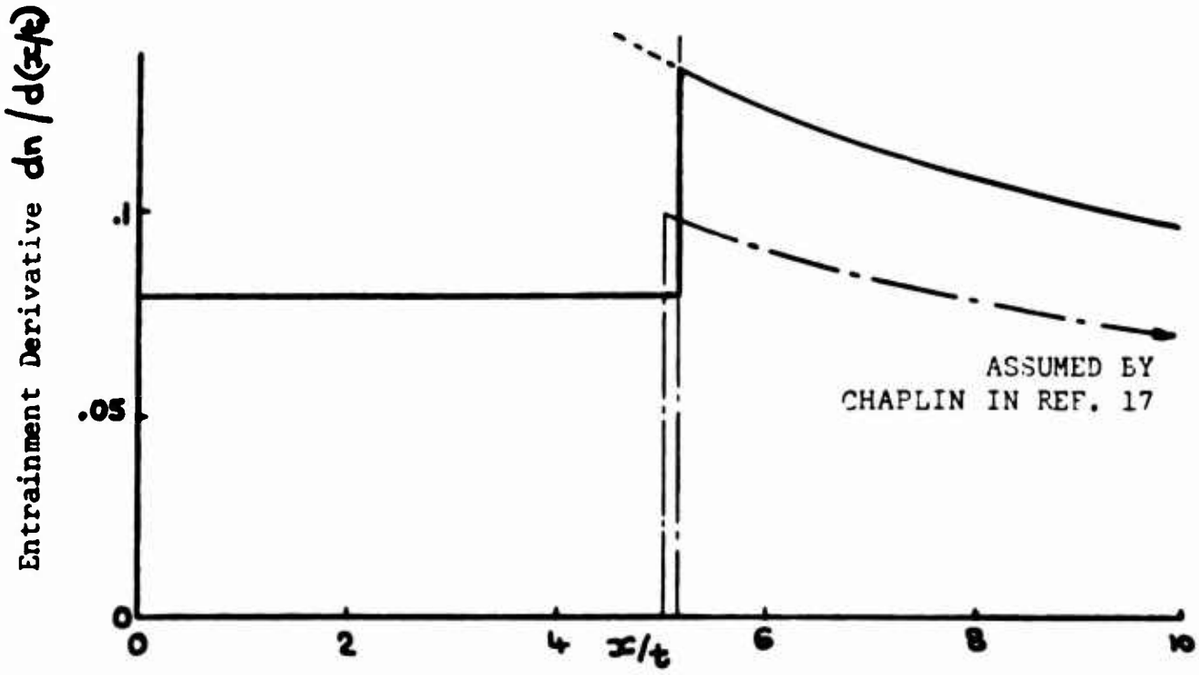

Figure 10. Variation of Entrainment Function Derivative $dn/d(x/t)$ With x/t.

In fact, for many applications, we can obviously take

$$\frac{dn}{d(x/t)} = .08 \tag{19}$$

- as a universal constant.

These values are much larger than those assumed by Chaplin in Reference 17, which are

$$n = 0 , \qquad \frac{dn}{d(x/t)} = 0 \qquad \left(\text{for } \frac{x}{t} < 5.0\right)$$

$$n = \sqrt{\frac{1}{5}\frac{x}{t}} - 1 , \qquad \frac{dn}{d(x/t)} = \frac{0.1}{\sqrt{\frac{1}{5}\frac{x}{t}}} \qquad \left(\text{for } \frac{x}{t} > 5.0\right)$$

1.5 Entrainment in a Jet With an Axial Free-Stream Flow Field.

When a jet exhausts into an axial free-stream (U_o), we assume, following a suggestion made by Kuchemann in Reference 1, that the rate of mixing is proportional to the shear velocity ($u - U_o$).

This amounts to multiplying the x-ordinates by the factor

$$\frac{v_j}{v_j - U_o} = \frac{1}{1 - U_o/v_j} \tag{20}$$

so that the entrainment functions become, from equations (17) and (18)

$$\left.\begin{aligned} n &= .08\left(\frac{x}{t}\right)\left(1 - \frac{U_o}{v_j}\right) && (x < x_o) \\ &= 0.62\sqrt{\frac{x}{t}\left(1 - \frac{U_o}{v_j}\right)} - 1 && (x > x_o) \end{aligned}\right\} \tag{21}$$

$$\left.\begin{aligned} \frac{dn}{d(x/t)} &= .08\left(1 - \frac{U_o}{v_j}\right) && (x < x_o) \\ &= \frac{0.31}{\sqrt{x/t}}\left(1 - \frac{U_o}{v_j}\right) && (x > x_o) \end{aligned}\right\} \tag{22}$$

Kuchemann's hypothesis is obviously limited to the consideration of entrainment in the vicinity of the nozzle if we take v_j to be the nozzle velocity; otherwise equations (21) would give infinite entrainment as $x \longrightarrow \infty$ resulting in infinite jet drag. The actual entrainment at infinity can be obtained by assuming v_j to be the local value, and substituting

$$v_j = \frac{v_{jo}}{1 + n} \qquad (x > x_o)$$

- into equation (22) and solving the resulting differential equation.

1.6 Entrainment in a Jet With a Normal Free-Stream Flow Field.

Because of the existence of the jet, a transverse flow field, as such, cannot occur across it. Instead, an initially normal airflow (of velocity U_o) will be arrested by the jet (resulting in a local static pressure differential of $\Delta p = \frac{1}{2}\rho U_o^2$) or will be deflected by the jet in a manner which will depend upon the strength and size of the jet and the boundary conditions.

Since the pressure rise Δp associated with stagnation of the free-stream flow will also be transmitted to the jet, there is no reason to expect that entrainment will be greater than for the static case, at least until the pressure becomes large enough for the fluid to be compressed. However, it is obviously desirable to obtain experimental verification for this hypothesis as soon as possible.

1.7 Total Pressure Loss Due to Static Mixing.

At constant static pressure, momentum remains constant along a jet, so that

$$\rho \int_0^\infty u^2 dA = \text{constant} \tag{23}$$

If we define $\dot{m}$ as the mass flow of a jet,

that is, $$\dot{m} = \rho \int_0^\infty u\, dA = \zeta(x) \tag{24}$$

- then the mean jet velocity U is defined by

$$\dot{m} U = \rho U \int_0^\infty u\, dA$$

or $$U = \frac{\int_0^\infty u^2 dA}{\int_0^\infty u\, dA} = \frac{\dot{m}_0 U_0}{\dot{m}} \tag{25}$$

The mean total head in the jet is therefore

$$P = p + \tfrac{1}{2}\rho U^2$$

$$P = p + \tfrac{1}{2}\rho U_0^2 \left(\frac{\dot{m}_0}{\dot{m}}\right)^2 \tag{26}$$

Thus the dynamic head in the jet is a unique function of (x/t).

That is, $$\frac{q}{q_o} = \left(\frac{\dot{m}_o}{\dot{m}}\right)^2 = f\left(\frac{x}{t}\right)$$

$$\left.\begin{aligned} &= \frac{1}{(1 + .08\, x/t)^2} && (x < x_o) \\ &= \frac{1}{.3844\, x/t} && (x > x_o) \end{aligned}\right\} \qquad (27)$$

This equation is plotted in Figure 11.

1.8 Momentum Change Due to a Static Pressure Change.

The momentum at any point in a jet is defined by

$$U = \sqrt{\frac{2}{\rho}(P - p)} \qquad (28)$$

- when U and P are the mean velocity and mean total head defined in the previous section.

Now $$P = p + \left(\frac{q}{q_o}\right) q_o = f_1(x) \qquad (29)$$

$$\dot{m} = \left(\frac{\dot{m}}{\dot{m}_o}\right) \dot{m}_o = f_2(x) \qquad (30)$$

At the initial (jet) pressure p_o

$$\dot{m} U = \dot{m}_o U_o \qquad (31)$$

$$P = p_o + \left(\frac{\dot{m}_o}{\dot{m}}\right)^2 q_o \qquad (32)$$

$$\dot{m} = \left(\frac{\dot{m}}{\dot{m}_o}\right) \dot{m}_o \qquad (33)$$

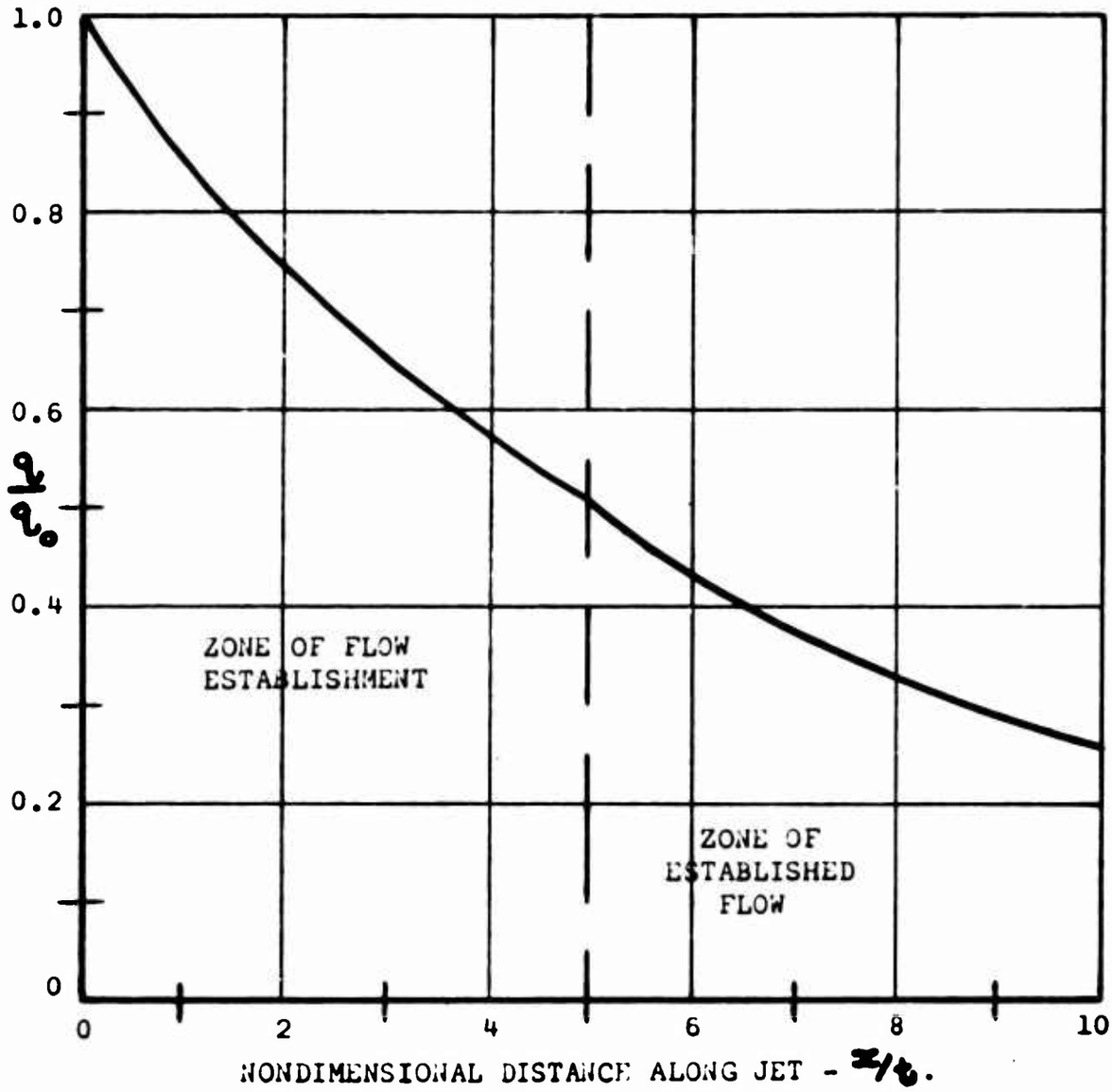

Figure 11. Ratio of Dynamic Pressure q in Jet To Initial Value q_o As A Function of Jet Length.

When the static pressure changes suddenly to p_1, at a plane in (y, z), the velocity changes suddenly also and becomes

$$v_1 = \frac{a}{\rho}(P_1 - p)$$

$$= \frac{a}{\rho}\left[p_0 - p_1 + \left(\frac{\dot{m}_0}{\dot{m}}\right)^2 q_0\right] \tag{34}$$

The momentum flux after the pressure change is

$$J_1 = \dot{m}\, v_1 = \frac{\dot{m}}{\dot{m}_0}\,\frac{a}{\rho}\left[(p_0 - p_1) + \left(\frac{\dot{m}_0}{\dot{m}}\right)^2 q_0\right] \tag{35}$$

$$\frac{J}{\dot{m}_0 v_0} = \frac{J_1}{J_0} = \frac{(p_0 - p_1)}{q_0}\left(\frac{\dot{m}}{\dot{m}_0}\right)^2 + 1 \tag{36}$$

Obviously if $p_0 > p_1$ there will be a gain in momentum flux across the static pressure discontinuity, and a loss if $p_0 < p_1$.

It is also of interest to express the momentum flux in relation to the value obtained if the jet pressure were ambient (p_a). This can be done by assuming either constant mass flow or constant total head at the nozzle.

When the nozzle mass flow is independent of nozzle static pressure, equation (36) obviously still applies.

When the nozzle total pressure is the constant quantity with respect to nozzle static pressure

$$P_0 = p_0 + \tfrac{1}{2}\rho v_0^2 = p_a + \tfrac{1}{2}\rho v_a^2$$

$$\therefore \frac{v_a}{v_0} = \sqrt{\frac{(p_0 - p_a)}{q_0} + 1} \tag{37}$$

$$\dot{m}_a = \rho A_0 v_a = \dot{m}_0\left(\frac{v_a}{v_0}\right) \tag{38}$$

and $$J_a = \dot{m}_a v_a = \dot{m}_o v_o \left(\frac{v_a}{v_o}\right)^2 \tag{39}$$

or $$\frac{J_a}{J_o} = \frac{(p_o - p_a)}{q_o} + 1 \tag{40}$$

so that $$\frac{J_1}{J_a} = \frac{J_1}{J_o}\,\frac{J_o}{J_a} = \frac{\sqrt{\frac{(p_o - p_1)}{q_o}\left(\frac{\dot{m}}{\dot{m}_o}\right)_1^2 + 1}}{\left[\frac{(p_o - p_a)}{q_o} + 1\right]} \tag{41}$$

In the special case when $p_1 = p_a$,

$$\frac{J_1}{J_a} = \frac{\sqrt{\frac{(p_o - p_a)}{q_o}\left(\frac{\dot{m}}{\dot{m}_o}\right)^2 + 1}}{\left[\frac{(p_o - p_a)}{q_o} + 1\right]} \tag{42}$$

Obviously $J_1 > J_a$ so long as the jet entrainment term ($\dot{m}/\dot{m}_o$) is finite and $p_o > p_a$. Thus we can summarize by saying that momentum flux is always increased when a jet passes into a reduced static pressure field, and that jet mixing actually increases the gain because of the increase in mass flow which it contributes.

1.9 Momentum Flux of Entrained Air.

Continuing the gross analysis of the two preceding sections, it is of interest to calculate the gross momentum flux of the entrained air. Since from equation (25),

$$\dot{m}_o v_o = \dot{m} v = \dot{m}_o (1+n)\left(\frac{v}{v_o}\right) v_o \tag{43}$$

- the entrained air momentum flux

$$J_n = n \dot{m}_o v = n \dot{m}_o \left(\frac{\dot{m}_o}{\dot{m}}\right) v_o$$

and $$\frac{J_n}{J_o} = \frac{n}{(n+1)} \tag{44}$$

The momentum flux of the air entrained on one side of the jet only (as in the cushion vortex problem) is, of course, half the value given by equation (44).

SECTION TWO

INDUCED FORCES DUE TO FREE-AIR ENTRAINMENT

We may represent the entrainment of air in a jet by a uniform half-line of sinks, the streamlines associated with which are as sketched in Figure 12. Since any streamline may be replaced by a solid boundary (such as the arbitrarily selected line x - o - x in Figure 12), we can calculate the pressure distribution at such a boundary. Moreover, we can apply our results to any jet thickness simply by separating and rotating the two halves of Figure 12, as shown in Figure 13. The rotation is necessary to allow for the increasing mass flow and diffusion of the jet as x increases, of course, but will most generally have a fairly small effect on the resulting pressure distribution.

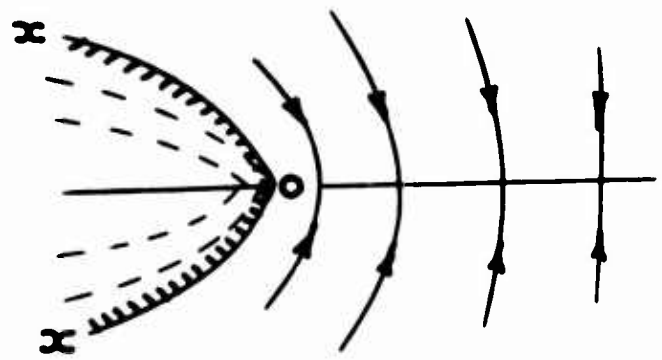

Figure 12. Half-Line of Sinks.

A limit solution is provided by the case of a two-dimensional jet issuing from a plane wall, as indicated in Figure 14. In this case the streamlines into the jet are all parallel, and the velocity is numerically equal to half the magnitude of the sink, M ft.^{3}/ft.^{2}sec.

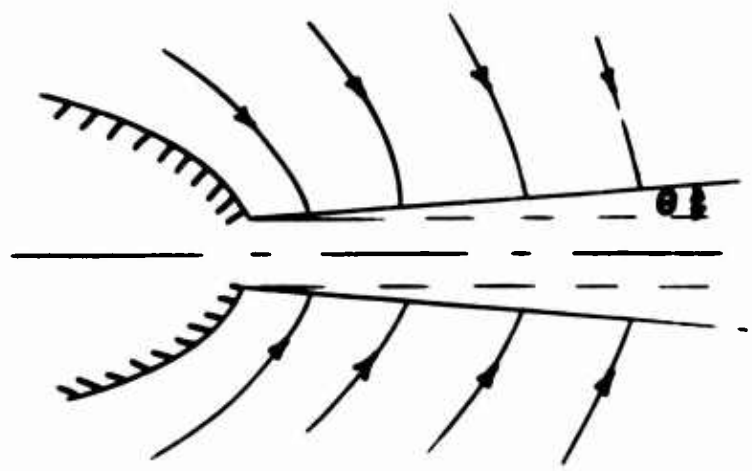

Figure 13. Simulation of a Thick Jet.

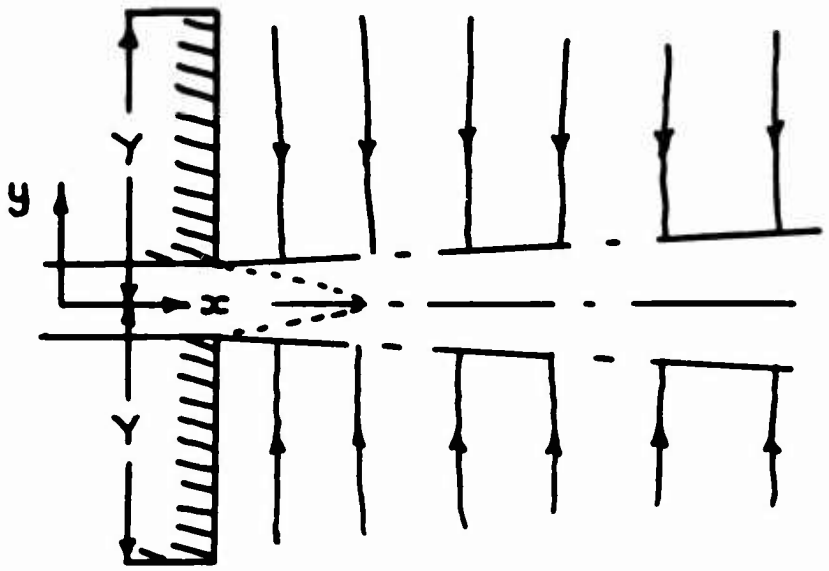

Figure 14. Two-Dimensional Jet Issuing From a Plane Wall.

The static pressure on the wall is therefore given by

$$\Delta p + \frac{1}{2}\rho v^2 = 0$$

or

$$\Delta p = -\frac{1}{2}\rho v^2 = -\frac{1}{2}\rho\left(\frac{M}{2}\right)^2 \tag{45}$$

Thus the "jet drag" force is

$$-\Delta F = \frac{1}{4}\rho \int_0^Y M^2\, dy = \frac{1}{4}\rho M^2 Y \tag{46}$$

- per unit width.

Now the sink magnitude is related to the entrainment function (n) by the equation

$$M = \frac{dn}{dx}\, t\, v_j = \frac{dn}{d(x/t)}\, v_j \tag{47}$$

(so that $\frac{v}{v_j} = \frac{1}{4}\frac{dn}{d(x/t)}$).

The jet thrust per unit length is

$$T_j = \rho t v_j^2 \tag{48}$$

Thus the ratio of jet drag to thrust is

$$\frac{-\Delta F}{T_j} = \frac{Y \rho v_j^2}{4 \rho t v_j^2} \left[\frac{dn}{d(x/y)}\right]^2$$

$$= \frac{1}{4}\left(\frac{Y}{t}\right)\left[\frac{dn}{d(x/y)}\right]^2 \tag{49}$$

If we use the approximation $dn/d(x/y) = .08$ [from equation (19)]

$$\frac{-\Delta F}{T_j} = .0016\left(\frac{Y}{t}\right)_r \tag{50}$$

Thus if $Y = t$, the loss is very much less than 1 per cent.

We can extend this simple case to include the influence of a free-stream velocity U_o, as shown in Figure 15 for the case of a jet issuing from a semi-infinite wedge.

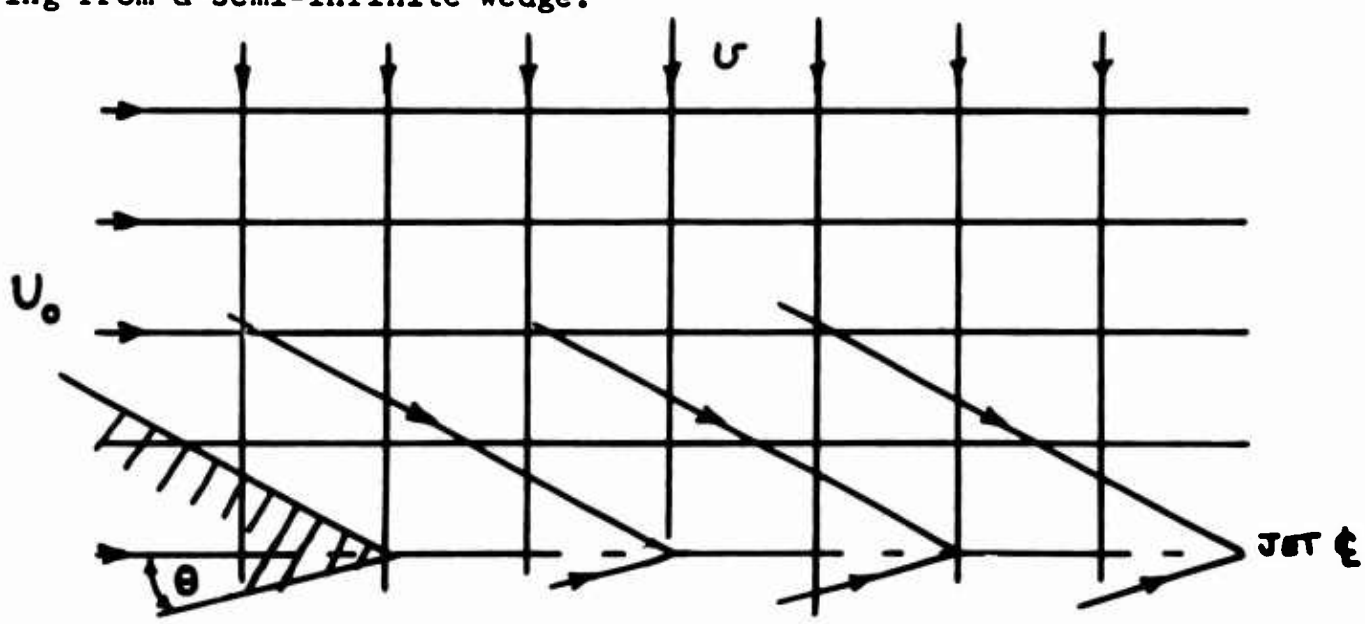

Figure 15. Two-Dimensional Jet From a Wedge in a Free-Stream Flow of Velocity $U_o = v/\tan\theta$

The resultant velocity is given by

$$V^2 = U_0^2 + v^2 \tag{51}$$

and the wedge half-angle by

$$\tan\theta = \frac{v}{U_0} \tag{52}$$

This analogy is very limited, however, in that, since v is a function of $(v_j - U_0)$, we can only obtain a solution for one particular value of U_0 for a given wedge angle. However, it is of value in enabling us to predict the more general effect of a free-stream velocity, using the following reasoning. When no mixing takes place, the flow picture is as shown in Figure 16 with a relatively high static pressure at the trailing edge. When mixing takes place, on the other hand, the air at the trailing edge is turned through a smaller angle $\theta - \phi$, where $\sin\phi = v/V$, so that the trailing edge static pressure is less, resulting in an apparent increase in drag due to mixing.

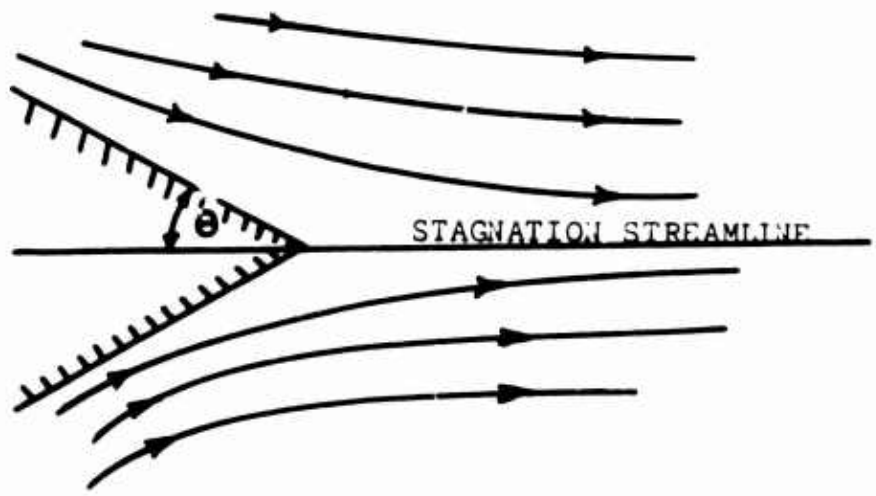

Figure 16. Flow Off a Wedge When No Jet Mixing Occurs.

2.1 Potential Flow Solution to the Jet Drag Problem.

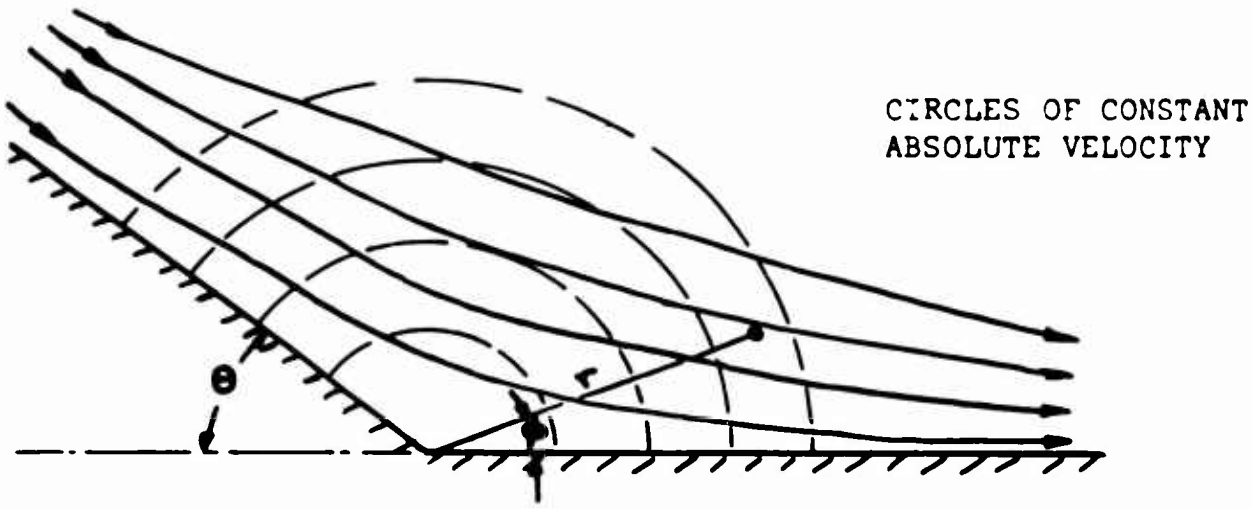

Figure 17. Flow in an Obtuse Angle.

The potential flow function in Figure 17 is

$$w = \frac{a}{n} z^n = \frac{a}{n}(x+iy)^n \qquad (1<n<2) \tag{53}$$

On polar coordinates, writing $z = re^{i\varphi}$

$$w = \frac{a}{n} r^n (\cos n\varphi + i \sin \varphi) \tag{54}$$

giving $$\phi = \frac{a r^n}{n} \cos n\varphi \tag{55}$$

$$\psi = \frac{a r^n}{n} \sin n\varphi \tag{56}$$

For $\psi = 0$, $\sin n\varphi = 0$, $\varphi = \frac{k\pi}{n}$ ($n = 0, 1, 2...$)

Thus, one boundary is given by the straight line at $\varphi = 0$, the second at $\varphi = \pi/n$.

That is, $\theta = \pi - \varphi = \pi\left(1 - \frac{1}{n}\right)$

so that $$n = \frac{1}{1 - \theta/\pi} \tag{57}$$

The radial and circumferential velocity components are

$$\tilde{u} = \frac{1}{r}\frac{\partial\psi}{\partial\varphi}$$

$$\tilde{v} = -\frac{\partial\psi}{\partial r}$$

- so that the resultant velocity

$$V^2 = \tilde{u}^2 + \tilde{v}^2 = \frac{1}{r^2}\left(\frac{\partial\psi}{\partial\varphi}\right)^2 + \left(\frac{\partial\psi}{\partial r}\right)^2$$

- which from equation (56) is

$$\frac{1}{r^2}\left(\frac{\partial\psi}{\partial\varphi}\right)^2 = \frac{1}{r^2}\left[\frac{a r^n}{n} n \cos n\varphi\right]^2 = a^2 r^{2(n-1)} \cos^2 n\varphi$$

$$\left(\frac{\partial\psi}{\partial r}\right)^2 = \left[a r^{n-1} \sin n\varphi\right]^2 = a^2 r^{2(n-1)} \sin^2 n\varphi$$

$$V^2 = a^2 r^{2(n-1)} \tag{58}$$

Thus, the absolute velocity is a function only of r, and $V \to \infty$ as $r \to \infty$

Since $p = p_a - \frac{1}{2}\rho V^2$

or $$-\Delta p = \frac{1}{2}\rho V^2 = \frac{1}{2}\rho\, a^2 r^{2(n-1)} \tag{59}$$

- the pressure distribution is known.

Let us define the velocity at some radius R as

$$U_R = a R^{n-1} \tag{60}$$

Then $$a = \frac{U_R}{R^{n-1}}$$

and $$-\Delta p = \frac{1}{2}\rho U_R^2 \left(\frac{r}{R}\right)^{2(n-1)} \tag{61}$$

A small increase Δn in n will give

$$\frac{\Delta p_{n+\Delta n} - \Delta p_n}{\frac{1}{2}\rho U_R^2} = \left(\frac{r}{R}\right)^{2(n+\Delta n-1)} - \left(\frac{r}{R}\right)^{2(n-1)} \tag{62}$$

Integrating between 0 and R

$$C_{\Delta F} = \int_0^R \frac{(\Delta p_{n+\Delta n} - \Delta p_n)\,dr}{\frac{1}{2}\rho U_R^2}$$

$$= R\left\{\frac{1}{2n+2\Delta n-1} - \frac{1}{2n-1}\right\} \tag{63}$$

and since Δn is small

$$(2n-1) + 2\Delta n = (2n-1)\left\{1 + \frac{2\Delta n}{(2n-1)}\right\} = \frac{(2n-1)}{\left[1 - \frac{2\Delta n}{(2n-1)}\right]}$$

$$C_{\Delta P} = \int_0^R \frac{\Delta p_{n+\Delta n} - \Delta p_n}{\frac{1}{2}\rho U_R^2 R}\,dr$$

$$= \frac{-2\Delta n}{(2n-1)^2} \tag{64}$$

Since $$n = \frac{1}{1 - \theta/\pi},$$

$$2n - 1 = \frac{1 + \theta/\pi}{1 - \theta/\pi} \tag{65}$$

Also $$n + \Delta n = \frac{1}{(1-\theta/\pi) - \delta/\pi} = \frac{1}{(1-\theta/\pi)} + \frac{\delta/\pi}{(1-\theta/\pi)^2}$$

$$\therefore\ 2\Delta n = \frac{2\ \delta/\pi}{(1-\theta/\pi)^2}$$

$$\frac{2\Delta n}{(2n-1)^2} \approx \frac{2\,\delta/\pi}{(1+\theta/\pi)^2} \tag{66}$$

- if δ/π is small in relation to $(1 - \theta/\pi)$. The change in drag due to the small angular change is of course $C_{\Delta F} \sin\theta$.

The small angular change δ is given by

$$\tan\delta = \frac{v}{U_R} \approx \delta \tag{67}$$

But $$v = v_J \frac{du}{d(x/t)} \quad \text{(from equation 47)}$$

$$= .04\, v_J \left(1 - \frac{U_R}{v_J}\right) \quad \text{(from equation 22)}$$

$$\therefore\ \delta = .04\, \frac{v_J}{U_R}\left(1 - \frac{U_R}{v_J}\right)$$

$$= .04\left(\frac{v_J}{U_R} - 1\right) \tag{68}$$

Thus $$C_{\Delta P} = \frac{.08}{\pi(1+\theta/\pi)^2}\left(\frac{v_J}{U_R} - 1\right) \tag{69}$$

- which has the same form as Kuchemann's static pressure equation given as equation (1). The actual force decrement in the direction of jet thrust is

$$\Delta F = 2 \times \frac{1}{2}\rho U_R^2 R \frac{.08}{\pi(1+\theta/\pi)^2}\left(\frac{v_j}{U_R} - 1\right)\sin\theta \tag{70}$$

and since the jet thrust is $\dot{m}_j v_j = \rho t v_j^2$

$$\frac{\Delta F}{J} = K\left(\frac{h}{t}\right)\left(\frac{U_R}{v_j}\right)^2\left(\frac{v_j}{U_R} - 1\right) \tag{71}$$

where $K = \dfrac{.08}{\pi(1+\theta/\pi)}$ (72)

For θ =	10°	20°	30°	40°	50°
K =	.0228	.0206	.0187	.0170	.0156

and $h = R\sin\theta$, as shown in Figure 18.

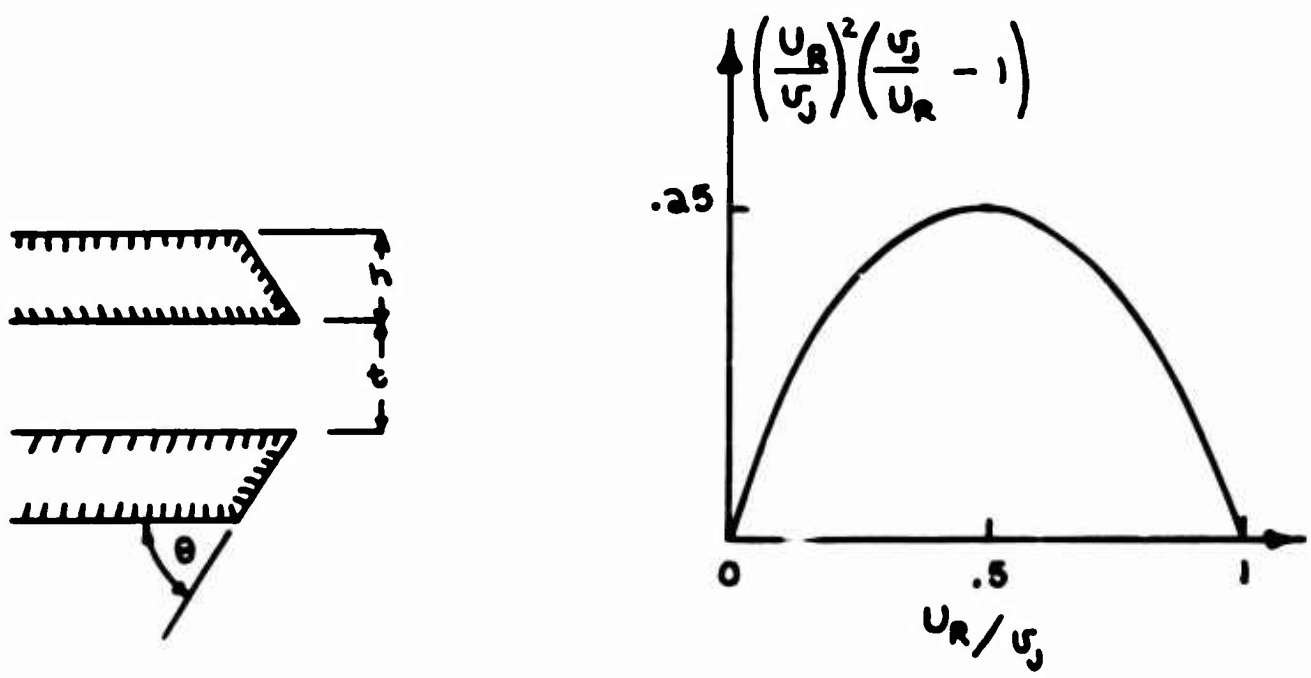

Figure 18. Definition of Geometry and Sketch of Velocity Ratio Function.

In Kuchemann's empirical equation (1), if the pressure change Δp is assumed to react over the entire rear end of the nozzle structure, then the coefficient $K = .01$. This difference is explainable on the basis of boundary layer effects, in that entrainment will tend to reduce the momentum thickness of the boundary layer.

2.2 Momentum Loss Under Static Conditions.

We have already obtained a solution for the limit case of Figure 14, and we now proceed to the more general case depicted in Figure 19.

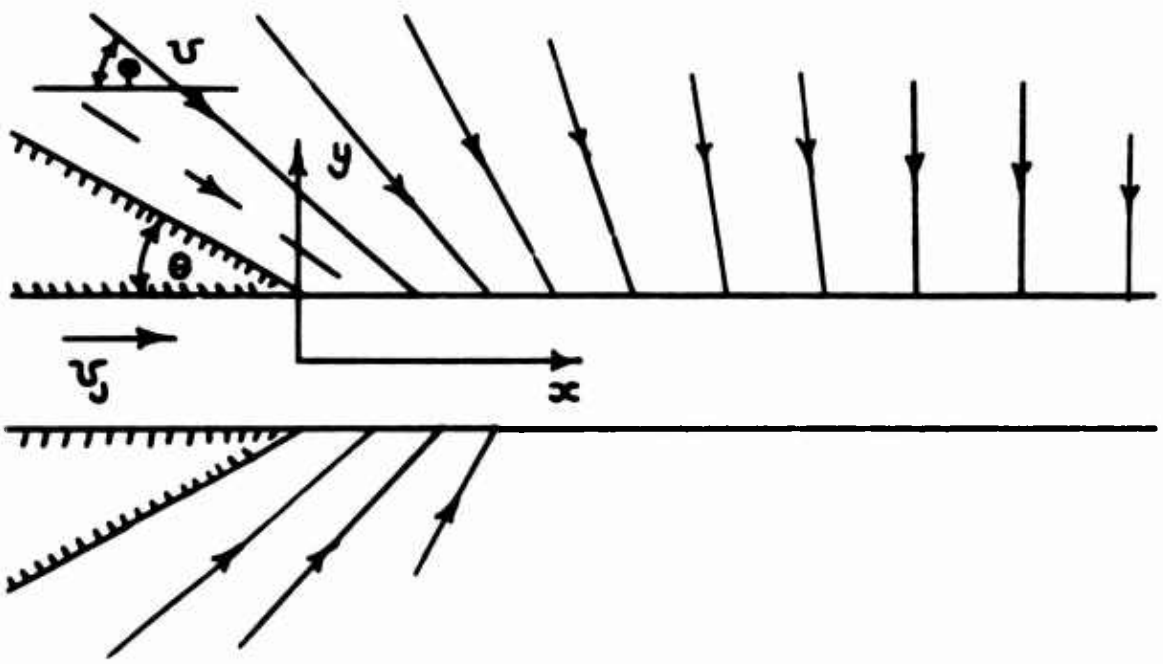

Figure 19. Two-Dimensional Static Jet Issuing From a Wedge.

Although, as indicated in Figures 12 and 13, this class of problem is amenable to a potential flow solution, our uncertainty as to the entrainment function, and the relatively small forces generated [as evidenced by equation (50)] would seem to render such sophistication out of place. In other words, although we have measured entrainment functions available for the case illustrated in Figure 14, we have arbitrarily to assume that these are also true for the case of Figure 19.

Ignoring boundary layer effects, the air moving next to the wedge wall, with a velocity v, is entrained in the length Δx of the jet immediately following the nozzle exit plane. From equation (17) the mass of this flow is

$$n\dot{m}_j = .04 \frac{\Delta x}{t} \dot{m}_j \tag{73}$$

The thickness of this layer is $\Delta x \sin\theta$ at the jet so that for continuity of mass flow

$$\Delta x \sin\theta \, v_\theta \rho = .04 \frac{\Delta x}{t} t \, v_j \rho$$

$$\frac{v_\theta}{v_j} = \frac{.04}{\sin\theta} \tag{74}$$

- where v_θ is the velocity immediately prior to entering the jet. At some distance away from the jet $v < v_\theta$, of course, because of the assumed flow pattern sketched in Figure 19.

If we ignore this, however, the local pressure differential will be

$$\Delta p = -\frac{1}{2} \rho v_\theta^2 \tag{75}$$

and the resultant horizontal force (on two wedge surfaces) is

$$\Delta F = 2 \times h \times \frac{1}{2} \rho v_j^2 \left(\frac{.04}{\sin\theta}\right)^2$$

since $T_j = \rho t v_j^2$

$$\frac{-\Delta F}{T_j} = \frac{.0016\,(h/t)}{\sin^2\theta} \tag{76}$$

- which agrees with equation (50) for $\theta = \pi/2$

In general, because of the acceleration of the entrained flow, equation (26) should usually result in an overestimate for large values of h/t, when the exterior jet surface is (relatively) plane. As shown in Section Five, however, discontinuities in the nozzle surface can result in much higher values of Δp than would be calculated from equation (76) if θ were measured close to the jet. A great deal more work remains to be done before this aspect can be clarified.

2.3 Discussion of Thrust Loss in an Axial Stream.

The greatest thrust loss in axial flow is seen to occur when $U_R = \frac{1}{2} V_J$, the condition for maximum propulsive efficiency. In this condition,

$$\text{for } h = t, \quad \frac{\Delta F}{T_J} = 0.5 \text{ per cent}$$

$$\text{for } h = 5t, \quad \frac{\Delta F}{T_J} = 2.5 \text{ per cent}$$

- results which indicate that the effect is small. In the case of a jet-flapped wing, however, particularly if the jet flap is partially deflected, the results of mixing can be very much more severe.

Under static conditions, the theory of Section 2.2 predicts a generally greater thrust loss than for the case of axial flow, rising to as high as 5 per cent for $\theta = 10°$ and $h/t = 1.0$ (Figure 20). These high values are by no means unreasonable, a static thrust loss of 5 per cent having been reported in at least one jet-flapped wing experiment.

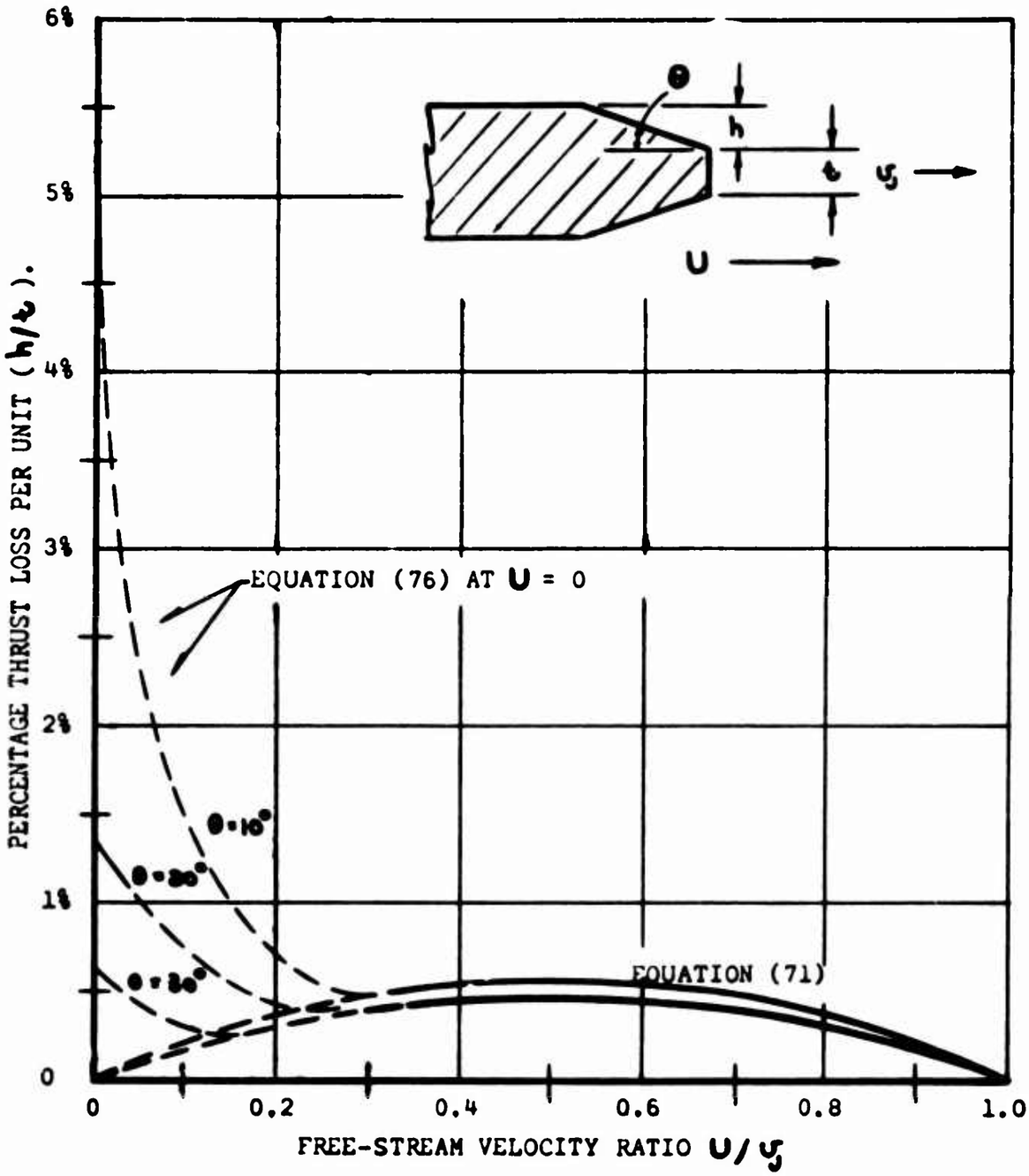

Figure 20. Thrust Loss For $h/t = 1.0$.

In addition, while we should not lose sight of the essentially heuristic arguments applied to the calculation of static thrust loss, particularly the assumption of constant velocity over the nozzle fairing, it should be borne in mind that this is a fair representation of a flow picture which occurs in many practical cases, due to the proximity of the ground, as illustrated in Figure 21.

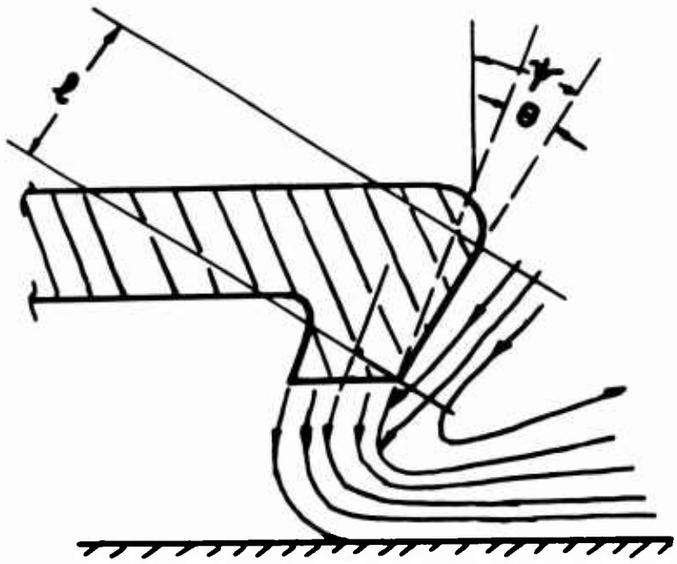

Figure 21. External Induced Air-Flow.

In such cases, the "negative lift" can be assumed to be approximately

$$\Delta L = \ell \, \Delta p \, \sin\psi$$

$$= -\,.0008 \, \rho \, v_j^2 \, \ell \, \frac{\sin\psi}{\sin^2\theta} \tag{77}$$

or

$$\frac{\Delta L}{J_j} = -\,.0008 \left(\frac{\ell}{t}\right) \frac{\sin\psi}{\sin^2\theta} \qquad (\theta \geqslant 0.1) \tag{78}$$

- the limit on θ being arbitrary.

2.4 Vorticity Induced in the Cushion Region of a GEM.

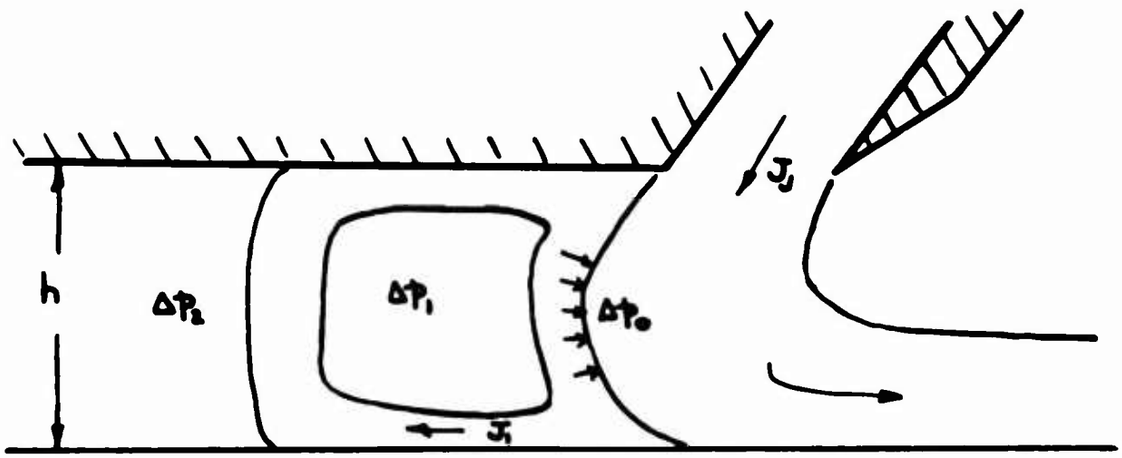

Figure 22. Geometry of Primary Cushion Vortex.

We assume that the viscous shear between the cushion air and an annular jet generates a vortex of momentum flux J_1, as shown in Figure 22.

Then $$\Delta p_0 = \frac{J_j}{h}(1+\sin\theta) \tag{79}$$

and for zero energy loss in the vortex

$$\Delta p_2 = \Delta p_0$$

But $$\Delta p_2 - \Delta p_1 = \frac{2J_1}{h} \tag{80}$$

$$\therefore \quad \Delta p_1 = \Delta p_2 - \frac{2J_1}{h}$$

or $$\frac{\Delta p_1}{\Delta p_2} = 1 - \frac{J_1}{J_j}\,\frac{1}{(1+\sin\theta)} \tag{81}$$

In order to predict the loss of lift occasioned by this effect, we need to know the ratio J_1/J_j and the cushion area covered by the vortex. Referring to Figure 23, we see that we can logically expect the entrainment in region A to be the value associated with entrainment of stationary atmosphere in a jet. In region B, however, the entrainment will be less than for a stationary atmosphere, because of the effect postulated in Section 1.5 of this report, occasioned by vortex rotation.

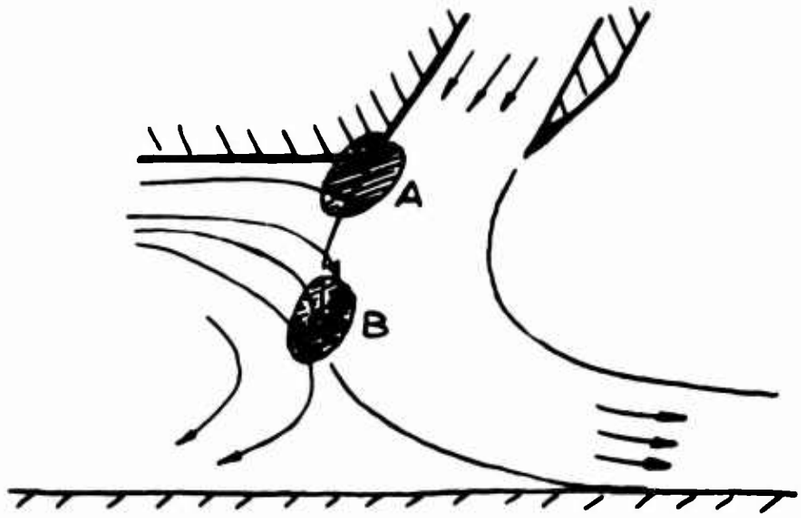

Figure 23. Geometry of Vortex Entrainment.

If the vortex is relatively weak, the entrainment ratio for stationary air may be an acceptable average to the complex entrainment picture actually occurring.

The length of the inner surface of the jet is defined by geometrical considerations, as indicated in Figure 24.

The circumference of the upper section is

$$S_1 = \theta r \qquad (82)$$

Now $h = r(1+\sin\theta)$

$$\therefore r = \frac{h}{1+\sin\theta} \qquad (83)$$

S_2 is defined as shown, being

$$S_2 = r\phi \qquad (84)$$

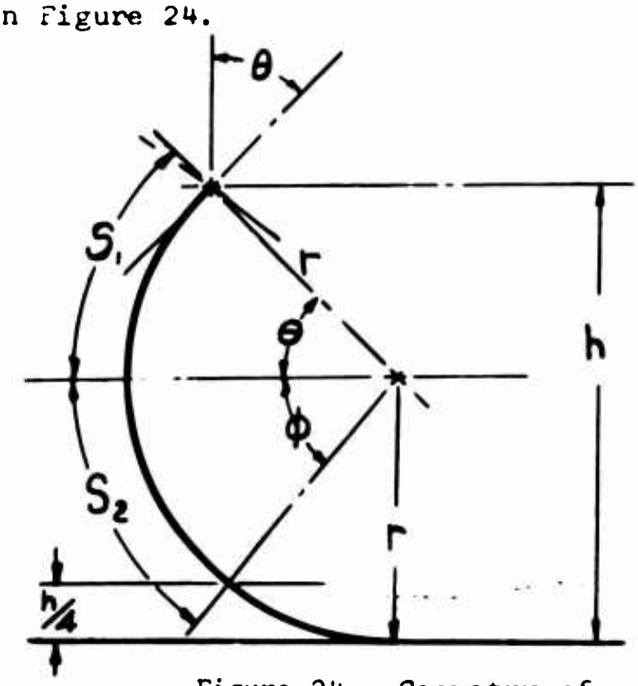

Figure 24. Geometry of Inner Jet Boundary.

where $\sin\phi = \frac{h}{r} - \sin\theta - \frac{h}{4r}$

$$= 3/4 - (1/4)\sin\theta \tag{85}$$

Thus the effective jet length is

$$S_1 + S_2 = \frac{h}{(1+\sin\theta)}\left[\theta + \sin^{-1}\left(\frac{3}{4} - \frac{1}{4}\sin\theta\right)\right] \tag{86}$$

- a relationship plotted in Figure 25. Obviously, it is sufficiently accurate to write

$$\left.\begin{aligned} S_1 + S_2 &= k\,h \\ \text{where } k &\approx 0.82 \end{aligned}\right\} \tag{87}$$

From equation (44) the momentum flux of the vortex is

$$\frac{J_1}{J_j} = \frac{\frac{1}{2}n}{n+1} \tag{88}$$

From equations (17) and (87)

$$n = .08 \times 0.82\,\frac{h}{t} \tag{89}$$

so that $\frac{J_1}{J_j} = \frac{.0328\,h/t}{(1+.0656\,h/t)}$ (90)

- a relationship which is plotted in Figure 26.

Substituting equation (90) in equation (81),

$$\frac{\Delta p_1}{\Delta p_2} = 1 - \frac{.0656\,h/t}{1+.0656\,h/t\;(1+\sin\theta)} \tag{91}$$

$$= 1 - \frac{.0656}{x + .0656\,(1+\sin\theta)} \tag{92}$$

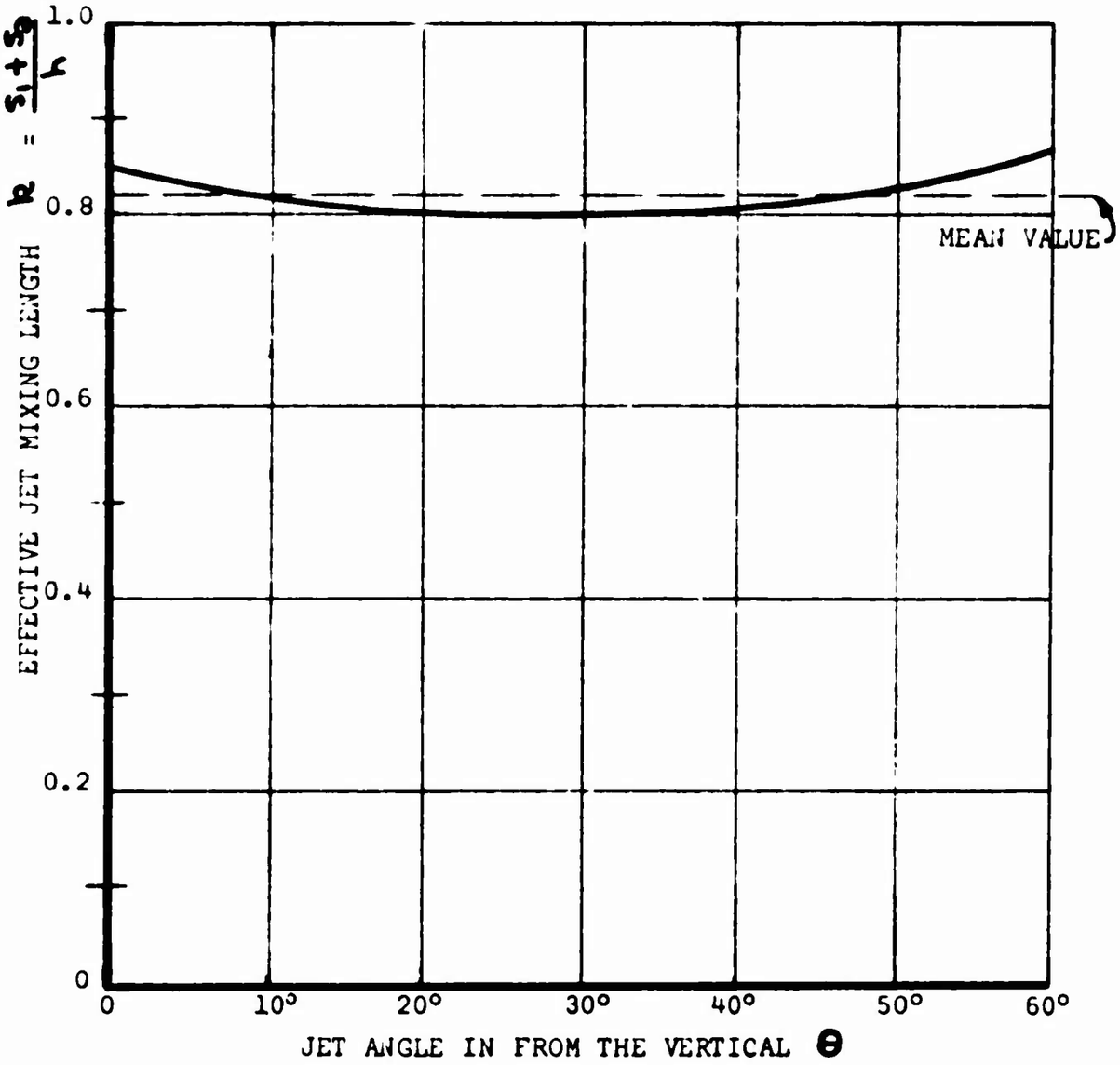

Figure 25. Effective Jet Mixing Length in Cushion.

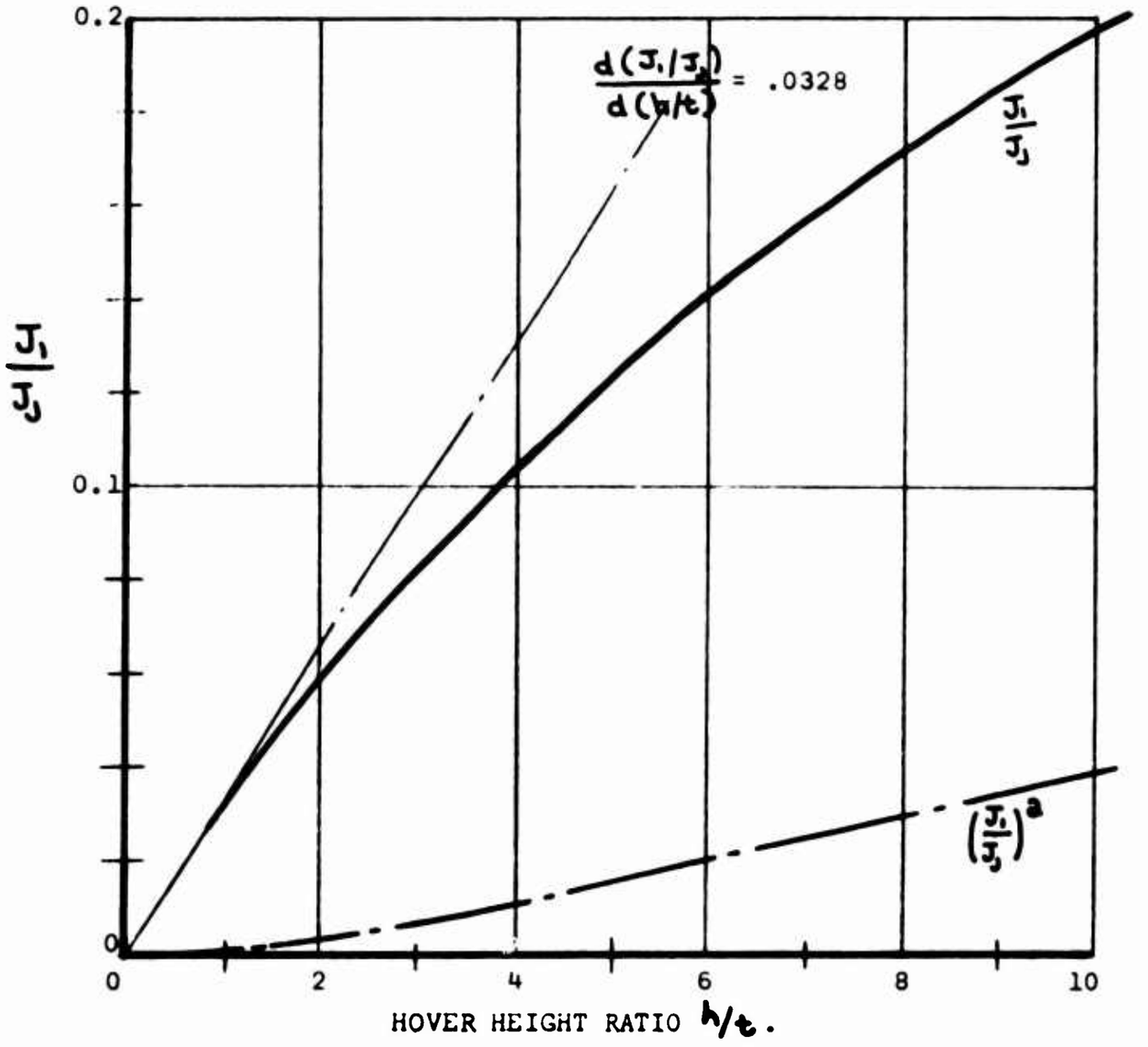

Figure 26. Ratio of Momentum Flux in the Primary Cushion Vorte · To That of the Jet.

where $x = \frac{t}{h}(1 + \sin\theta)$

In-board of the primary cushion vortex will be a secondary vortex, as shown in Figure 27.

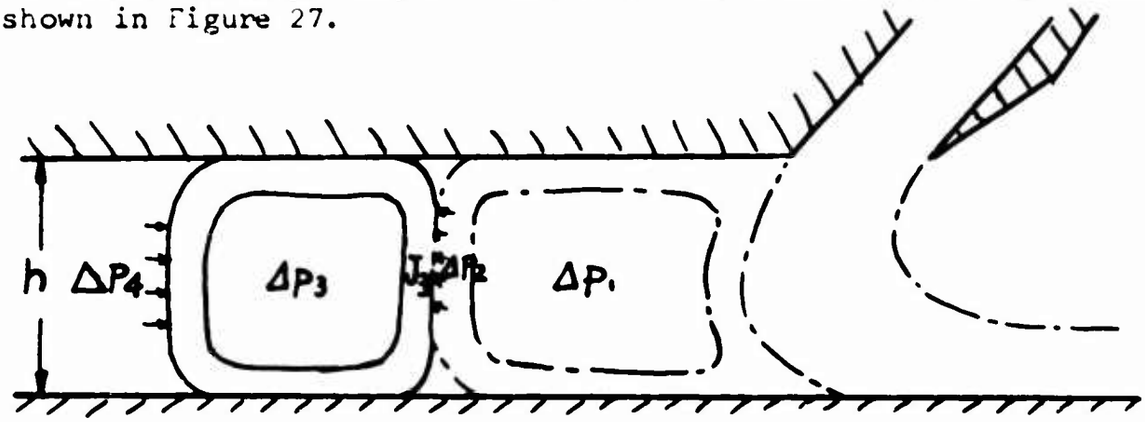

Figure 27. Geometry of Secondary Cushion Vortex.

Making the same assumptions as before,

$$\frac{J_3}{J_1} = \frac{\frac{1}{2}n}{n+1} \tag{93}$$

$$\Delta p_4 - \Delta p_3 = \frac{2J_3}{h}$$

$$\therefore \Delta p_3 = \Delta p_4 - \frac{2J_3}{h}$$

but $\Delta p_4 = \Delta p_0 = \frac{J_1}{h}(1 + \sin\theta)$

$$\frac{\Delta p_3}{\Delta p_4} = \frac{\Delta p_3}{\Delta p_0} = 1 - \frac{J_3}{J_1}\frac{2}{(1+\sin\theta)}$$

$$= 1 - \frac{J_3}{J_1}\frac{J_1}{J_1}\frac{2}{(1+\sin\theta)}$$

$$= 1 - \left(\frac{J_1}{J_1}\right)^2 \frac{2}{1+\sin\theta} \tag{94}$$

Equations (91) and (94) are plotted in Figure 28, where it is seen that the influence of the secondary vortex is quite small.

BLANK PAGE

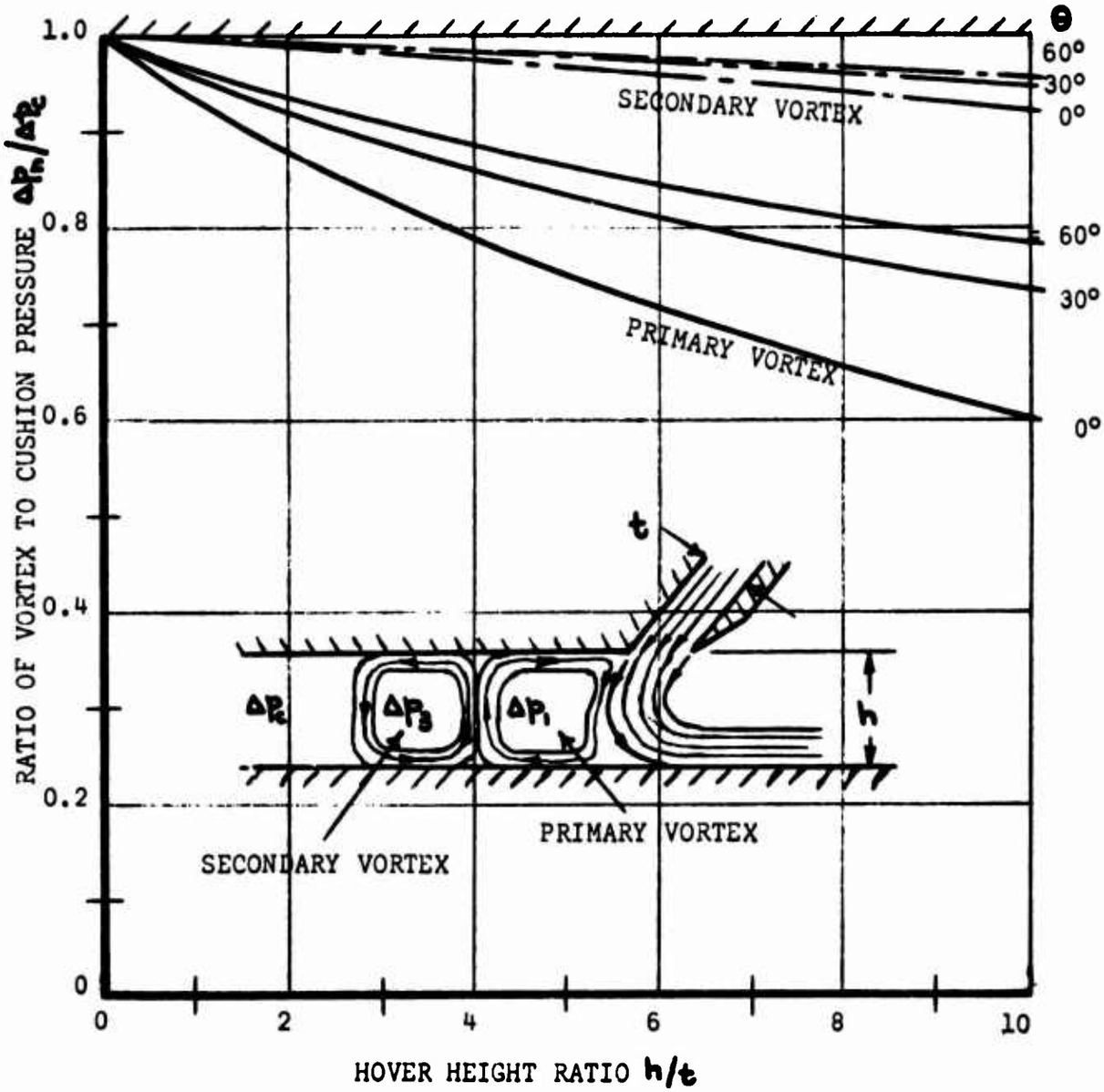

Figure 28. Static Pressure in Cushion Vortices As A Ratio of Basic Cushion Pressure. (No Momentum Loss).

It should be noted that the theoretical pressure distribution will be similar to Figure 29, if the cushion vortex hypothesis is valid, so that pressure measurement with a limited number of static pressure taps may give misleading results. A measurement at (A) would give too high a reading, and at (B) too low a reading.

It is important to note, however, that the total lift will not be influenced by vortex flow if it has zero loss and if the vortices are "square", because the vertical momentum is equal to the horizontal momentum.

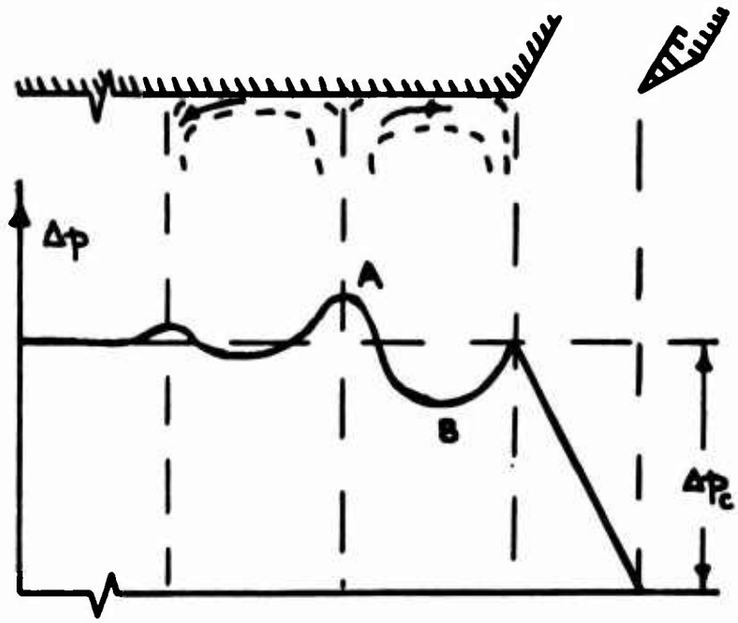

Figure 29. Theoretical Static Pressure Distribution Under a GEM.

If we assume 100 per cent momentum loss, the horizontal momentum flux is J_1 instead of $2J_1$ so that the pressure decrements are half the values given by equations (91) and (94), and the lift loss would be approximately the value to be expected from this decrement.

In practice the pressure distribution is not so regular as that sketched in Figure 29, and tends to be of the type sketched in Figure 30. By assuming a rectangular primary vortex we can obtain an average value for Δp_1. Some experimental results averaged in this manner are compared with theory in Figure 31.

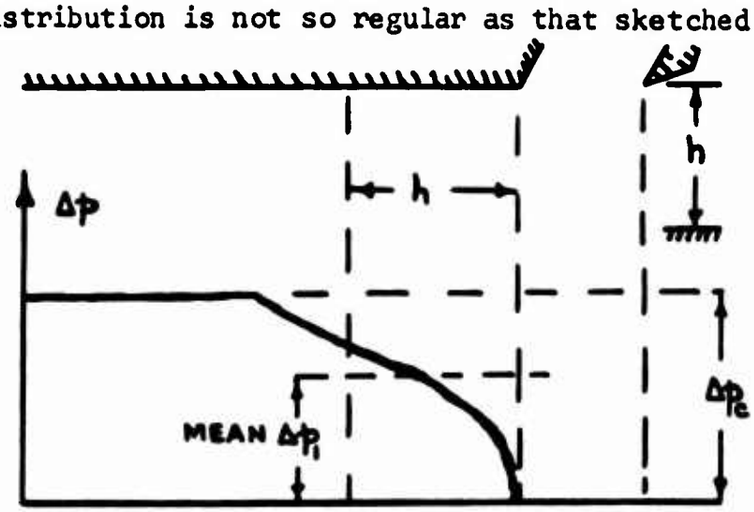

Figure 30. Idealization of Actual Cushion Pressure Distribution.

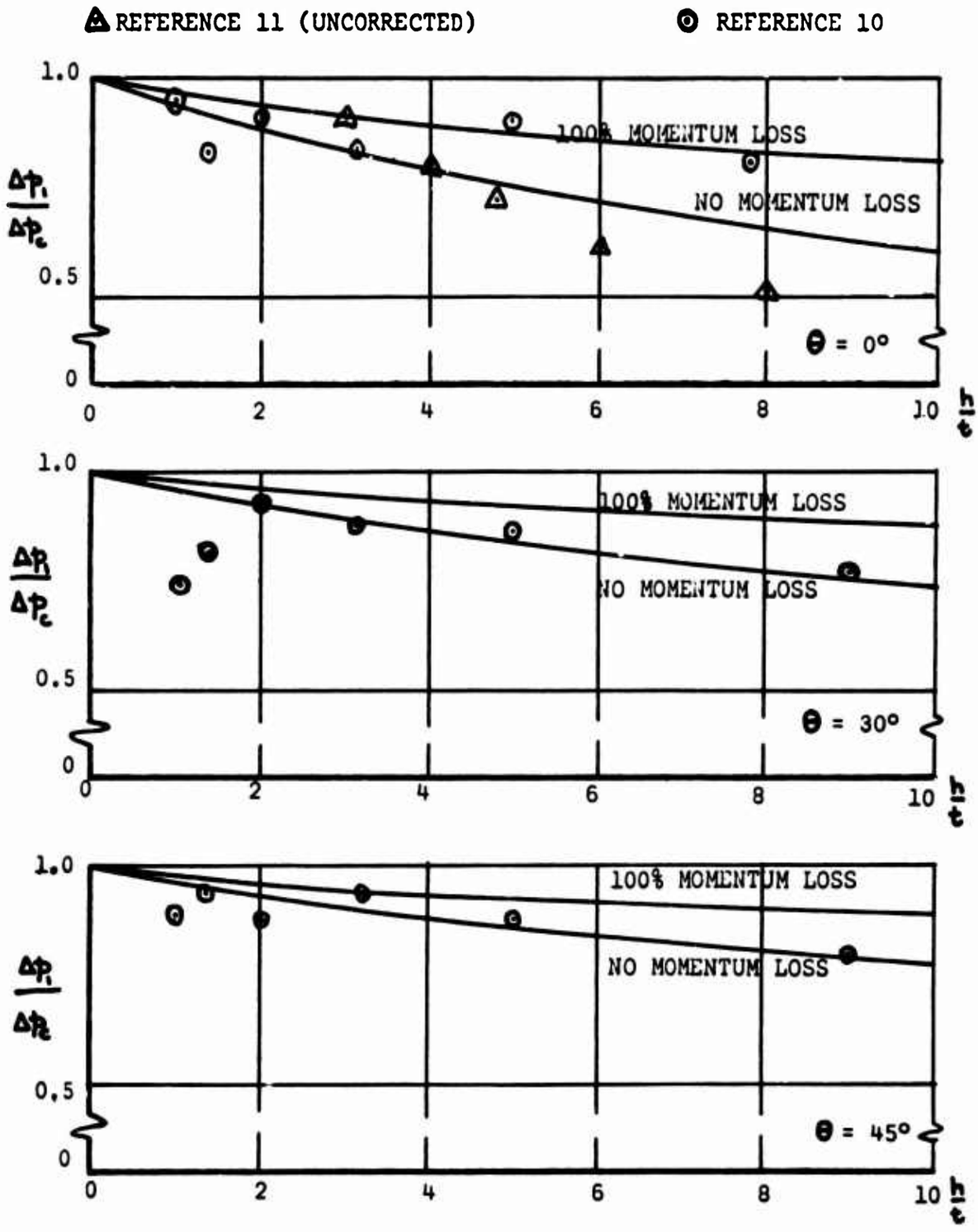

Figure 31. Calculated Vortex Pressure Compared With Experiments Reported in Reference 10.

Although there is apparently a great deal of scatter, particularly at low lift ratios, the general trends seem to be in fair agreement. Moreover, there are so many practical difficulties in experimental work of this type that it is unsafe to place too much reliance upon the experimental measurements. For example, the cushion pressure, measured at the center of the rig, is plotted in Figure 32 for the Reference 11 experiments. We know from experience that layered jet theory always gives good agreement with theory under these conditions, so that cushion air leakage must be occurring, to give the effect analyzed in Reference 12. This is a very common problem with two-dimensional test rigs, although it is also possible that ΔP_{JN} is measured some distance upstream of the nozzle and that significant losses occur after the measuring station.

In either case, we can correct the Reference 11 measurements of Δp_r by ratioing the decrement by the values of theory to experiment in Figure 32. The results of such a correction are plotted in Figure 33, and the agreement between theory and experiment is now obviously much better than in Figure 31. The fact that the measured Δp_1 is less than the theoretical value at large lift values is explainable by the fact that we have used equation (15) throughout to calculate entrainment, rather than equations (15) and (16) together.

We conclude, tentatively, that the primary vortex pressure decrement can be assumed to act over a distance (h) in from the nozzle, where h is the hover height, and that the value given by equation (91) should be used.

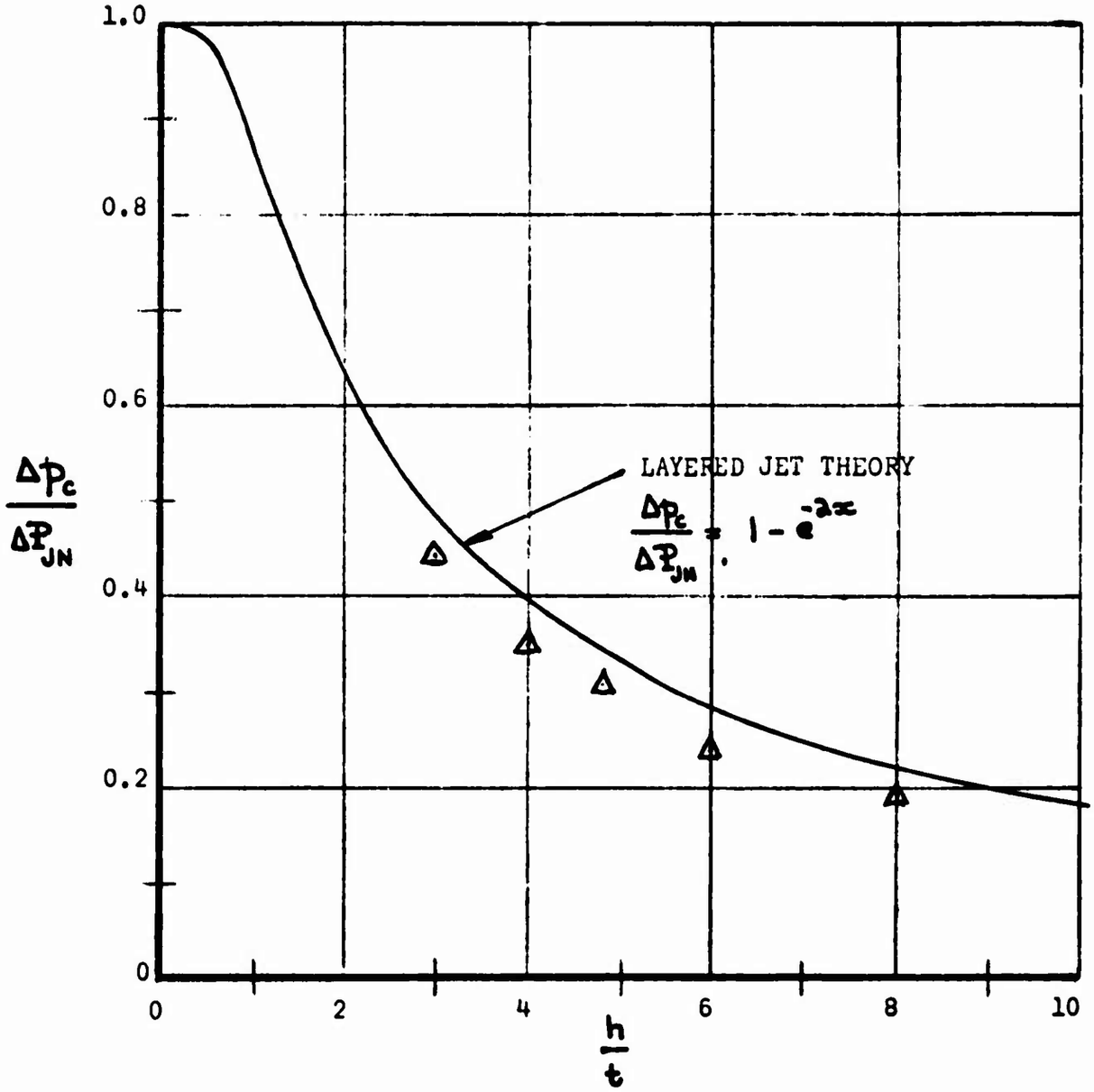

Figure 32. Measured Cushion Pressure From Reference 11 Compared With Theory $\theta = 0$.

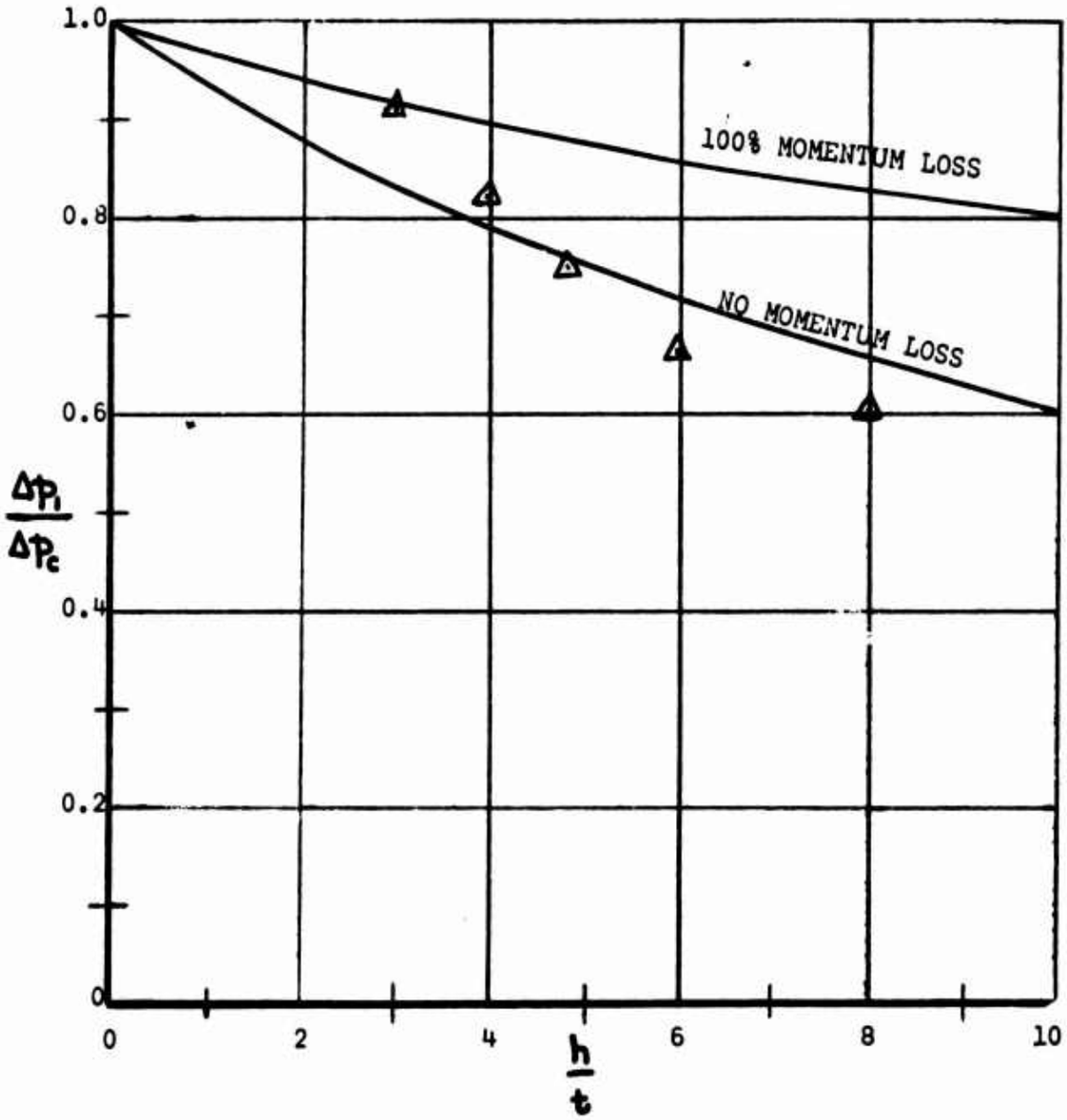

Figure 33. Reference 11 Vortex Pressure Data Corrected For Test Rig Leakage $\theta = 0$.

2.5 The Effect of Raising the Cushion Volume.

If the height of the cushion (h_a) is greater than the height of the jet nozzle (h_1), then equation (81) becomes

$$\frac{\Delta p_1}{\Delta p_c} = 1 - \frac{J_1}{J_j}\,\frac{h_1}{h_a}\,\frac{a}{(1+\sin\theta)} \qquad (94)$$

indicating that the vortex pressure decrement is reduced by the factor h_1/h_a.

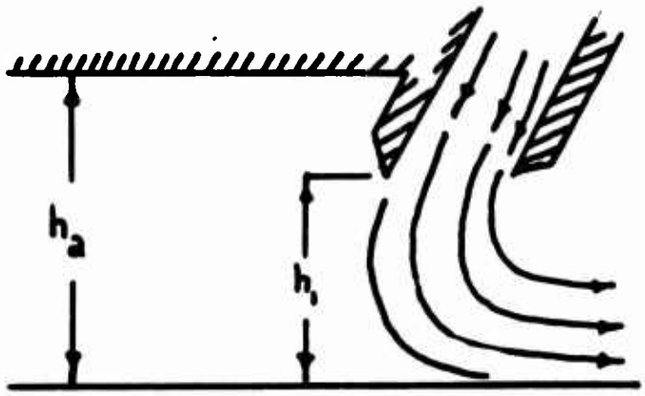

Figure 34. Increased Cushion Volume.

Thus, increasing the cushion volume reduces the lift loss due to cushion vorticity if the present assumptions are correct.

2.6 Loss of Cushion Lift Due to Cushion Vortex Flow.

We are now in a position to calculate the loss of lift due to cushion vorticity, since we assume equation (91) to act over a distance h in from the nozzle. For a rectangular cushion planform, as shown in Figure 35, the normal cushion area is

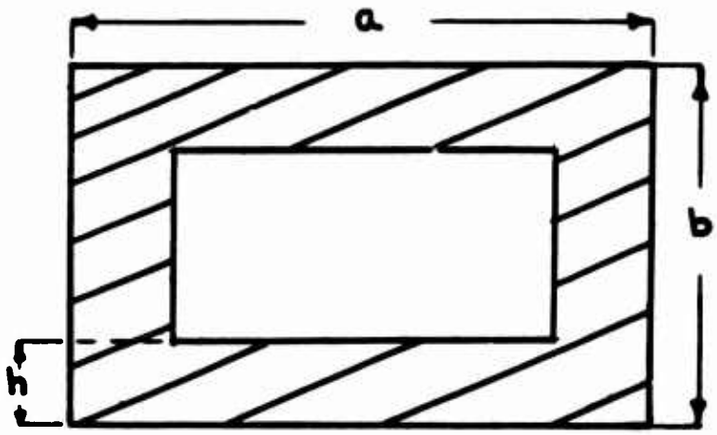

Figure 35. Rectangular Cushion Planform.

$$A_c = ab$$

The area over which the reduced pressure acts is

$$\Delta A_c = 2ah + 2(b-2h)h$$

$$= 2h(a+b-2h) \qquad (95)$$

The cushion lift is

$$L_c = \Delta p_c A_c - (\Delta p_c - \Delta p_1)\,\Delta A_c$$

$$\frac{L_c}{\Delta p_c A_c} = 1 - \frac{\Delta A_c}{A_c}\left[1 - \frac{\Delta p_1}{\Delta p_c}\right] \tag{96}$$

Substituting equation (91) for

$$\frac{L_c}{\Delta p_c A_c} = 1 - \frac{.1312\left(\frac{h}{t}\right)^2\left(\frac{t}{b}\right)\left\{1 + \frac{b}{a}\left[1 - 2\left(\frac{h}{t}\right)\left(\frac{t}{b}\right)\right]\right\}}{\left[1 + .0656\left(\frac{h}{t}\right)\right](1 + \sin\theta)} \tag{97}$$

For a circular cushion planform, of diameter D

$$\left.\begin{aligned} \frac{\Delta A_c}{A_c} &= \frac{\frac{\pi D^2}{4} - \frac{\pi}{4}(D - 2h)^2}{\frac{\pi D^2}{4}} \\ &= 4\left(\frac{h}{D}\right)\left[1 - \frac{h}{D}\right] \\ &= 4\left(\frac{h}{t}\right)\left(\frac{t}{D}\right)\left[1 - \left(\frac{h}{t}\right)\left(\frac{t}{D}\right)\right] \end{aligned}\right\} \tag{98}$$

The ratio $\Delta L_c / \Delta p_c A_c$ is plotted in Figure 36 for a circular planform for $\theta = 30°$. Since the theory can only apply if

$$2h < D$$

we have a limitation

$$\frac{h}{t} \leqslant \frac{1}{2(t/D)} \tag{99}$$

- the equality representing the entire cushion filled by the primary vortex. Naturally, we cannot expect this to occur in practice because of the rapid acceleration of the vortex air which would be required near the center of the cushion. Thus the cut-off value of h/t will be less than that indicated in Figure 36.

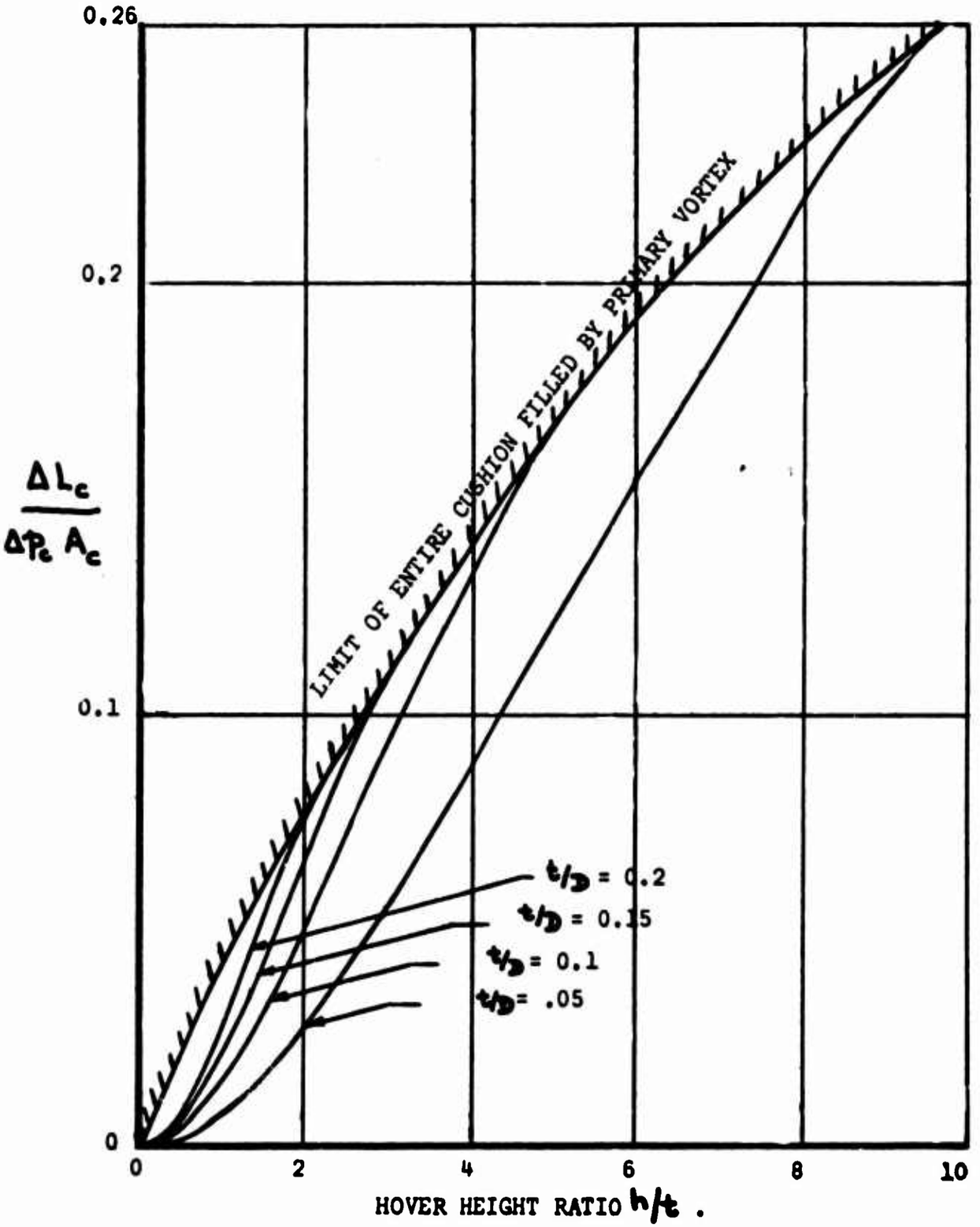

Figure 36. Loss of Cushion Lift Due to Primary Vortex - Circular Planform, θ = 30°.

Very often, as shown in Figure 37, an annular jet is thick enough for viscous mixing to have very little effect upon the total lift of the vehicle.

2.7 The Existence of Cushion Vorteces.

Whether or not a vortex pattern is set up in the cushion will presumably depend upon three-dimensional flow effects which are beyond the scope of this investigation. When more refined analyses of this flow are carried out, we can expect to discover parameters which will indicate whether a vortex can exist.

Even when no vortex exists, however, we can expect entrainment of the cushion air to occur, resulting in a net momentum loss and hence a reduction in cushion pressure.

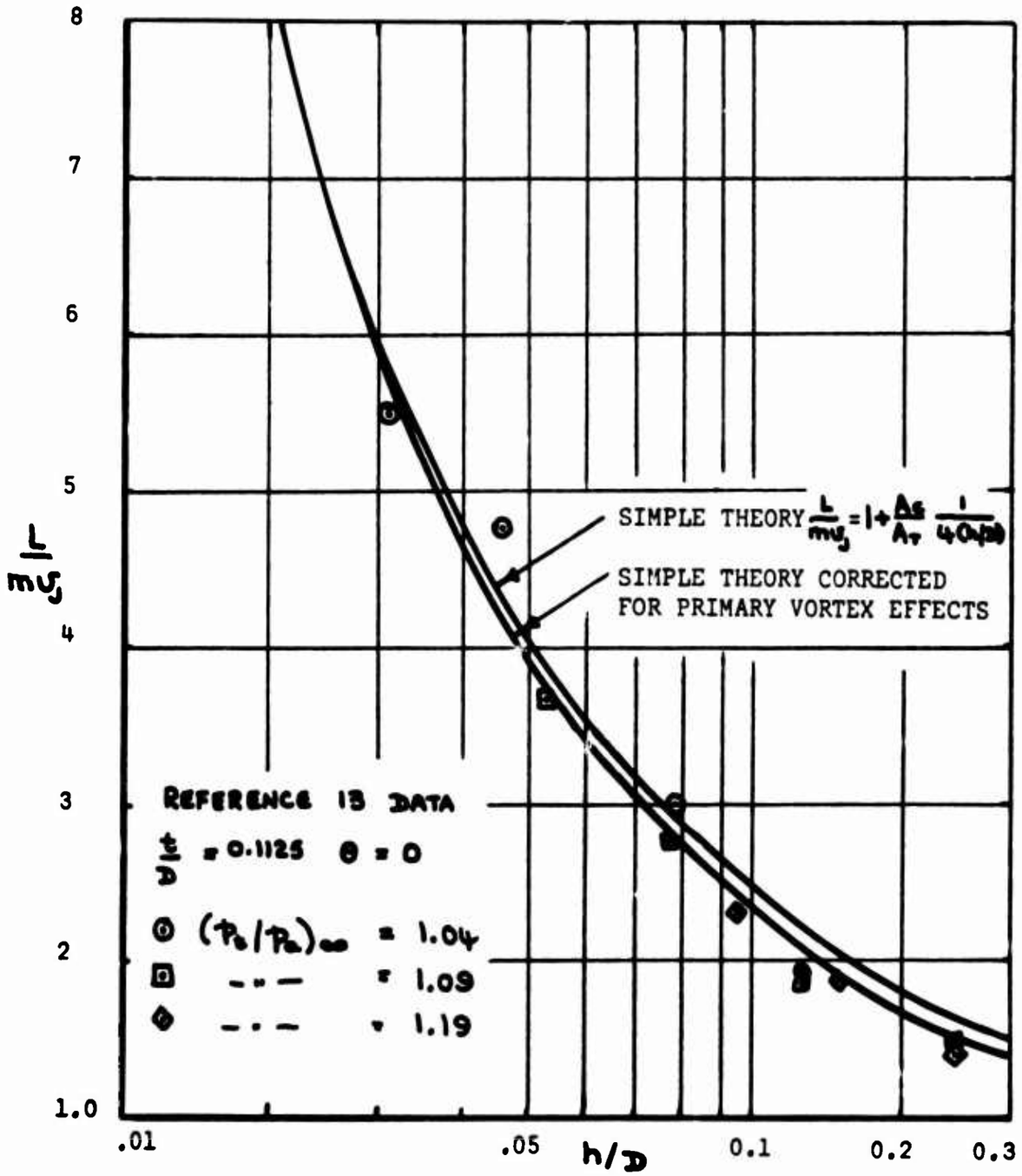

Figure 37. Model Data for Total Lift Compared With Theory.

SECTION THREE

MIXING LOSSES IN AN ANNULAR JET

In this section we shall attempt to solve the familiar problem of the cushion pressure generated by an annular jet, but with the effects of mixing included.

We shall also eliminate another approximation; namely, the familiar one that the horizontal momentum flux is $J_J(1+\sin\theta)$. In fact, referring to Figure 38, the horizontal momentum flux is

$$J_{JN} \sin\theta + J_{JO} \tag{100}$$

where $$J_{JO} > J_{JN}$$

- because the mean static pressure of the jet is lower after it strikes the ground.

3.1 Thin Jet Theory.

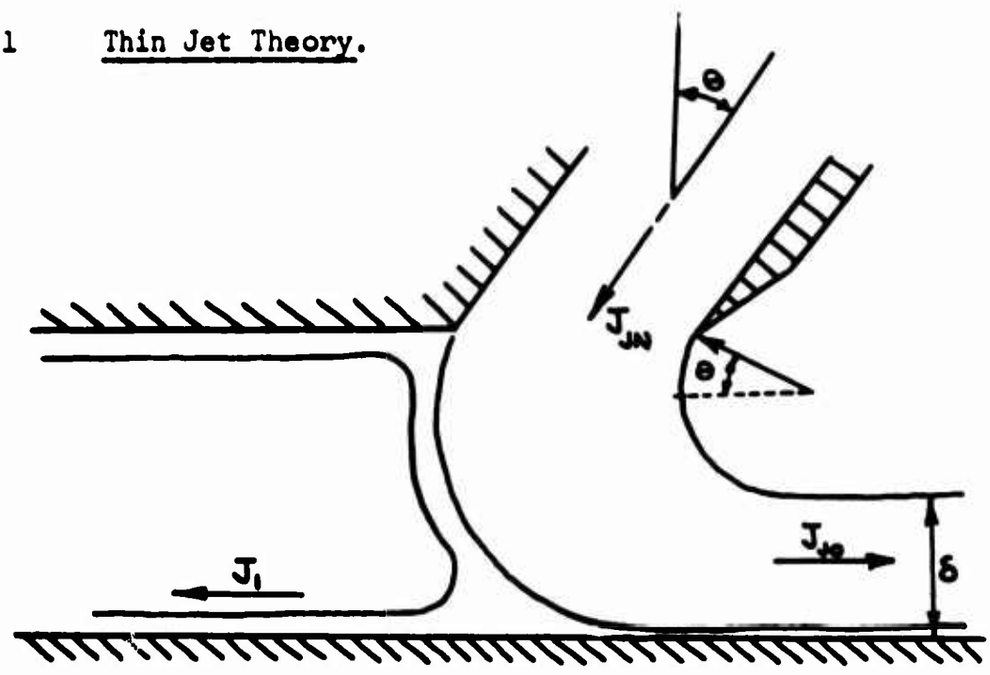

Figure 38. Basic Geometry.

From Figure 38 the effective mixing length of the outside of the jet is approximately

$$s = r\left(\frac{\pi}{2} + \theta\right) \tag{101}$$

where $\delta - h = r(1 + \sin\theta)$

Writing $\delta \approx t$ because of entrainment

$$r = \frac{h - t}{1 + \sin\theta} \tag{102}$$

and

$$s = \frac{(h - t)\left(\frac{\pi}{2} + \theta\right)}{1 + \sin\theta} \tag{103}$$

The mean mixing length is the average of this and equation (87),

that is, $$\frac{s_m}{h} = 0.41 + \frac{\left(1 - \frac{t}{h}\right)\left(\frac{\pi}{2} + \theta\right)}{2(1 + \sin\theta)} \tag{104}$$

The relationship $f(\theta)$ is plotted in Figure 39, and we can obviously take a mean value of $f(\theta) = 1.44$

so that $$\frac{s_m}{h} = 0.41 + 0.72\left(1 - \frac{t}{h}\right) \tag{105}$$

- as plotted in Figure 40.

From equations (17) and (27)

$$\frac{\dot{m}_{JO}}{\dot{m}_{JN}} = 1 + .04\left(\frac{s_m}{h}\right)\left(\frac{h}{t}\right) \tag{106}$$

$$\frac{q_{JO}}{q_{JN}} = \frac{1}{\left[1 + .08\left(\frac{s_m}{h}\right)\left(\frac{h}{t}\right)\right]^2} \tag{107}$$

Also $$J_{JO} = \dot{m}_{JO} v_{JO} = \left(\frac{\dot{m}_{JO}}{\dot{m}_{JN}}\right)\left(\frac{v_{JO}}{v_{JN}}\right)\dot{m}_{JN} v_{JN} = \left(\frac{\dot{m}_{JO}}{m_{JN}}\right)\left(\frac{v_{JO}}{v_{JN}}\right) J_{JN} \tag{108}$$

But $$\Delta P_{JN} = \frac{1}{2}\Delta p_c + \frac{1}{2}\rho v_{JN}^2 \tag{109}$$

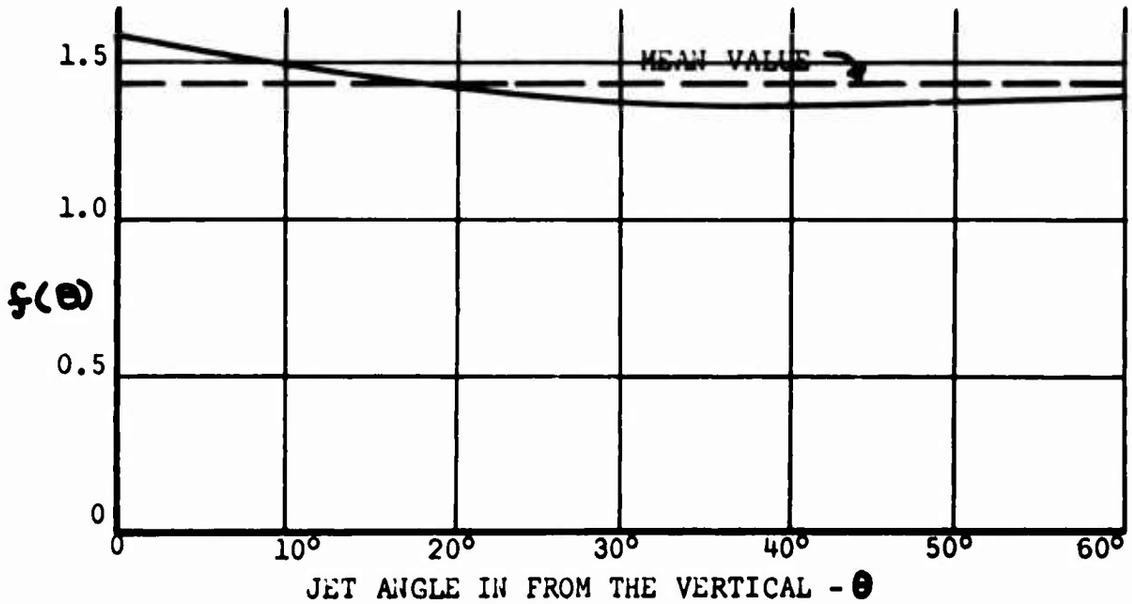

Figure 39. Plot of $f(\theta) = (\xi + \theta)/(1 + \sin\theta)$ Against θ.

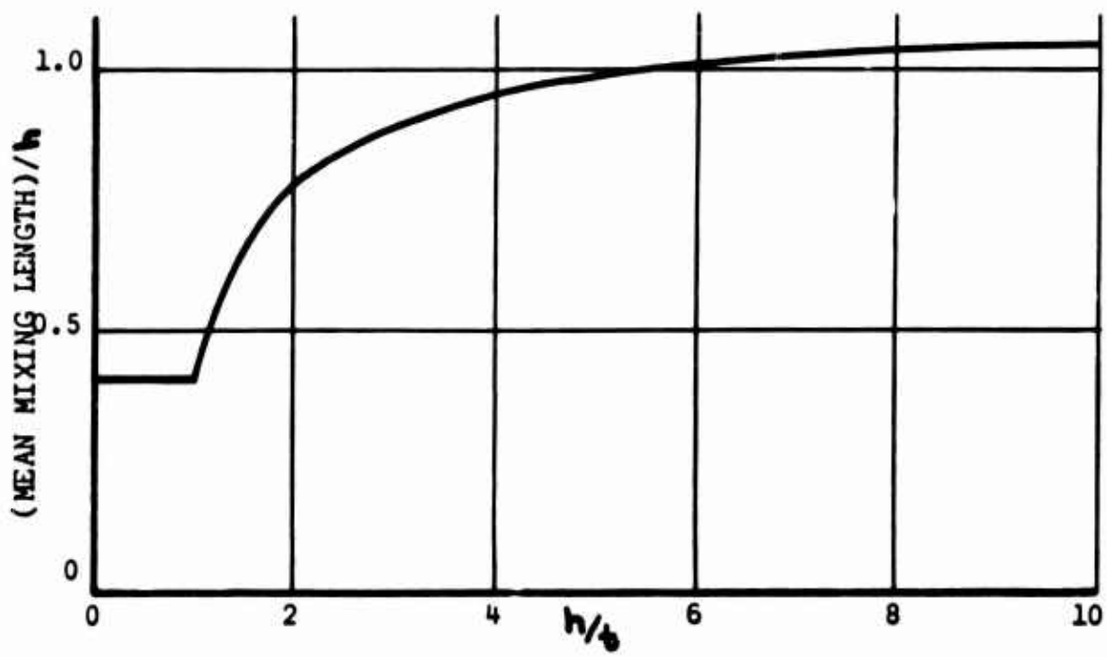

Figure 40. Mean Mixing Length Ratio ℓ_m/h To Point Where Jet Static Pressure is Ambient.

$$\left.\begin{aligned} \Delta P_{JO} &= \frac{1}{2}\Delta p_c + \frac{1}{2}\rho v_{JN}^2\left(\frac{q_{JO}}{q_{JN}}\right) \\ &= \frac{1}{2}\rho v_{JO}^2 \end{aligned}\right\} \tag{110}$$

$$v_{JO} = \sqrt{\frac{\Delta p_c}{\rho} + v_{JN}^2\left(\frac{q_{JO}}{q_{JN}}\right)} \tag{111}$$

Substituting for v_{JN}^2

$$v_{JO} = \sqrt{\frac{\Delta p_c}{\rho} + \left[\frac{2\Delta P_{JN}}{\rho} - \frac{\Delta p_c}{\rho}\right]\left(\frac{q_{JO}}{q_{JN}}\right)}$$

$$= \sqrt{\frac{\Delta p_c}{\rho}\left[1 - \frac{q_{JO}}{q_{JN}}\right] + 2\frac{\Delta P_{JN}}{\rho}\left(\frac{q_{JO}}{q_{JN}}\right)} \tag{112}$$

$$= \sqrt{\frac{2\Delta P_{JN}\left(\cancel{q_{JO}/q_{JN}}\right) + \Delta p_c\left[1 - \cancel{q_{JO}/q_{JN}}\right]}{2\Delta P_{JN} - \Delta p_c}} \tag{113}$$

Thus the total horizontal momentum flux gives

$$\Delta p_c = \frac{J_{JN}}{h}\left[\sin\theta + \left(\frac{\dot{m}_{JO}}{\dot{m}_{JN}}\right)\left(\frac{v_{JO}}{v_{JN}}\right)\right] \tag{114}$$

where $\left(\frac{\dot{m}_{JO}}{\dot{m}_{JN}}\right)\left(\frac{v_{JO}}{v_{JN}}\right) > 1.0$

From equation (109)

$$J_{JN} = \dot{m}_{JN} v_{JN} = \rho t v_{JN}^2$$

$$= t\left[2\,\Delta P_{JN} - \Delta P_E\right]\left[\sin\theta + \left(\dot{m}_{JO}/\dot{m}_{JN}\right)\left(v_{JO}/v_{JN}\right)\right]$$

$$\frac{\Delta P_E}{\Delta P_{JN}} = \frac{t}{h}\left(2 - \frac{\Delta P_E}{\Delta P_{JN}}\right)\left\{\sin\theta + \left[1 + .04\left(\frac{\delta_m}{h}\right)\left(\frac{h}{t}\right)\right]\sqrt{\frac{2\left(\dot{m}_{JO}/\dot{m}_{JN}\right) - \Delta P_E/\Delta P_{JN}\left[1 - \dot{m}_{JO}/\dot{m}_{JN}\right]}{2 - \Delta P_E/\Delta P_{JN}}}\right\} \tag{115}$$

After some manipulation, this reduces to

$$a\left(\frac{\Delta P_E}{\Delta P_{JN}}\right)^2 + b\left(\frac{\Delta P_E}{\Delta P_{JN}}\right) + c = 0$$

where

$$a = \frac{\left(h/t + \sin\theta\right)^2}{\left[1 + .04\left(\frac{\delta_m}{h}\right)\left(\frac{h}{t}\right)\right]^2} - \left[1 - \frac{q_{JO}}{q_{JN}}\right] \tag{116}$$

$$b = 2 - \frac{4\sin\theta\left(\frac{h}{t} + \sin\theta\right)}{\left[1 + .04\left(\frac{\delta_m}{h}\right)\left(\frac{h}{t}\right)\right]^3}$$

$$c = \frac{4\sin^2\theta}{\left[1 + .04\left(\frac{\delta_m}{h}\right)\left(\frac{h}{t}\right)\right]^2} - 4\left(\frac{q_{JO}}{q_{JN}}\right)$$

and of course

$$\frac{q_{JO}}{q_{JN}} = \frac{1}{\left[1 + .08\left(\frac{\delta_m}{h}\right)\left(\frac{h}{t}\right)\right]^2} \tag{107}$$

$$\frac{\delta_m}{h} = 0.41 + 0.72\left(1 - \frac{t}{h}\right) \tag{105}$$

This equation is plotted in Figure 41 for $\theta = 60°$ and is seen to give slightly more cushion pressure than simple thin jet theory for $h/t < 3$ and rather less for $h/t > 4$. In other words, at low hover heights $J_{je} > J_{jN}$ because the mean jet pressure is greater than ambient prior to striking the ground. At higher heights this is more than offset by the loss of momentum flux due to entrainment of cushion air.

3.2 Layered Jet Theory.

The effect of entrainment of cushion air is already incorporated in layered jet theory, as given in Reference 12, for example. Thus the only additional factor which needs to be incorporated is the acceleration of the air due to $J_{je} > J_{jN}$. Although it is obviously possible to carry out a detailed analysis of these effects, the equations are so complicated that more useful results are obtained by devising an expression for the mom ntum ratio ($\sin\alpha$) from the thin jet theory of the previous section. The obvious rationale for this procedure is, of course, that mixing only becomes important for the larger values of h/t where thin jet theory is, in any case, adequate.

Layered jet theory (Reference 12) gives

$$\frac{\Delta p_c}{\Delta p_{jN}} = 1 - e^{-2x} \tag{117}$$

where $x = \frac{t}{h}\left(\sin\alpha + \sin\theta\right)$

and $\sin\alpha$ is the ratio of the exhausted momentum to the total nozzle momentum. In terms of Figure 38,

$$\sin\alpha = \frac{J_{ve}}{J_{jN}} \tag{118}$$

- since the vortex air recirculates and does not reduce Δp_c as such. Thus, from equation (108),

$$\sin\alpha = \frac{\dot{m}_{ve}}{\dot{m}_{jN}} \frac{V_{ve}}{V_{jN}} \tag{119}$$

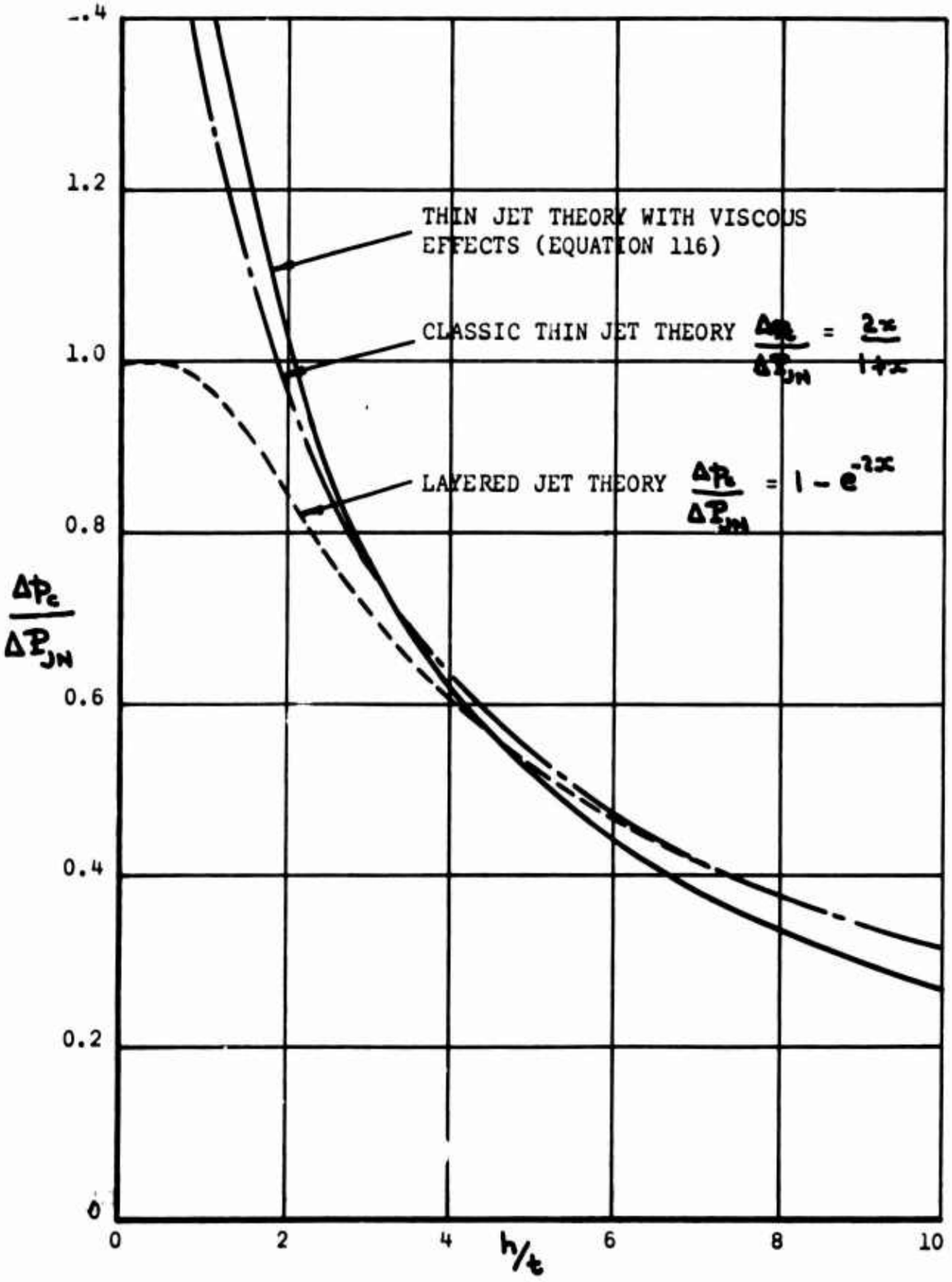

Figure 41. Comparison of Cushion Pressure Theories For θ = 60°.

- and from equations (106) and (113),

$$\sin\alpha = \left(\frac{\dot{m}_{Jo}}{\dot{m}_{JN}}\right)\sqrt{\frac{2\,\Delta P_{JN}\left(\frac{q_{Jo}}{q_{JN}}\right) + \Delta p_c\left[1-\left(\frac{q_{Jo}}{q_{JN}}\right)\right]}{2\,\Delta P_{JN} - \Delta p_c}} \tag{120}$$

If this is substituted into equation (117), it is obviously impossible to solve explicitly. Obviously, it is most convenient, therefore, to obtain a graphical solution, and this is done by first plotting

$$\sin\alpha = \left(\frac{\dot{m}_{Jo}}{\dot{m}_{JN}}\right)\sqrt{\frac{\frac{q_{Jo}}{q_{JN}} + \frac{1}{2}\frac{\Delta p_c}{\Delta P_{JN}}\left[1 - \frac{q_{Jo}}{q_{JN}}\right]}{1 - \frac{1}{2}\frac{\Delta p_c}{\Delta P_N}}} \tag{121}$$

as a function of $\frac{h}{t}$ for various values of $\Delta p_c / \Delta P_{JN}$. From equation (117) we get the relationship

$$x = \frac{1}{2}\log_e\left|\frac{1}{1-\Delta p_c/\Delta P_{JN}}\right| \tag{122}$$

$$\therefore \sin\alpha = \frac{1}{2}\frac{h}{t}\log_e\left|\frac{1}{1-\Delta p_c/\Delta P_{JN}}\right| - \sin\theta \tag{123}$$

The intersections of equations (121) and (123) will obviously give the correct values of sin α, which can then be used in equation (117).

As an alternative (approximate) approach, the ratio of the thin jet values for $\Delta p_c/\Delta P_{JN}$ (Figure 41 for example) can be used to ratio the values obtained from equation (117) provided that this is not done below about h/t = 4.0.

3.3 Calculation of Sin α for Zero Mixing.

When there is no mixing loss, sin α > 1.0. From Bernoulli,

$$\frac{1}{2}\rho v_{Jo}^2 = \Delta P_{JN} \tag{124}$$

$$\therefore \quad J_{Jo} = \dot{m}_J v_{Jo} = \dot{m}_J\sqrt{\frac{2}{\rho}\Delta P_{JN}} \tag{125}$$

But from Reference 14

$$\dot{m}_J = t\sqrt{2\rho\,\Delta P_{JN}}\;\frac{(1-e^{-x})}{x} \tag{126}$$

$$J_{JN} = t\;\Delta P_{JN}\;\frac{1-e^{-2x}}{x} \tag{127}$$

$$\therefore\ \sin\alpha = \frac{J_{JO}}{J_{JN}} = 2\,\frac{1-e^{-x}}{1-e^{-2x}} \tag{128}$$

$$\therefore\quad x = 2\frac{t}{h}\,\frac{1-e^{-x}}{1-e^{-2x}} + \frac{t}{h}\sin\theta \tag{129}$$

- an equality to which no explicit solution can be written.

From equation (122) by equating x,

$$\frac{1}{2}\log_e\frac{1}{1-\frac{\Delta p_c}{\Delta P_{JN}}} = 2\frac{t}{h}\,\frac{1-e^{-x}}{\Delta p_c/\Delta P_{JN}} + \frac{t}{h}\sin\theta \tag{130}$$

and since $e^{-2x} = 1 - \dfrac{\Delta p_c}{\Delta P_{JN}}$

$$e^{-x} = \sqrt{1-\frac{\Delta p_c}{\Delta P_{JN}}}$$

$$\frac{t}{h}\left\{\frac{2\left[1-\sqrt{1-\Delta p_c/\Delta P_{JN}}\right]}{\Delta p_c/\Delta P_{JN}} + \sin\theta\right\} = \frac{1}{2}\log_e\frac{1}{1-\frac{\Delta p_c}{\Delta P_{JN}}} \tag{131}$$

Thus we can use this equation to plot $\Delta p_c/\Delta P_{JN}$ as a function of t/h. This has been done in Figure 42, for $\theta = 60°$ and is seen to give somewhat higher values of Δp_c than the simple layered jet theory. The inclusion of mixing losses will reduce these values, of course, as in Figure 41.

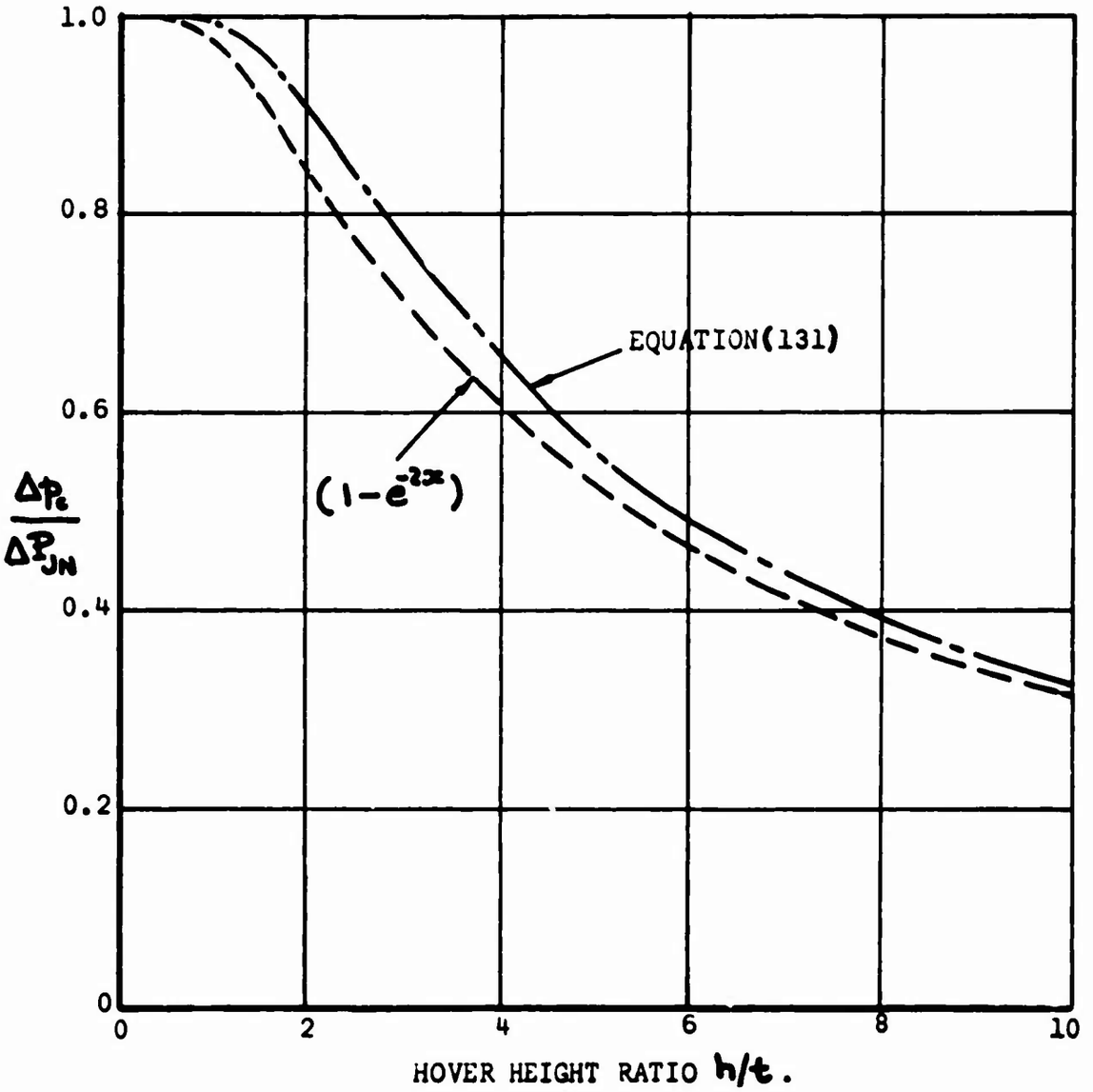

Figure 42. Effect of Allowing For Jet Expansion To Ambient Without Mixing. θ = 60°.

SECTION FOUR

MIXING LOSSES IN A RECIRCULATING JET

The basic geometry of a recirculating jet is illustrated in Figure 43, where entrainment is seen to be possible in three areas. It is possible for entrainment of the outside air to influence only that part of the flow which is exhausted outwards, provided that this portion of the jet is thick enough. In this case there is no total pressure loss in the recirculating jet, and the effect of entrainment on the outwardly exhausting air is as discussed in the previous section for an annular jet.

The effective entrainment in the cavity zone can be zero if a stable, loss-free vortex is established. In configurations so far tried, however, there has been no possibility of such vortex flow, because of the large diffusion losses which would occur. Thus, present cavity zone geometries can be regarded as giving the "worst-case" loss of free-air entrainment in the jet.

Finally, in the third mixing zone, the relatively slow-moving re-entrant jet can be assumed to experience free-air entrainment on its cushion side.

We shall now analyze each of these losses in detail, in order to determine the total pressure loss attributable to all three causes. The analysis will be restricted to constrained vortex flow.

4.1 Free-Air Entrainment Losses.

This problem was examined in Reference 15 for the case of 100 per cent recirculating flow, where it is shown that the length of jet affected is

$$\frac{S_F}{h} = \frac{\frac{\pi}{2} - \theta_1}{1 - \sin\theta_1} \tag{132}$$

This equation is plotted in Figure 44. From equation (107), the dynamic head reduction attributable to mixing over this length is

$$\frac{q}{q_{JN}} = \frac{1}{\left[1 + .04\left(\frac{S_F}{h}\right)\left(\frac{h}{t}\right)\right]^2} \tag{133}$$

BLANK PAGE

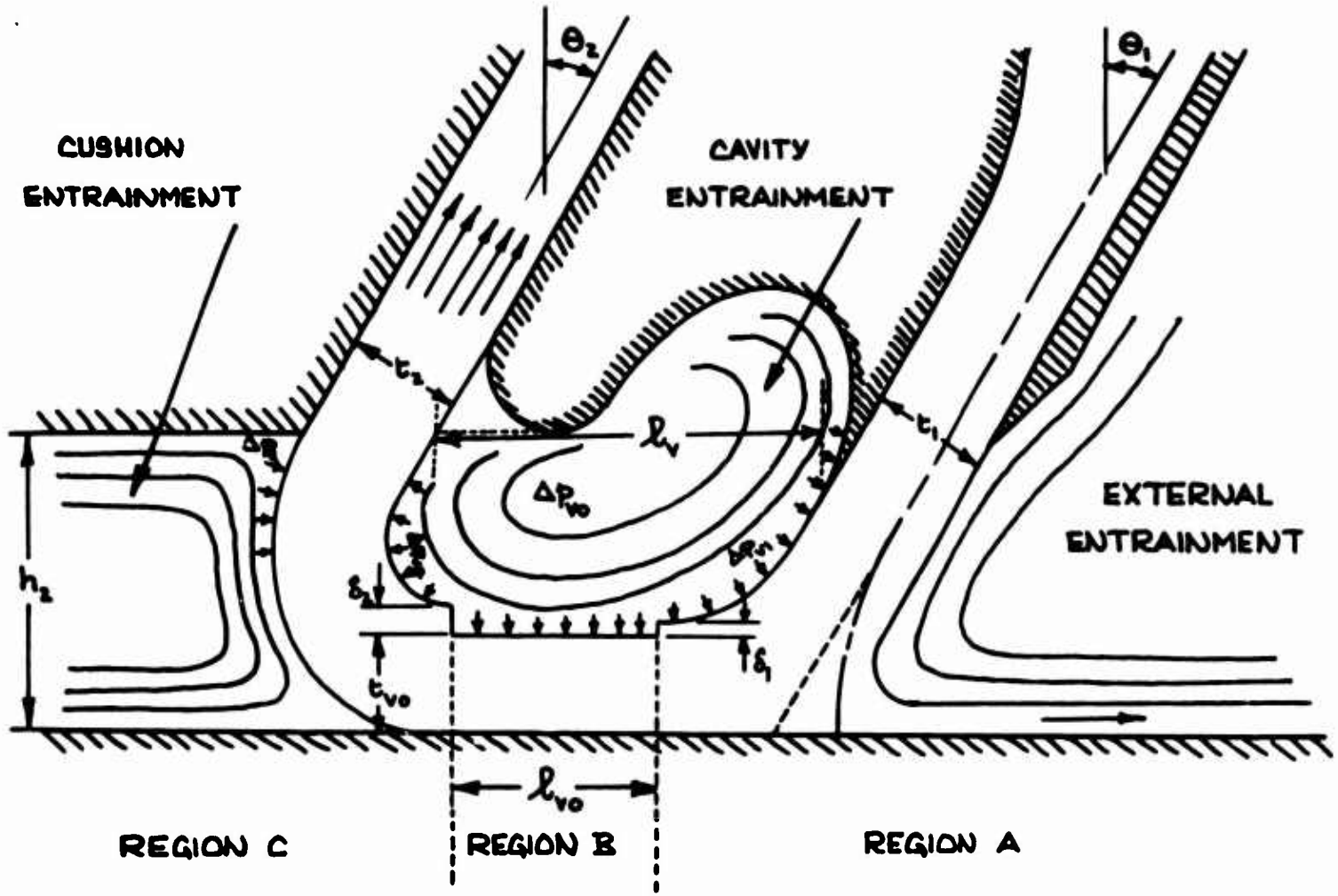

Figure 43. Partially Recirculating Jet.

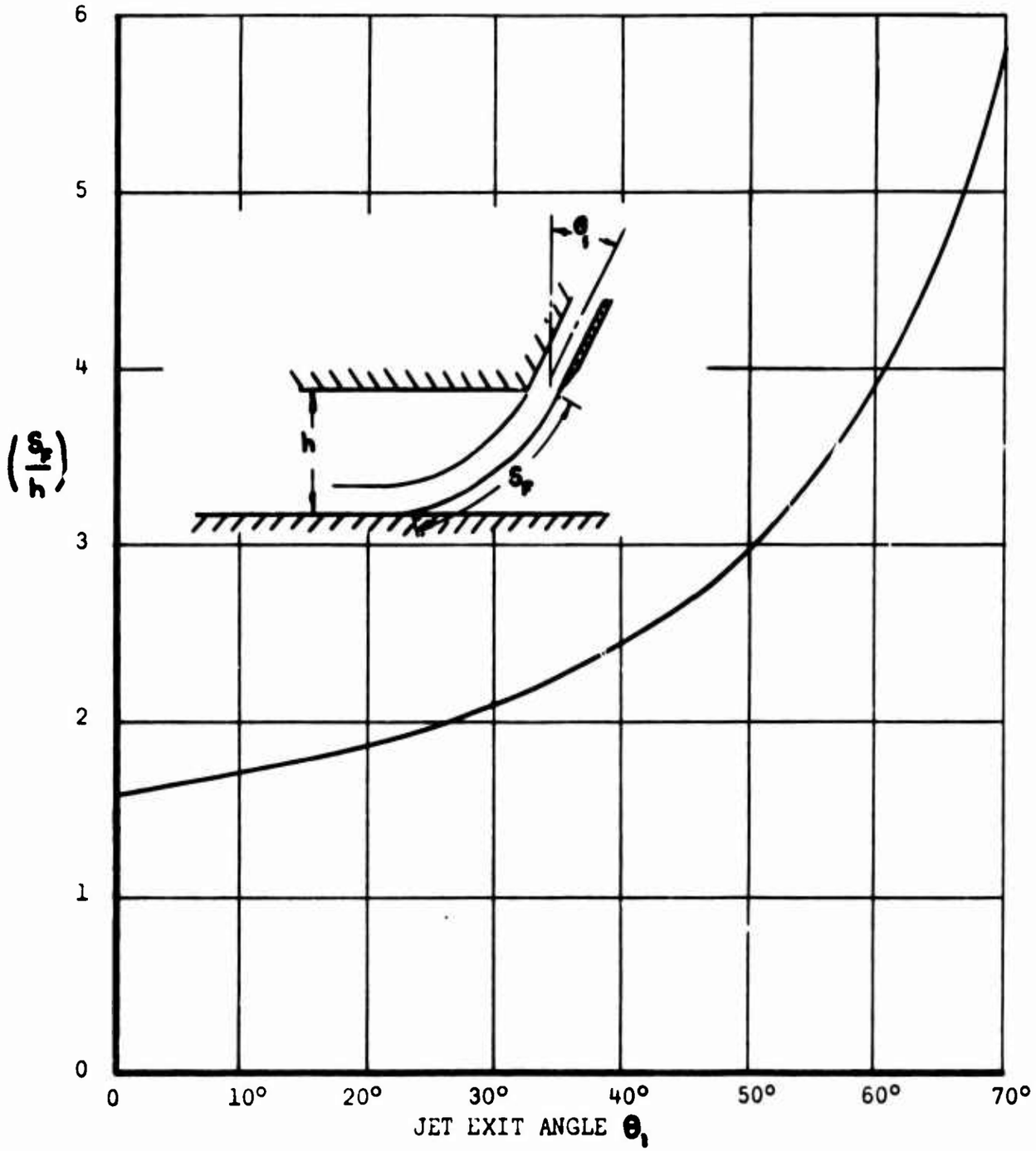

Figure 44. Free-Air Entrainment Periphery for Recirculating Jet.

If we assume that the static pressure is essentially ambient in the outer portions of the jet,

$$\Delta P_{JN} = \frac{1}{2}\rho V_{JNF}^2 = q_{JN}$$

$$\therefore \quad q_F = \left(\frac{q}{q_{JN}}\right) q_{JN} = \frac{\Delta P_{JN}}{\left[1 + .08\left(\frac{\delta_F}{h}\right)\left(\frac{h}{t}\right)\right]^2} \tag{134}$$

over the <u>outer half of the jet</u>.

4.2 Cavity Zone Entrainment Loss.

Assuming that no cavity vortex flow is generated, we can assume static entrainment.

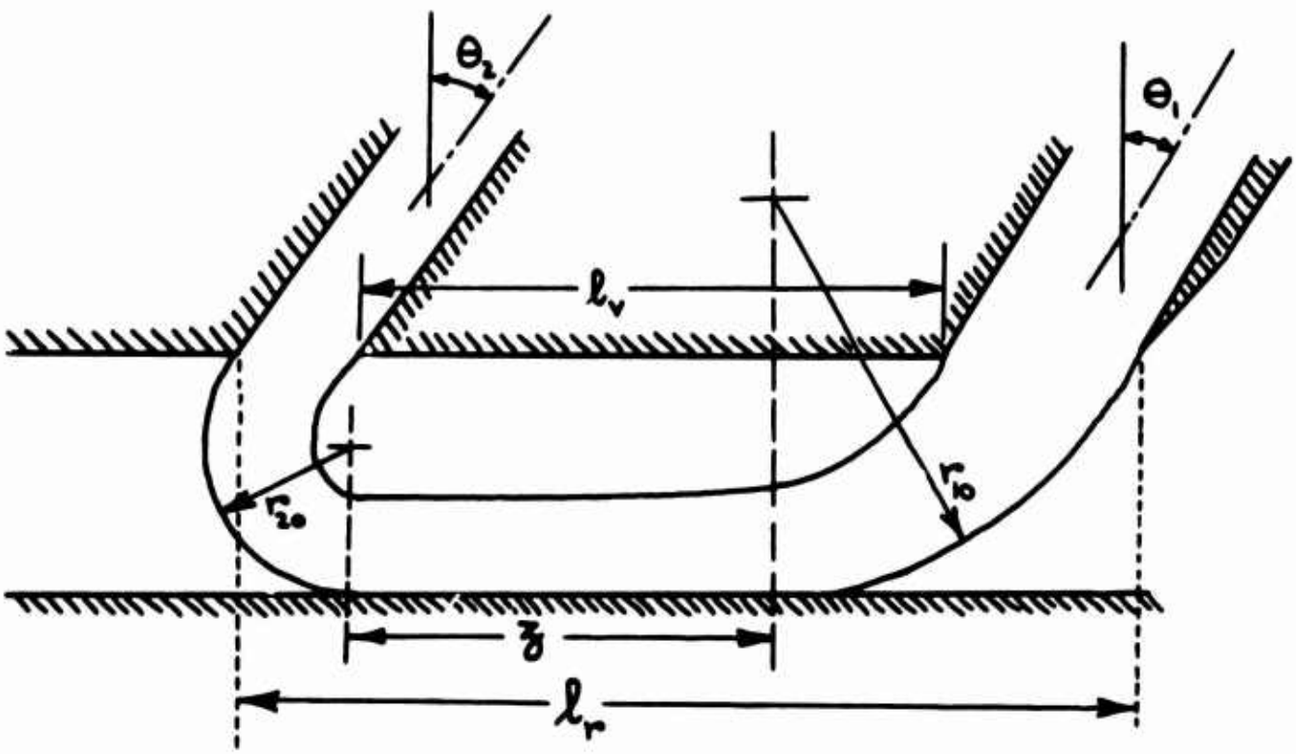

Figure 45. Geometry of Jet External Surface.

From Figure 45 and equation (102),

$$\left.\begin{aligned} \frac{r_{10}}{h} &= \frac{1}{1-\sin\theta_1} \\ \frac{r_{20}}{h} &= \frac{1}{1+\sin\theta_2} \end{aligned}\right\} \tag{135}$$

From the geometry

$$\ell_r = r_{10}\cos\theta_1 + r_{20}\cos\theta_2 + z$$

$$\frac{z}{h} = \frac{\ell_r}{h} - \frac{\cos\theta_1}{1-\sin\theta_1} - \frac{\cos\theta_2}{1+\sin\theta_2} \tag{136}$$

(Note that the critical height postulated in Reference 15 is reached when $z = 0$ in this equation.)

The inner jet radii are, approximately,

$$\left.\begin{aligned} \frac{r_{11}}{h} &= \frac{1-t/h}{1-\sin\theta_1} \\ \frac{r_{21}}{h} &= \frac{1-t/h}{1+\sin\theta_2} \end{aligned}\right\} \tag{137}$$

- assuming that the jet thickness is equal to the exit plane thickness, for simplicity. Thus the periphery in the entrainment zone is

$$\frac{S_v}{h} = \frac{z}{h} + \frac{(\frac{\pi}{2}-\theta_1)(1-t/h)}{1-\sin\theta_1} + \frac{(\frac{\pi}{2}+\theta_2)(1-t/h)}{1+\sin\theta_2} \tag{138}$$

Substituting equation (136) for ℓ_r/h,

$$\frac{S_v}{h} = \frac{\ell_r}{h} - \frac{\cos\theta_1}{1-\sin\theta_1} - \frac{\cos\theta_2}{1+\sin\theta_2} + \left(1-t/h\right)\left\{\frac{\frac{\pi}{2}-\theta_1}{1-\sin\theta_1} + \frac{\frac{\pi}{2}+\theta_2}{1+\sin\theta_2}\right\} \quad (139)$$

If we assume that the pressure Δp_v acts over the inner half of the jet

$$\Delta P_{JN} = \Delta p_v + \tfrac{1}{2}\rho v_{JNV}^2$$

$$\therefore \quad q_{JN} = \Delta P_{JN} - \Delta p_v$$

$$q_v = \frac{q}{q_{JN}} q_{JN} = \frac{\Delta P_{JN} - \Delta p_v}{\left[1 + .08\left(\frac{S_v}{h}\right)\left(\frac{h}{t}\right)\right]^2}.$$

and
$$\frac{\Delta P_{v1}}{\Delta P_{JN}} = \frac{\Delta p_v}{\Delta P_{JN}} + \frac{q_v}{\Delta P_{JN}} = \frac{\Delta p_v}{\Delta P_{JN}}\left[1 - \frac{1}{\left[1+.08\left(\frac{S_v}{h}\right)\left(\frac{h}{t}\right)\right]^2}\right] + \frac{1}{\left[1+.08\left(\frac{S_v}{h}\right)\left(\frac{h}{t}\right)\right]^2} \quad (140)$$

measured at the intake nozzle, over the <u>inner half</u> of the jet.

4.3 Cushion Zone Entrainment Loss.

The jet periphery in the cushion is

$$\frac{S_c}{h} = \frac{\frac{\pi}{2} + \theta_2}{1+\sin\theta_2} \quad (141)$$

Assuming the pressure Δp_c to act over the outer half of the jet,

$$\Delta p_c + q_{co} = \Delta P_{JN} - q_{JN}\left(1 - q_F/q_{JN}\right)$$

$$q_{co} = \Delta P_{JN} - q_{JN}\left(1 - q_F/q_{JN}\right) - \Delta p_c$$

$$= \frac{\Delta P_{JN} - q_{JN}\left(1 - q_F/q_{JN}\right) - \Delta p_c}{\left[1 + .08\left(\frac{S_c}{h}\right)\left(\frac{h}{t}\right)\right]^2} \quad (142)$$

Substituting equation (134),

$$\frac{\Delta P_{c1}}{\Delta P_{JN}} = \frac{\Delta P_c}{\Delta P_{JN}} - \frac{q_c}{\Delta P_{JN}}$$

$$= \frac{\Delta P_c}{\Delta P_{JN}}\left[1 - \frac{1}{\left[1+.08\left(\frac{S_c}{h}\right)\left(\frac{h}{t}\right)\right]^2}\right] + \frac{1}{\left[1+.08\left(\frac{S_c}{h}\right)\left(\frac{h}{t}\right)\right]^2}$$

$$- \frac{1}{\left[1+.08(S_c/h)(h/t)\right]^2}\left\{1 - \frac{1}{\left[1+.08(S_c/h)(h/t)\right]^2}\right\} \tag{143}$$

- measured at the intake, over the outer half of the jet. The mean total pressure at the intake is obviously the mean of equations (140) and (143).

If there is no cavity loss, the mean will be

$$\frac{\Delta P_1}{\Delta P_{JN}} = \frac{1 + \Delta P_{c1}/\Delta P_{JN}}{2} \tag{144}$$

If there is no free-air loss, due to insulation by the primary air, we can take $S_F = 0$.

4.4 Comparison With Experiment.

Reference 16 contains some measurements of exit and re-entry total head for a partial recirculation system, the exit total head varying linearly across the exit plane. For the test model (Martin Model #1) $\theta_1 = \theta_2 = 30°$, $\ell_r = 41.86$ in., $t = 6.76$ in. From equation (136) the "critical height" would therefore be given by

$$\frac{\ell_r}{h_{crit}} = \cos\theta\left[\frac{1}{1-\sin\theta} + \frac{1}{1+\sin\theta}\right] = 2.31$$

$$\frac{h_{crit}}{t} = \frac{h_{crit}}{\ell_r}\,\frac{\ell_r}{t} = 2.68.$$

The experimental data is for values of h/t at, or in excess of, this critical value.

Assuming no loss in momentum flux attributable to mixing, the theoretical values of cavity and cushion pressure are plotted for this model in Figure 46, some experimental values of ΔP_c being plotted for comparison. Because both the nozzle pressure distribution and the mass augmentation ratio m/m' vary for the test data, the agreement is not good, in Figure 46, but the absolute order of the values is obviously reasonable.

These calculated values of Δp_c and Δp_v have been used to calculate the total pressure drop, which is the mean of equations (140) and (143), the results being plotted in Figure 46. The agreement with experiment is evidently good, particularly when we remember that, in the model tests, the exit nozzle total distribution was highly nonuniform.

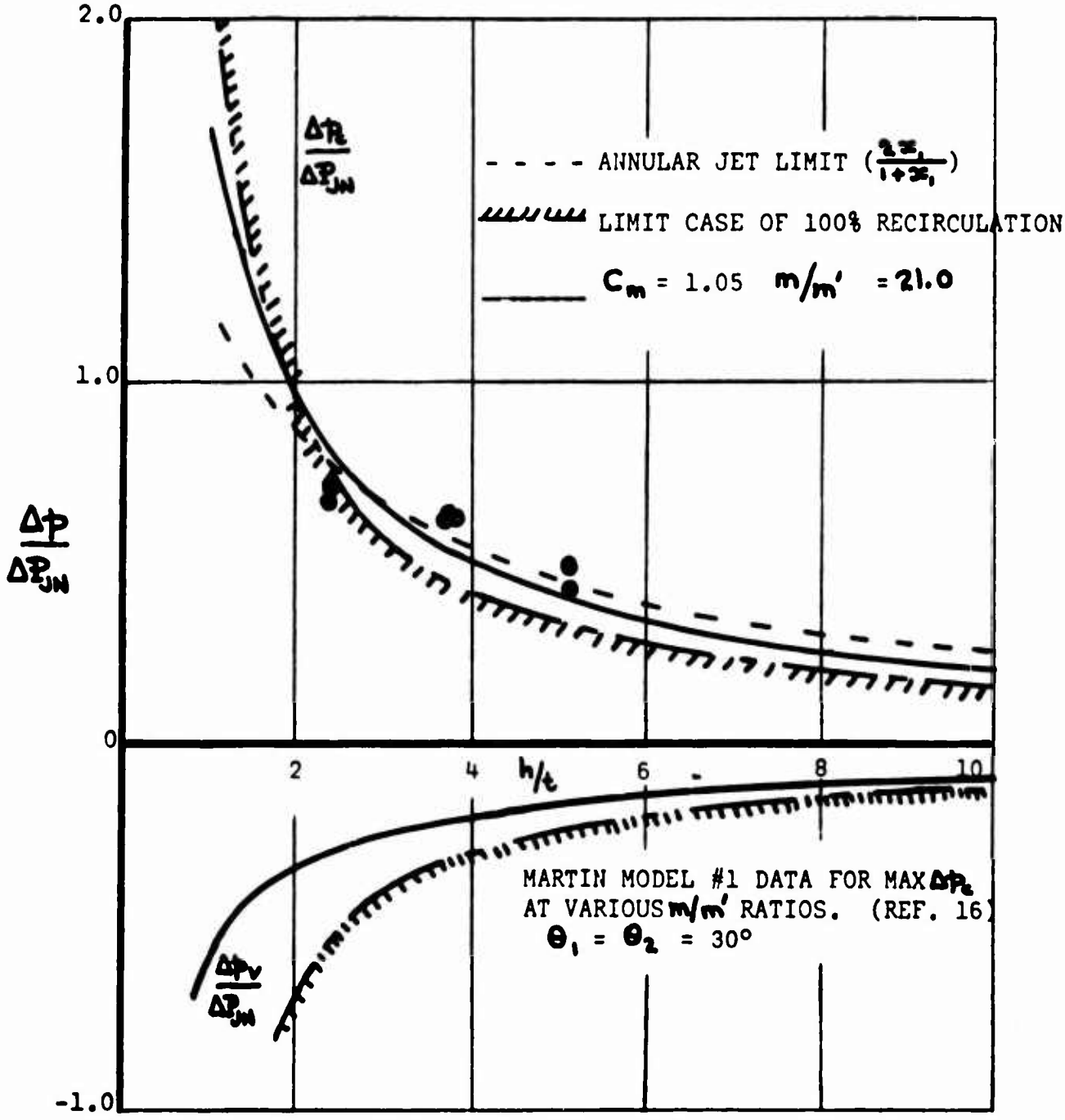

Figure 46. Theoretical Cushion and Cavity Pressure For a Recirculation Test Rig. $\theta_1 = \theta_2 = 30°$.

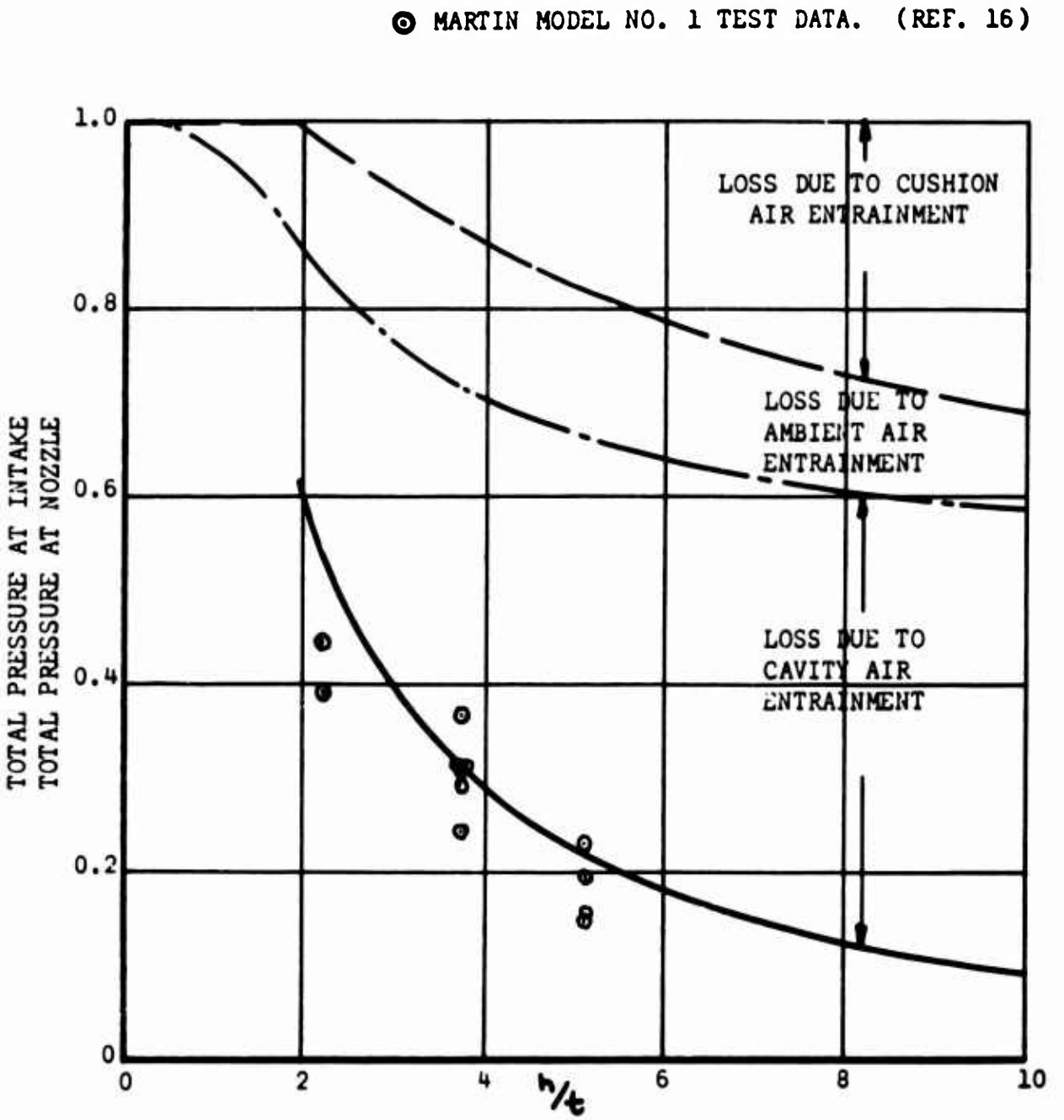

Figure 47. Predicted and Measured Total Head Loss for Martin Model No. 1.

SECTION FIVE

SOME EXPERIMENTAL MEASUREMENTS OF STATIC PRESSURE NEAR A NOZZLE

A full-scale Frost Fan two-dimensional test rig (Reference 15) was instrumented with static pressure taps. Figure 48 shows the location of the taps relative to the fan inlet and the results obtained are presented in Figures 49 to 56.

From Reference 15, Appendix E, the Frost Fan gives a momentum flux of

$$bJ = 1.675\left(\frac{RPM}{1000}\right)^2 \quad (lb) \tag{145}$$

$$J = \rho t\, v_j^2 \qquad = 0.829\left(\frac{RPM}{1000}\right) \quad (lb.ft.)$$

From equations (74) and (75) the static pressure decrement near the nozzle will be

$$\Delta p = -\frac{1}{2}\rho\left(\frac{.04}{\sin\theta}\right)^2 v_j^2 \quad = -\frac{1}{2}\left(\frac{.04}{\sin\theta}\right)\frac{J}{t} \tag{146}$$

or $$\sin\theta = \frac{1}{\sqrt{-\Delta p\, 1250\, t/J}} \tag{147}$$

At 1000 r.p.m. $$\frac{1250t}{J} = \frac{0.765}{.829} \times 125 = 115.2$$

$$\therefore \sin\theta = \frac{.0932}{\sqrt{-\Delta p}} \tag{148}$$

The pressure decrements close to the nozzle, corrected as $(r.p.m.)^2$ to 1000 r.p.m., are plotted in Figure 57. Using the mean of these values, the effective value of θ is plotted in Figure 58. Since the nominal outside value of θ is 45°, close to the nozzle, and the inside value is 90°, it is obvious that the entrainment is much greater than would be indicated by the local geometry.

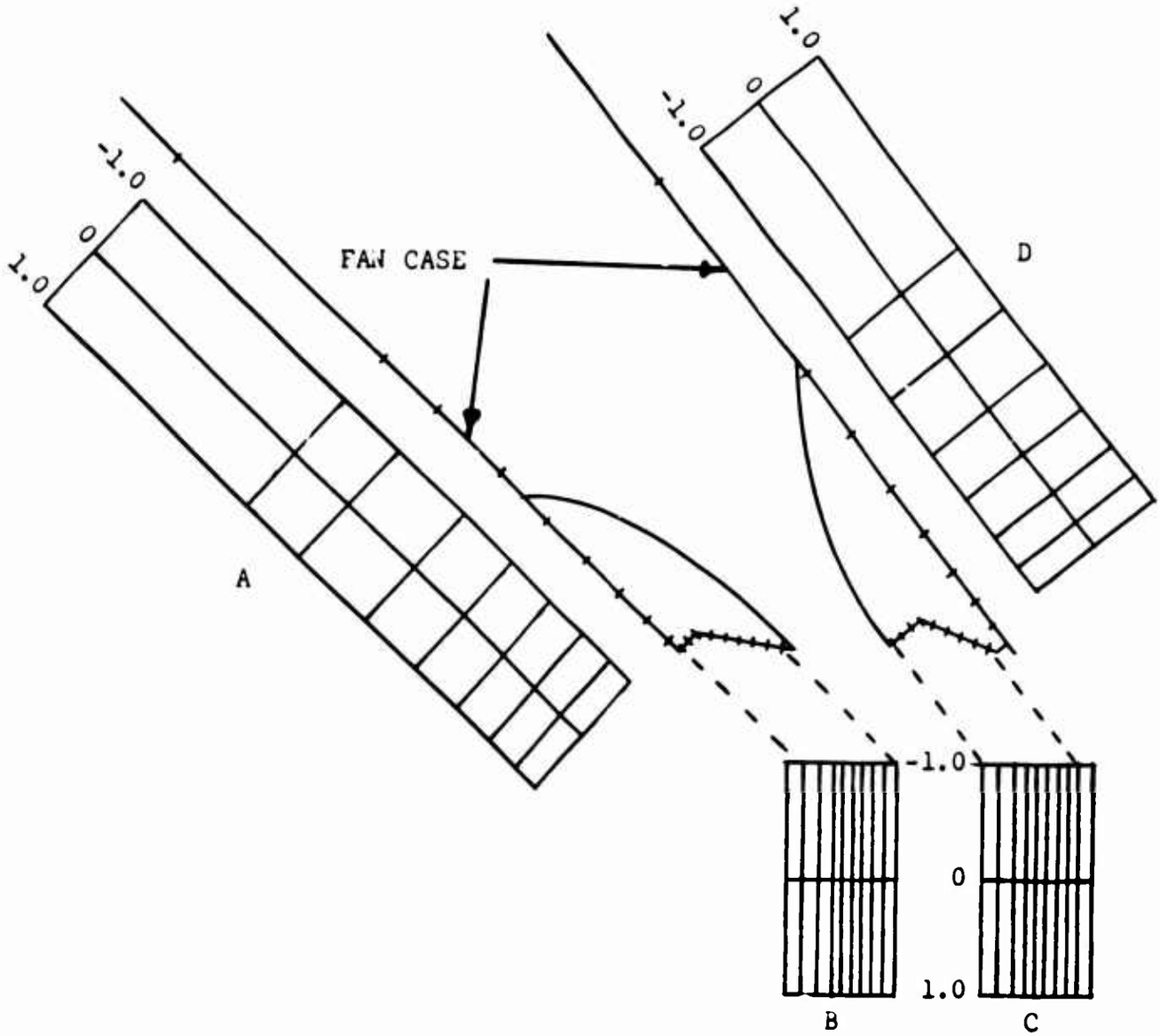

Figure 48. Location of Pressure Taps.

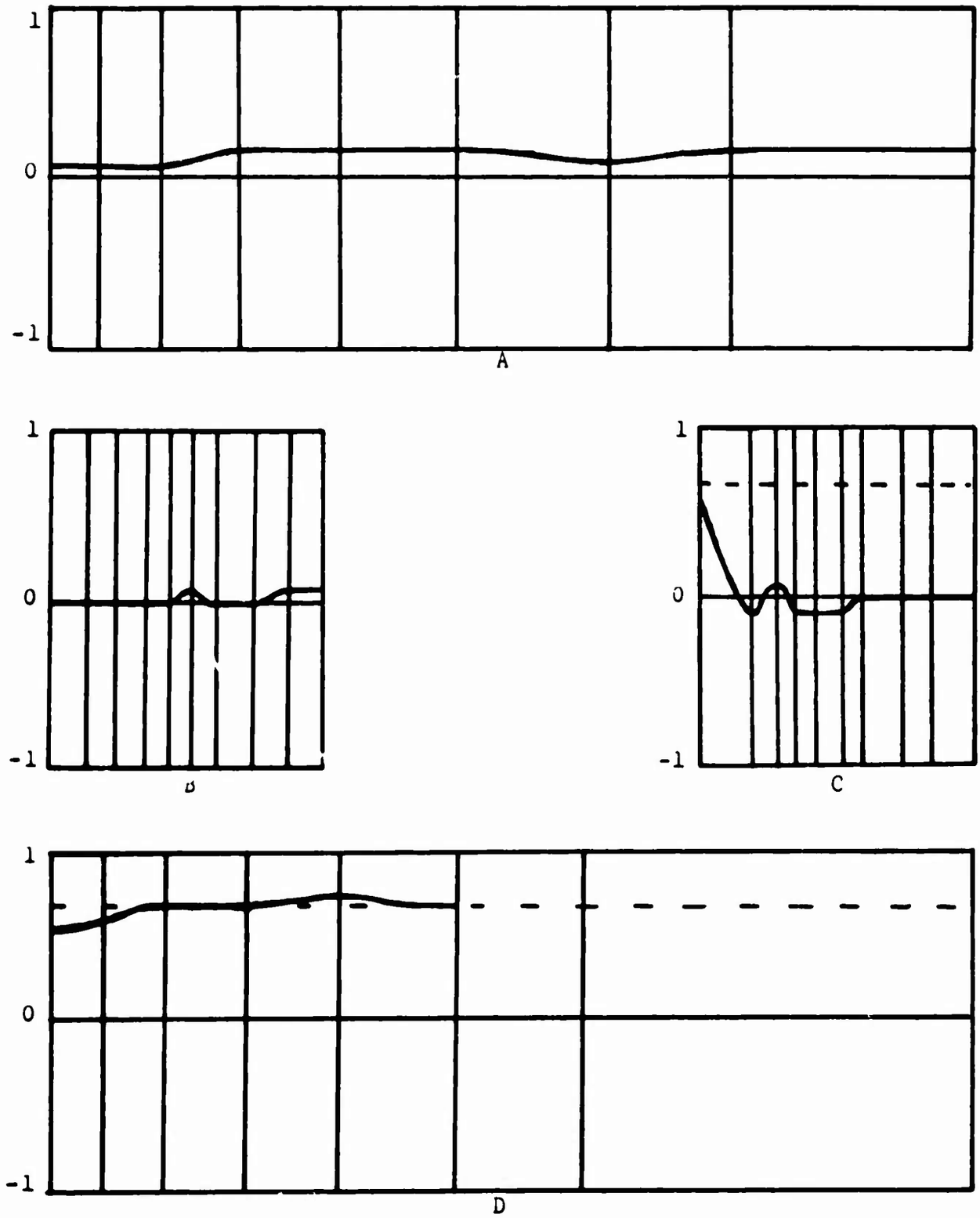

- - - - NOMINAL CUSHION PRESSURE = 0.66 LB./FT.^{2}

Figure 49. Static Pressure Measurement
Series D, Group II, Run No. 9. (1000 RPM, h = 22.75").

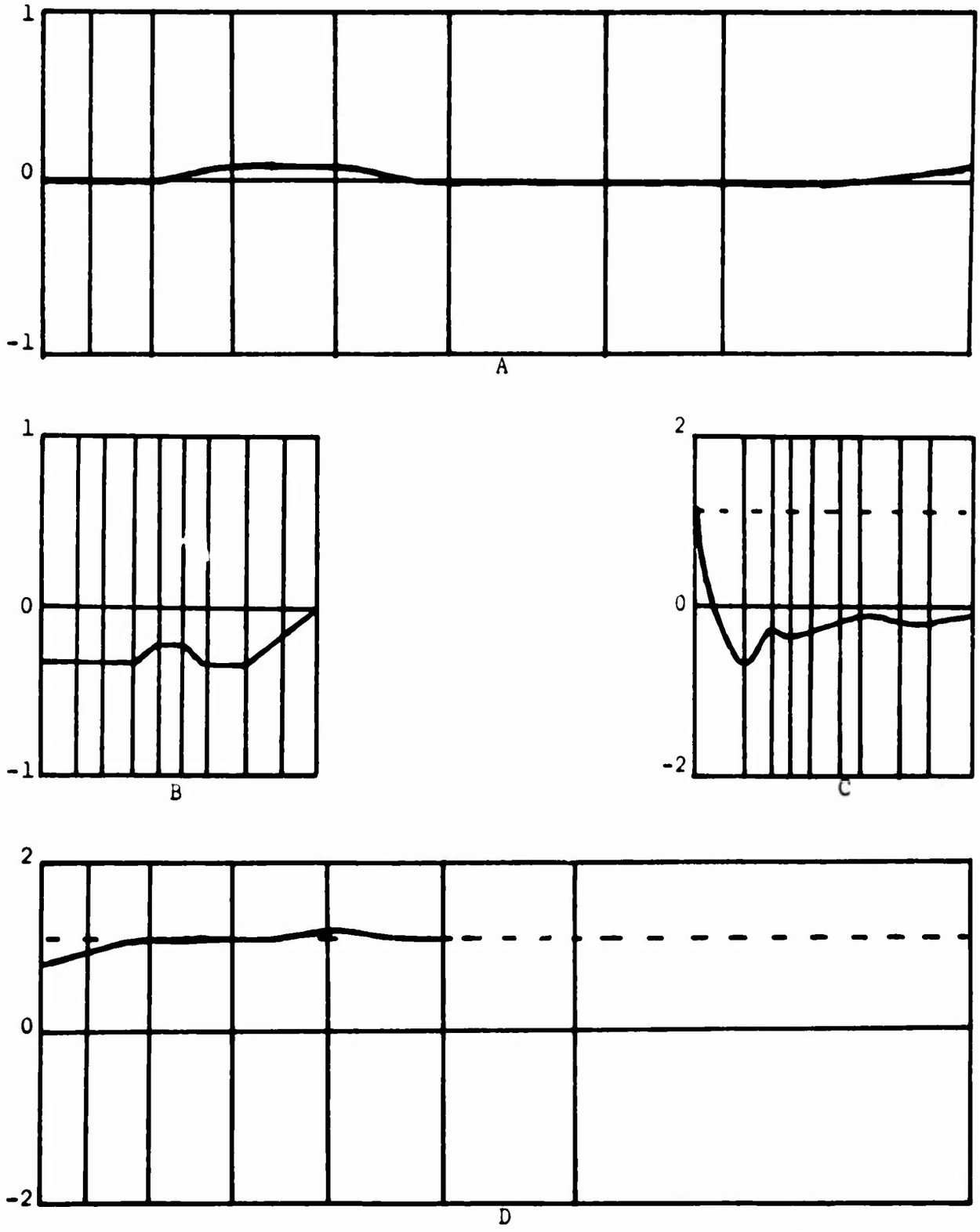

- - - - NOMINAL CUSHION PRESSURE = 1.1 LB./FT.^{2}

Figure 50. Series D, Group II, Run No. 10.
(1400 RPM, h = 22.75").

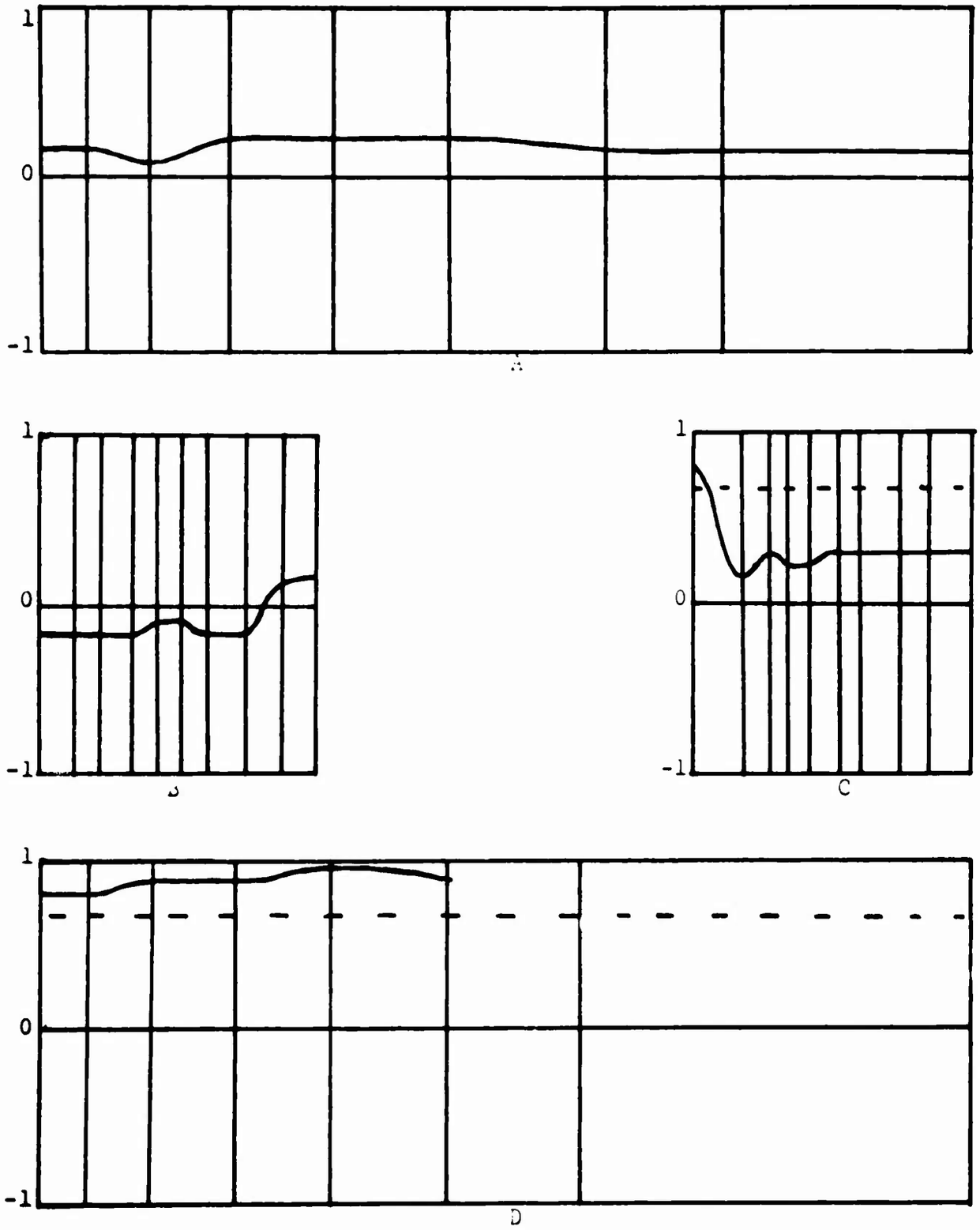

- - - - NOMINAL CUSHION PRESSURE = 0.66 LB./FT.^{2}

Figure 51. Series D, Group II, Run No. 11.
(1000 RPM, **h** = 13.75").

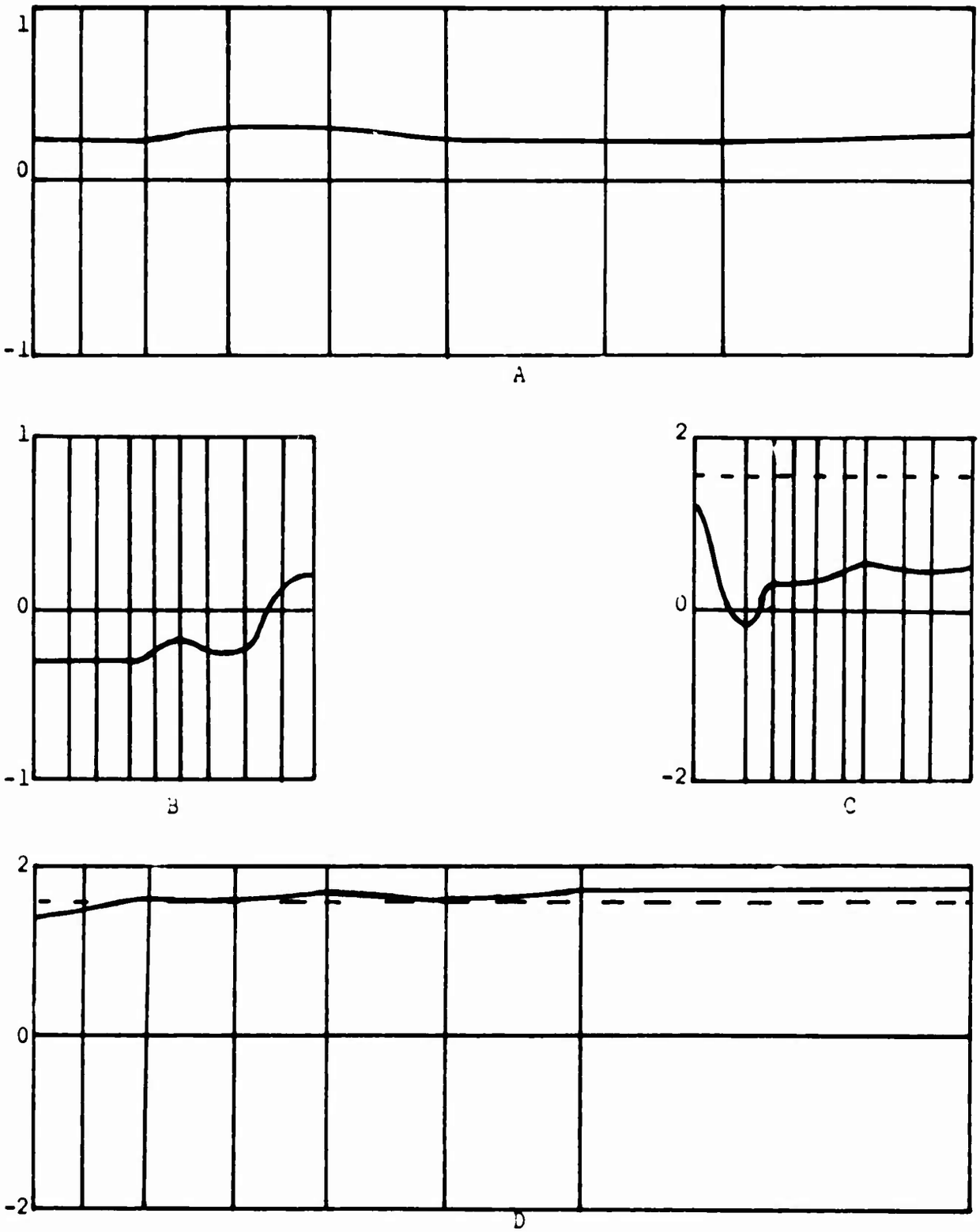

- - - - NOMINAL CUSHION PRESSURE = 1.53 LB./FT.^{2}

Figure 52. Series D, Group II, Run No. 12.
(1400 RPM, h = 13.75").

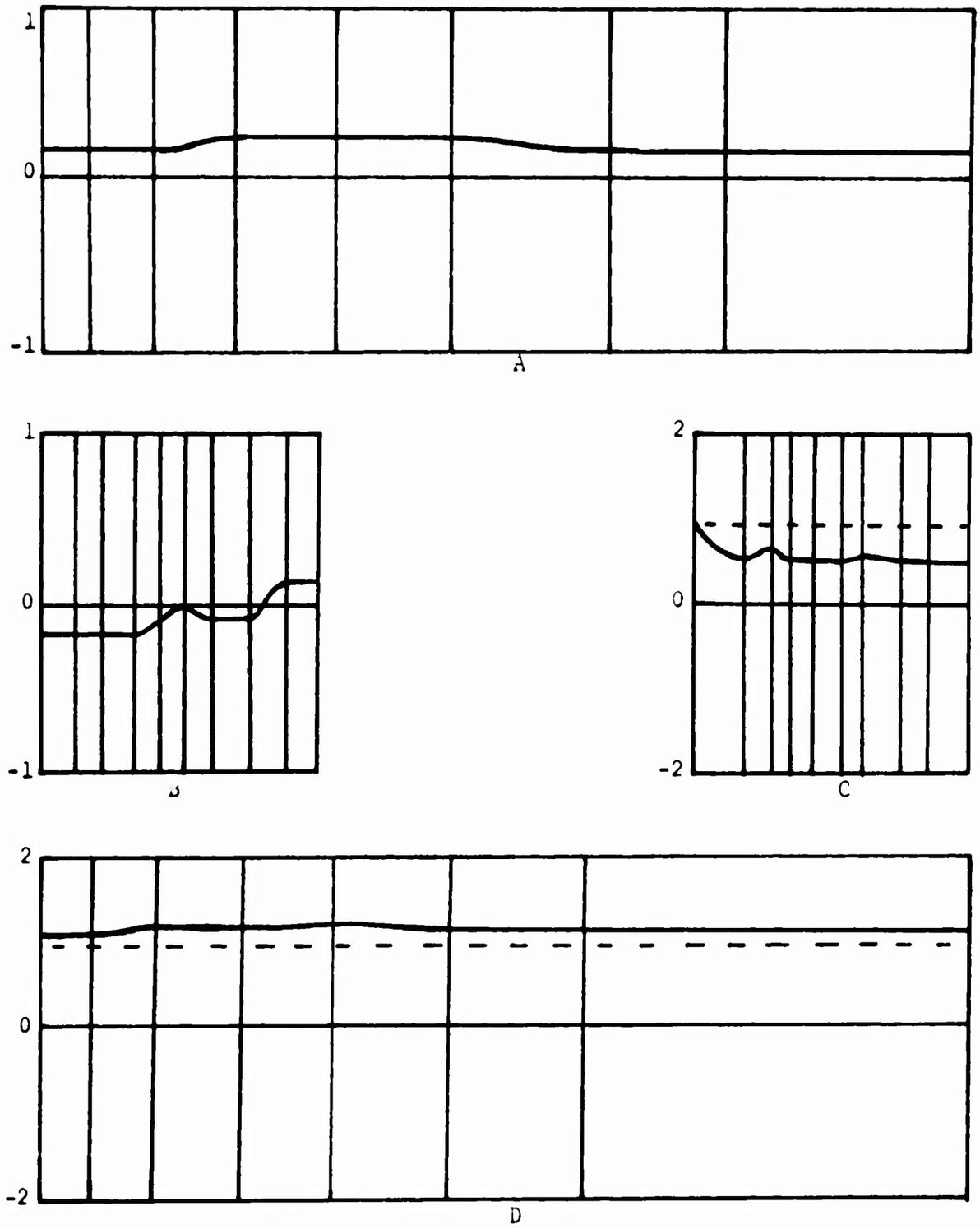

- - - - NOMINAL CUSHION PRESSURE = 0.95 LB./FT.^{2}

Figure 53. Series D, Group II, Run No. 13.
(1000 RPM, h = 9.25").

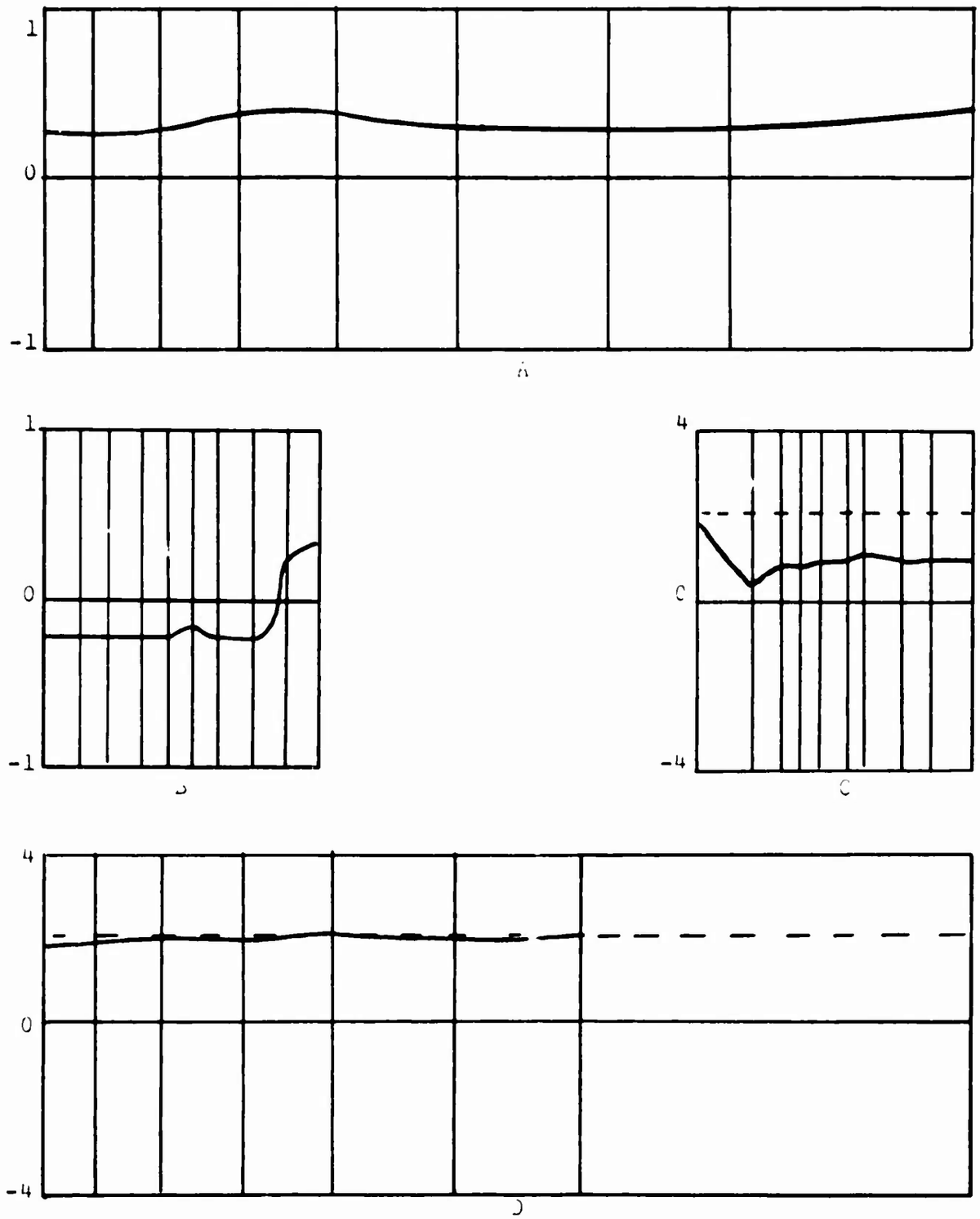

- - - - NOMINAL CUSHION PRESSURE = 2.12 LB./FT.^{2}

Figure 54. Series D, Group II, Run No. 14.
(1400 RPM, h = 9.25").

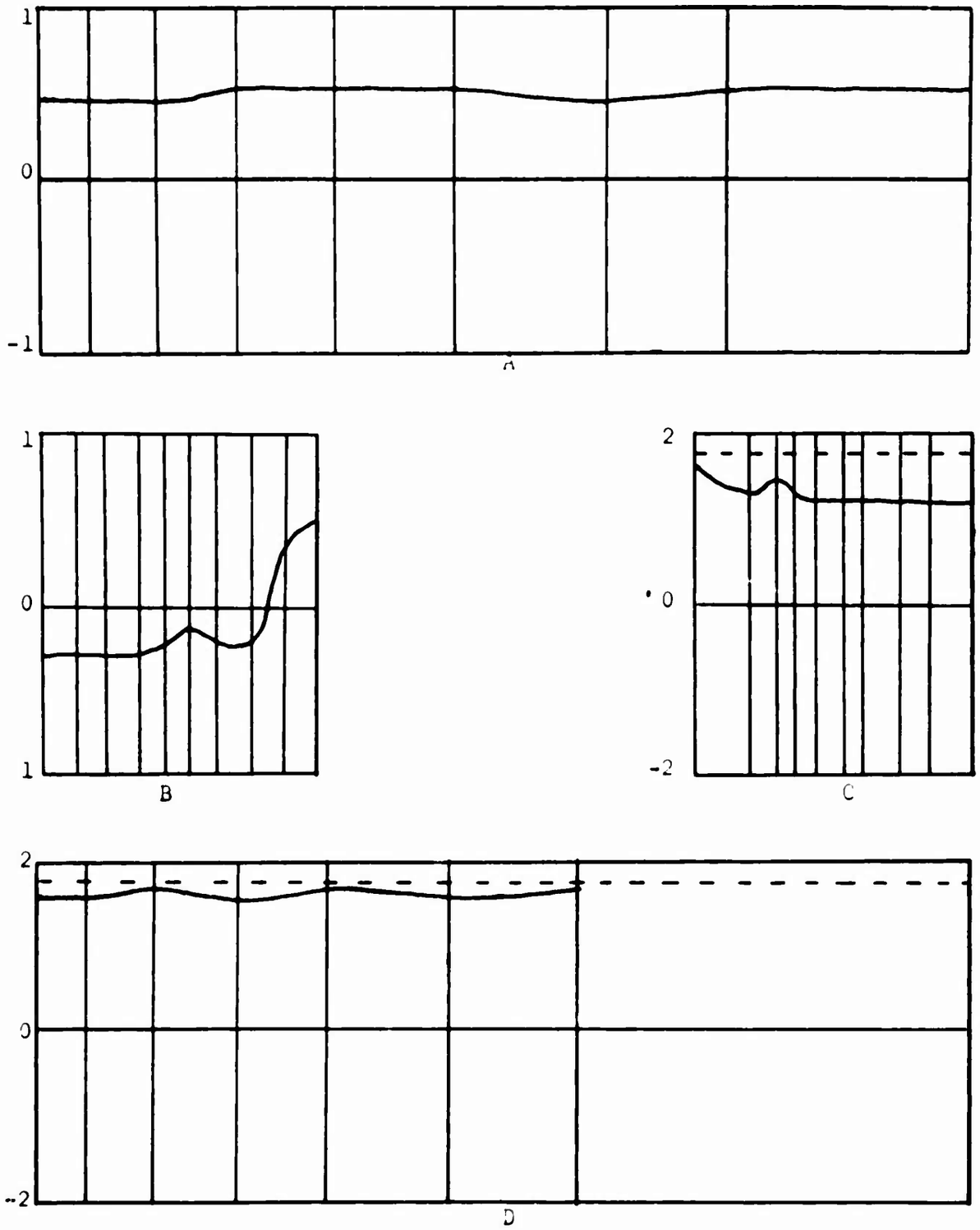

- - - - NOMINAL CUSHION PRESSURE = 1.75 LB./FT.^{2}

Figure 55. Series D, Group II, Run No. 15.
(1000 RPM, h = 4.5").

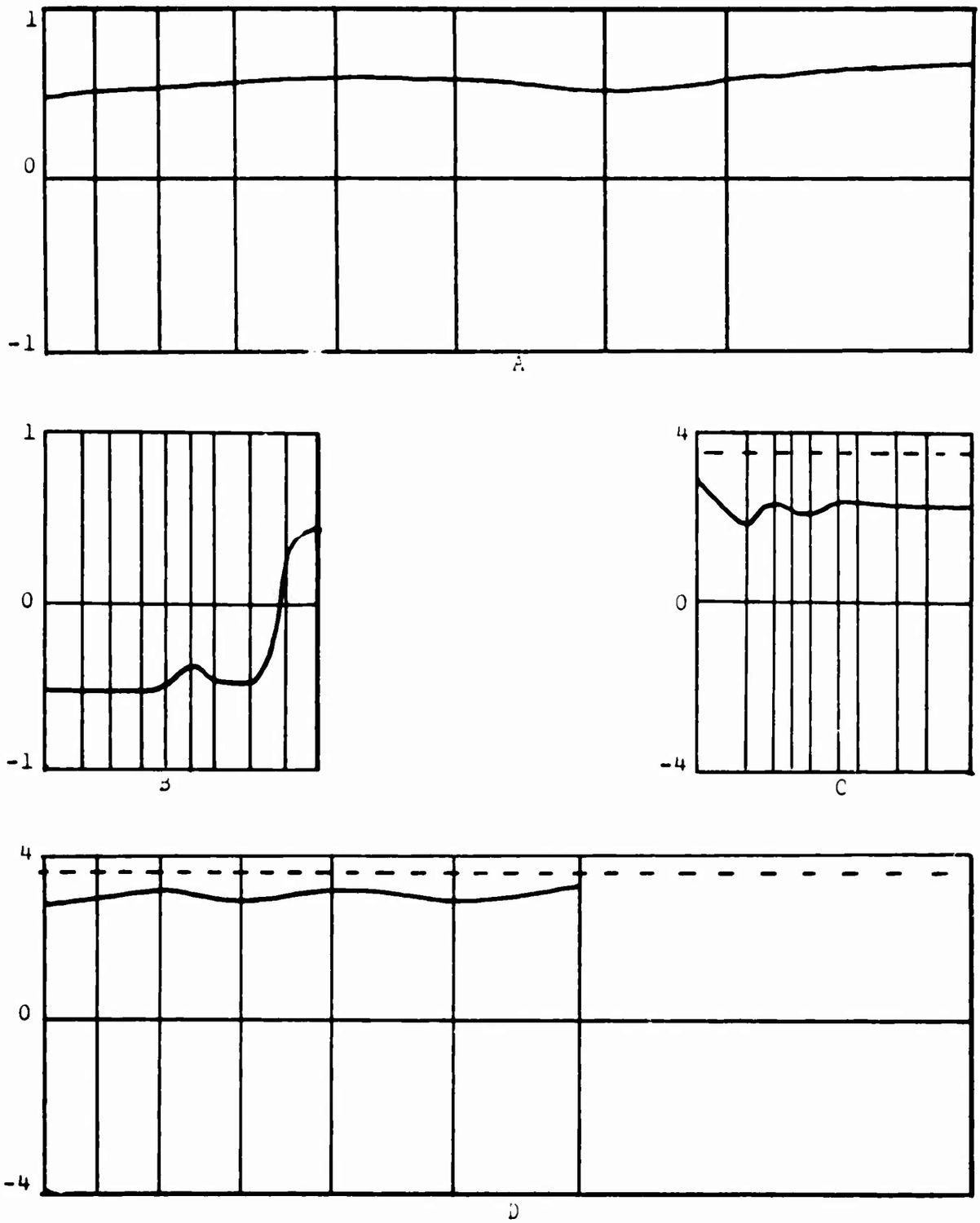

- - - - NOMINAL CUSHION PRESSURE = 3.58 LB./FT.^{2}

Figure 56. Series D, Group II, Run No. 16.
(1400 RPM, **h** = 4.5").

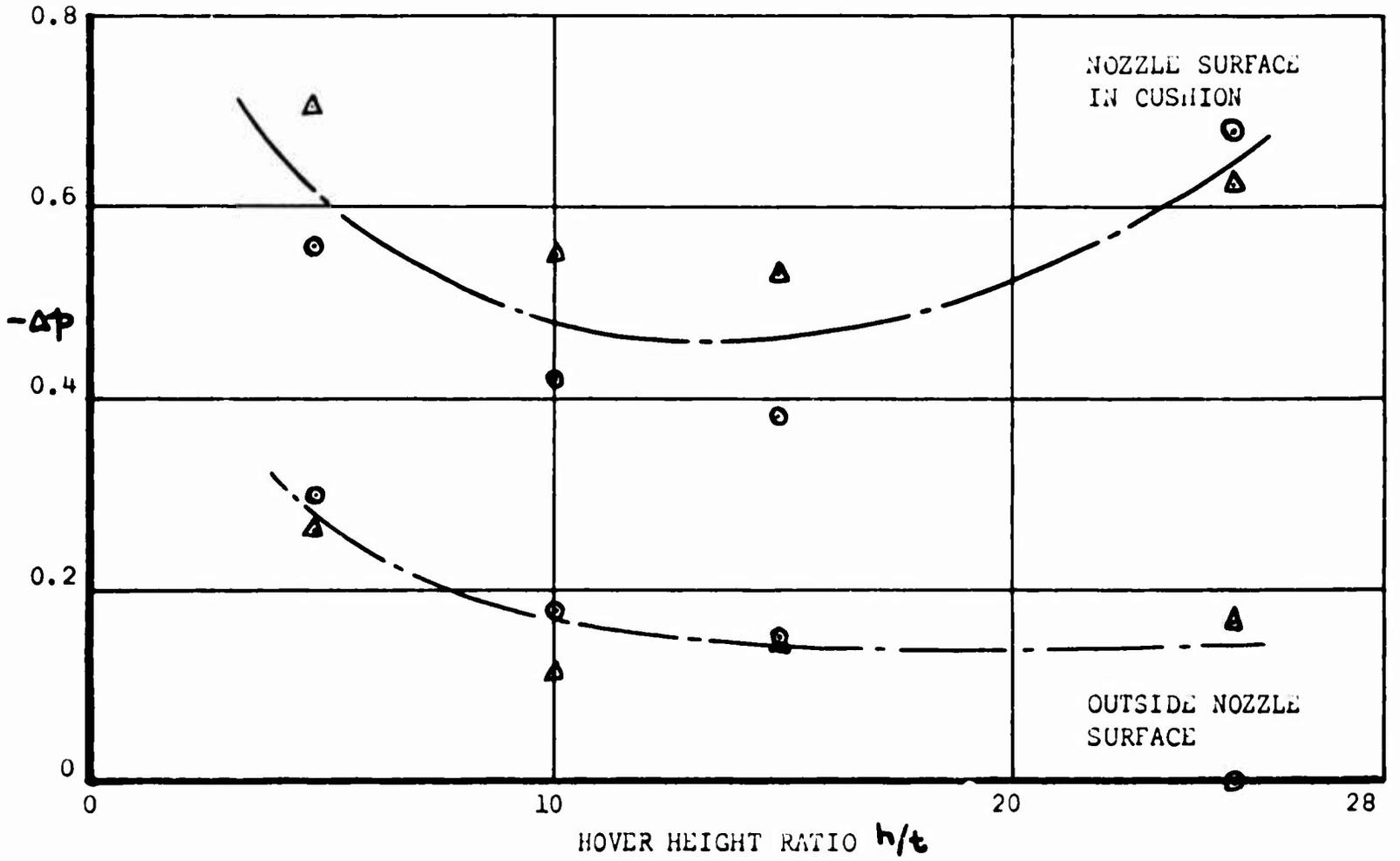

Figure 57. Nozzle Static Pressure Decrement On Internal and External Surface. (Corrected to 1000 RPM).

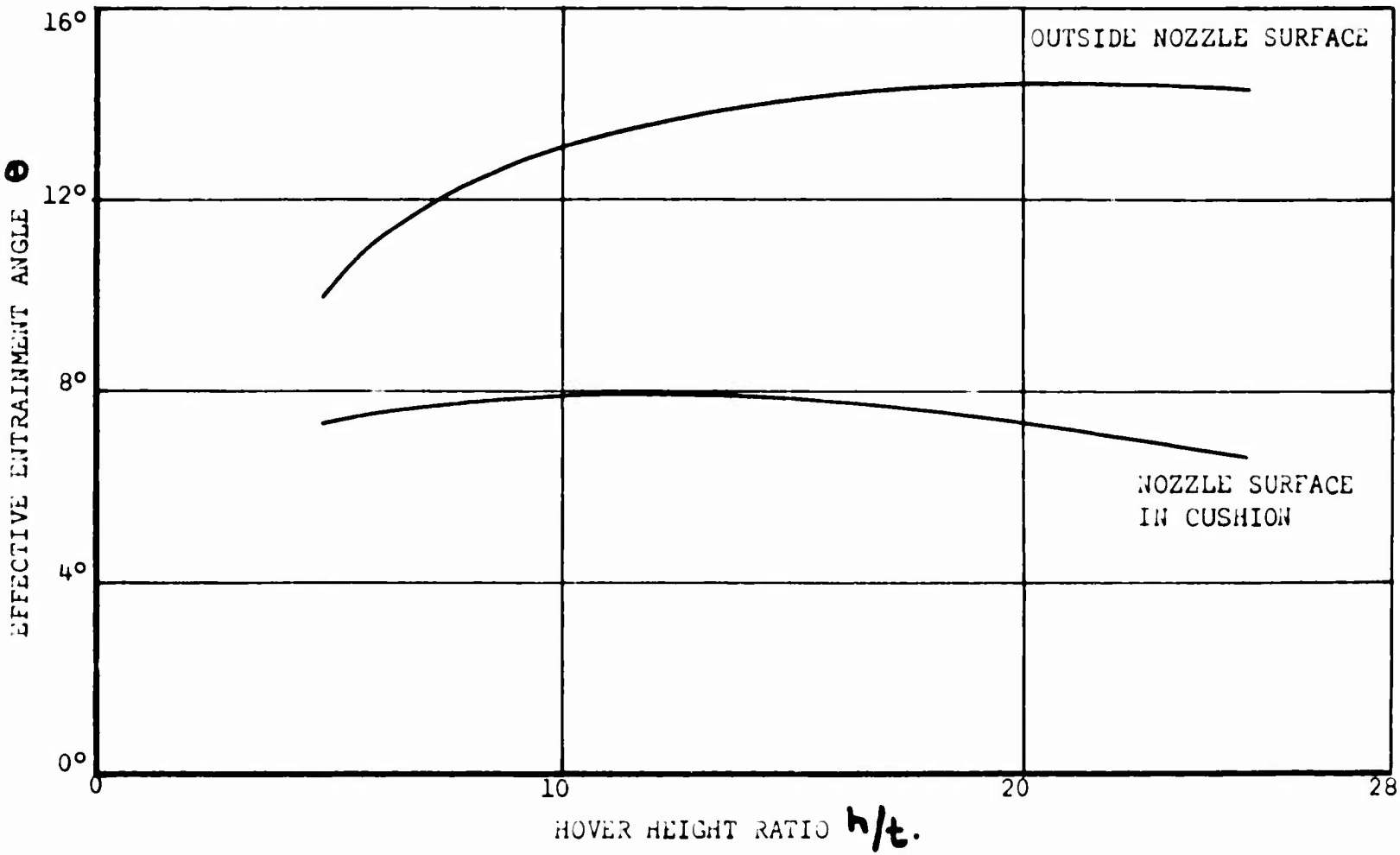

Figure 58. Effective Entrainment Angles For Frost Fan Test Rig.

BIBLIOGRAPHY

1. Kuchemann, Dietrich and Weber, Johanna, Aerodynamics of Propulsion, McGraw Hill, London, England, 1953.

2. Payne, Peter R., "Jet Drag of Wings with Jet Flaps", Aircraft Engineering, Vol. XXX, No. 349, March 1958.

3. Stratford, B.S., "Mixing and the Jet Flap", Aeronautical Quarterly, Vol. VII, August 1956.

4. Stratford, B.S., "A Further Discussion of Mixing and the Jet Flap", Aeronautical Quarterly, Vol. VII, August 1956.

5. von Karman, Theodore, Theoretical Remarks on Thrust Augmentation, Reissner Anniversary Volume, J. W. Edwards, Ann Arbor, Mich., 1949, p. 461.

6. Albertson, M. L., Dai, Y. B., Jensen, R. A., and Rouse, Hunter, "Diffusion of Submerged Jets", Transactions of the American Society of Civil Engineers, Vol. 115, 1950.

7. Tollmein, Walter, "Calculation of Turbulent Expansion Processes", NACA TM 1085, National Advisory Committee for Aeronautics, Washington 25, D.C., 1926.

8. Forthmann, E., "Turbulent Jet Expansion", NACA TM 789, National Advisory Committee for Aeronautics, Washington 25, D.C., 1934.

9. Liepmann, H. W., Lanfer, J., "Investigations of Free Turbulent Mixing", NACA TN 1257, National Advisory Committee for Aeronautics, Washington 25, D.C., 1947.

10. Carmichael, B. H., "Hovering Two-Dimensional Annular Jet Performance Experiments", Publication No. V-1053, Aeronutronic, Division of Ford Motor Co., Newport Beach, Calif., Nov. 1960.

11. Yen, Ben-Chie, "Patterns of Flow Under a Two-Dimensional GEM", Iowa Institute of Hydraulic Research, ONR Contract Nonr 1509(03), Iowa University, Iowa City, Iowa, Jan. 1962.

12. Payne, Peter R., "The Influence of Leakage on the Performance of an Annular Jet GEM", Frost Engineering Report No. 197-3, Contract DA 44-177-AMC-71(T), Frost Engineering Development Corporation, Englewood, Colorado, Sept. 1963.

13. Kuhn, R. E., Carter, A. W., "Research Related to Ground Effect Machines", Princeton Symposium on Ground Effect Vehicles, Oct. 1959.

14. Payne, Peter R., "A Note on the Optimum Thickness and Angle of an Annular Jet With Zero Translation Velocity", Frost Engineering Report No. 142-5, Contract DA 44-177-AMC-5(T), Frost Engineering Development Corporation. Englewood, Colorado, Feb. 1963.

15. Payne, Peter R., "Preliminary Studies of the Application of Peripheral Fans to Ground Effect Machines", Frost Report No. 142-18, Contract DA 44-177-AMC-5(T), Frost Engineering Development Corp., Englewood, Colo., Oct. 1963.

16. Ortell, A., "Recirculation Principle for Ground Effect Machine Two-Dimensional Tests", TCREC Tech. Report 62-66, U. S. Army Transportation Research Command, Fort Eustis, Va., June 1962.

17. Chaplin, Harvey R., "Effect of Jet Mixing on the Annular Jet", DTMB Report 1375, David Taylor Model Basin, Washington 7, D.C., Feb. 1959.

BLANK PAGE

APPENDIX I

AN ANNULAR JET VERY CLOSE TO THE GROUND

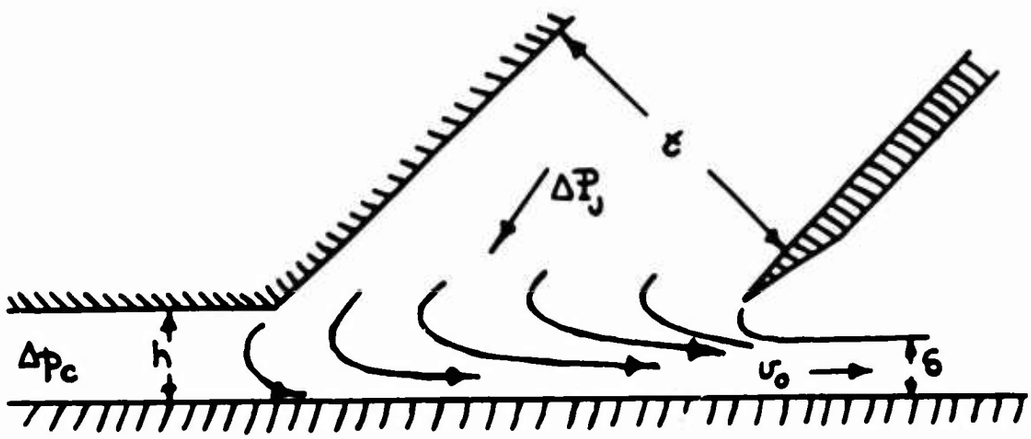

Figure 59. Annular Jet Very Close to the Ground.

Consider the case of Figure 58 where $h \to 0$. The air in the duct is essentially stationary, so that its static pressure is equal to its total pressure and

$$\Delta p_c = \Delta P_J \tag{149}$$

The vehicle thus behaves as a plenum chamber, and the air mass flow, for an outer periphery $\mathcal{C}$ is

$$\dot{m}_J = \mathcal{C} h C_D v_o \rho \tag{150}$$

But $\Delta P_J = \frac{1}{2} \rho v_o^2$ so that $v_o = \sqrt{\frac{2}{\rho} \Delta P_J}$ (151)

$$\therefore \dot{m}_J = \mathcal{C} h C_D \sqrt{2 \rho \Delta P_J} \tag{152}$$

The jet power is $\frac{1}{2} \dot{m}_J v_o^2$

That is, $E_J = \mathcal{C} h C_D \sqrt{\frac{2}{\rho}} \Delta P_J^{3/2}$ (153)

APPENDIX II

EFFECTIVE PERIPHERY OF A CIRCULAR ANNULAR JET

In the three-dimensional theory of annular jets we use the relationship

$$C\,h\,\Delta p_c = J_j(\eta + \sin\theta) \tag{154}$$

- to determine the cushion pressure Δp_c. In other words, the pressure Δp_c acts on an area Ch to give the horizontal momentum flux $J_j(\eta + \sin\theta)$.

We normally take $C = \pi D$, where D is the outside diameter of the nozzle, but we shall now estimate this quantity more precisely, using the assumptions of Figure 59, which follows the theory of Section 2.4 of this report.

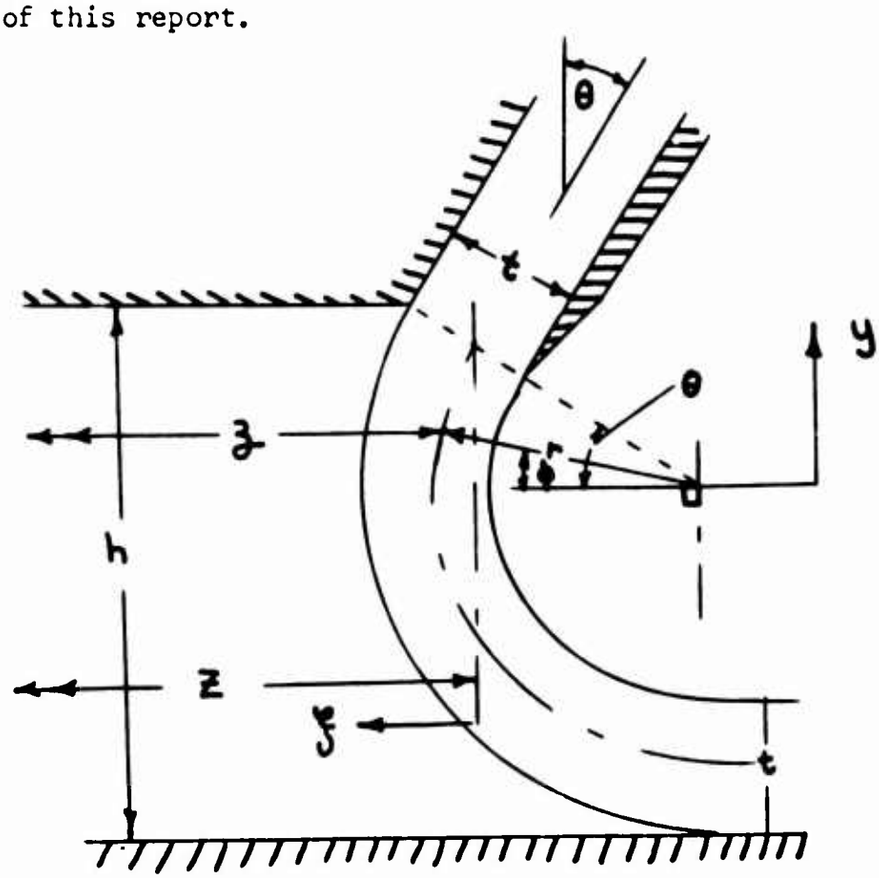

Figure 60. Assumed Jet Geometry.

Obviously, $h = r(1+\sin\theta) + \frac{1}{2}t$

$$\therefore\ r = \frac{h - \frac{1}{2}t}{(1+\sin\theta)} \tag{155}$$

Relative to the jet ℄ in the nozzle exit plane, the radius of curvature is centered about a point $r\sin\theta$ outboard. Thus the jet is a distance ξ

$$\xi = r\cos\phi - r\cos\theta \tag{156}$$

- inboard of the nozzle ℄ . Thus if Z is the radius to the nozzle ℄ and z the radius to the jet ℄ , both measured from the cushion center.

$$z = Z - \xi = Z - r(\cos\phi - \cos\theta) \tag{157}$$

Taking the upper half of the jet first

$$\sin\phi = y/r$$

$$\therefore\ \cos\phi = \sqrt{1-(y/r)^2}$$

$$z = Z - \frac{(h-\frac{1}{2}t)}{(1+\sin\theta)}\left[\sqrt{1-(y/r)^2} - \cos\theta\right] \tag{158}$$

The incremental vertical area is $2\pi z\,dy$. Thus the total vertical area of the upper half of the jet ℄ is

$$\Delta A_{v1} = 2\pi\int_{y=0}^{y=r\sin\theta}\left[Z - \frac{(h-\frac{1}{2}t)}{(1+\sin\theta)}\sqrt{1-(y/r)^2} + \frac{(h-\frac{1}{2}t)}{(1+\sin\theta)}\cos\theta\right]dy$$

After some manipulation,

$$\Delta A_{v1} = 2\pi Z\left[r\sin\theta + \frac{r^2}{2Z}\sin\theta\cos\theta - \frac{r^2\theta}{2Z}\right] \tag{159}$$

for the lower half of the jet, exclusive of the area $\frac{1}{2} t \, 2\pi(z + r\sin\theta)$ immediately in contact with the ground plane

$$A_{v2} = 2\pi \int_0^r \left[z - \left(\sqrt{r^2 - y^2} - r\cos\theta \right) \right] dy$$

$$= 2\pi z \left[\left(1 + \frac{r}{z} \cos\theta \right) r - \frac{r^2}{2z} \frac{\pi}{2} \right] \tag{160}$$

Thus the total vertical area is

$$\frac{C}{2\pi z} = \frac{1}{2} \frac{t}{h} + \frac{\left(1 - \frac{1}{2}\frac{t}{h}\right)}{(1 + \sin\theta)} \left[1 + \left(1 + \frac{1}{2} \frac{t}{h} \frac{h}{z} \right) \sin\theta \right]$$

$$+ \frac{h}{z} \frac{\left(1 - \frac{1}{2}\frac{t}{h}\right)^2}{(1 + \sin\theta)^2} \left[\frac{1}{2} \sin\theta \cos\theta - \frac{\theta}{2} + \cos\theta - \frac{\pi}{4} \right] \tag{161}$$

When $h/t < 1.0$, we take $C = \pi D$, where D is the diameter of the outer nozzle edge.

We evaluate this for the case $\theta = 0$ considered in Section 2.4 of this report.

$$\frac{C}{2\pi z} = \frac{1}{2} \frac{t}{h} + \left(1 - \frac{1}{2}\frac{t}{h}\right) + \frac{h}{z} \left(1 - \frac{1}{2}\frac{t}{h}\right)^2 \left(1 - \frac{\pi}{4}\right)$$

$$= 1 + 0.215 \frac{h}{z} \left(1 - \frac{1}{2}\frac{t}{h}\right)^2$$

$$= 1 + 0.215 \frac{h}{z} \left[1 - \frac{1}{2} \left(\frac{t}{z}\right) \left(\frac{z}{h}\right) \right]^2 \tag{162}$$

For the Reference 13 model, $\frac{t}{D} = .1125$,

$$\therefore z = \frac{D - t}{2}$$

$$\frac{z}{h} = \frac{1}{2}\left(\frac{D}{h} - \frac{t}{h}\right) = \frac{1}{2}\,\frac{D}{h}\left(1 - \frac{t}{D}\right)$$

$$= 0.44375$$

$$\frac{t}{z} = 2.255\,\frac{t}{D} = 0.254$$

The ratio $C/\pi D$ is plotted in Figure 60 for the Reference 13 model and is seen to be greater than unity for $h/D > 0.3$. Thus the cushion pressure will decrease more rapidly with height above this value.

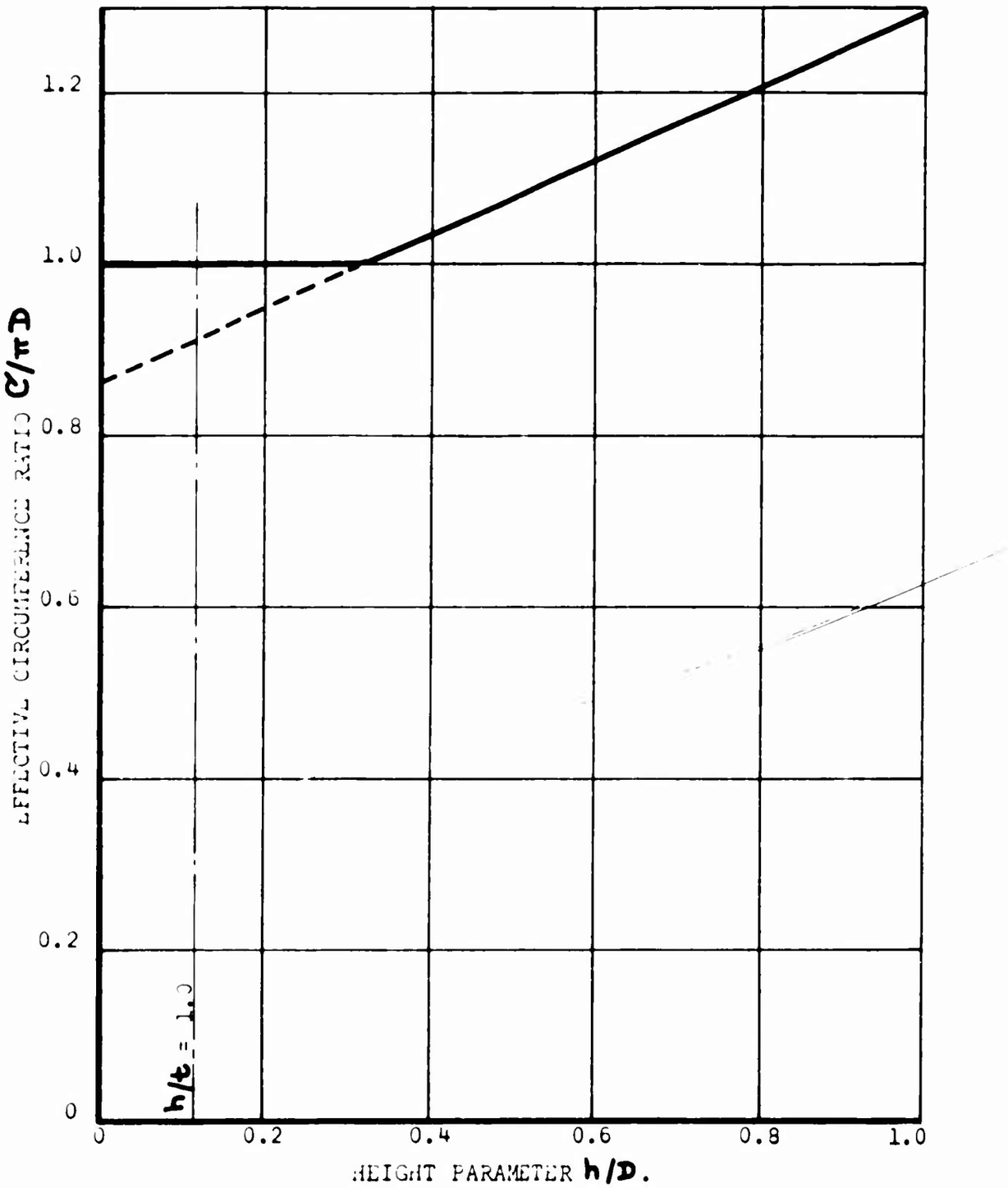

Figure 61. Effective Jet Circumference For $\theta = 0$, $t/D = 0.1125$

APPENDIX III

AN EXACT SOLUTION FOR A LAMINAR JET

Schlichting [1] and Bickley [2] have obtained a laminar solution for a plane jet issuing from a slot, as sketched in Figure 61.

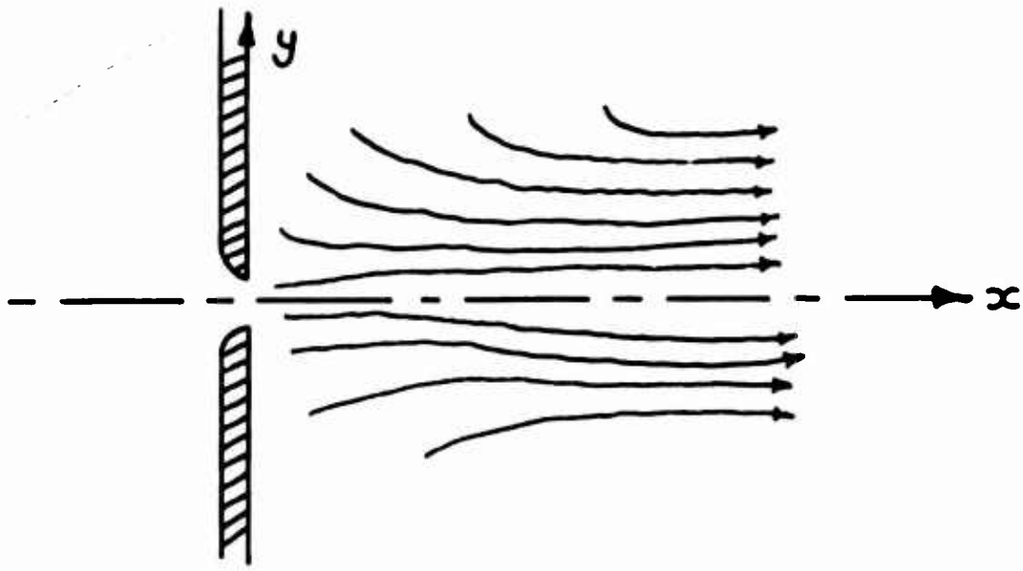

Figure 62. Laminar Jet From a Slot.

Taking x, y ordinates about the jet ℄, and assuming the jet is infinitely narrow (but of finite momentum M_o), they show that the "boundary layer" approximation to the Navier-Stokes equations is [from (4)]

$$u \frac{\partial u}{\partial x} + v \frac{\partial v}{\partial x} = \frac{\mu}{\rho} \frac{\partial^2 u}{\partial y^2} \tag{163}$$

(i.e., the pressure term is neglected because the stream lines are nearly parallel)

and $$\frac{\partial u}{\partial x} + \frac{\partial v}{\partial y} = 0 \tag{164}$$

- - - - - - - - - - -

(1) H. Schlichting, "Laminar Strahlausbrectung" ZAMM Bd. 13, 1933.

(2) W. Bickley, "The Plane Jet," Phil. Mag. 7, 23, 1937.

The boundary conditions are

$$y = 0;\ v = 0,\ \frac{\partial u}{\partial y} = 0$$
$$y = \infty;\ u = 0 \tag{165}$$

From equation (5) the total jet momentum

$$M_0 = 2\rho \int_0^\infty u^2\, dy = \text{constant} \tag{166}$$

The approximate solution to these equations is

$$u = 0.4543\left(\frac{M_0}{\rho^2 \nu x}\right)^{\frac{1}{3}} \operatorname{sech}^2 \xi \tag{167}$$

$$v = 0.5503\left(\frac{M_0}{\rho x^2}\right)^{\frac{1}{3}} \left(2\xi \operatorname{sech}^2 \xi - \tanh \xi\right) \tag{168}$$

where $$\xi = 0.2752 \left(\frac{M_0}{\rho \nu^2}\right)^{1/3} \left(\frac{y}{x^{2/3}}\right) \tag{169}$$

The mass flow across any section of the jet is

$$\dot{m} = 2\rho \int_0^\infty u\, dy = 3.3019\, \rho \left(\frac{M_0 \nu x}{\rho}\right)^{\frac{1}{3}} \tag{170}$$

These approximations apply if $M_0 x/\rho \nu^2$ is large and cannot therefore be applied to determine the pressure distribution on the wall at $x = 0$.

C.1 Comparison With a Turbulent Jet.

Laminar flow is characterized by the Newtonian relationship

$$\text{stress} = \mu \frac{du}{dy} \tag{171}$$

- where μ is the viscosity of the fluid and is assumed to be a constant. One approach to turbulent mixing problems is to assume that the eddy viscosity ϵ is statistically constant, and that laminar solutions can be applied to turbulent phenomena when μ is replaced by ϵ.

Writing the jet momentum

$$M_o = \rho t u_o^2 = \dot{m}_J u_o = \frac{\dot{m}_J^2}{\rho t}$$

- we have, from equation (170),

$$\frac{\dot{m}}{\dot{m}_J} = 3.302 \, \rho \left[\frac{\nu}{\rho^2 \dot{m}_J} \right]^{\frac{1}{3}} \left(\frac{x}{t} \right)^{\frac{1}{3}} \tag{172}$$

It is immediately obvious that this equation is quite different from equation (16) in the main body of this report, implying that the linear relationship of equation (171) cannot be applied to turbulent mixing processes.

BLANK PAGE

DISTRIBUTION

U. S. Army Materiel Command	7
U. S. Army Mobility Command	3
U. S. Strike Command	1
Office of Chief of R&D, D/A	2
Office of the Asst. Secy. of Defense for R&E	1
U. S. Army Transportation Research Command	64
U. S. Army Research and Development Group (Europe)	2
U. S. Army Human Engineering Laboratories	1
Army Research Office-Durham	2
U. S. Army Polar Research and Development Center	1
U. S. Army Medical Research and Development Command	1
U. S. Army Combat Developments Command Aviation Agency	1
U. S. Army Combat Developments Command Transportation Agency	1
U. S. Army Combat Developments Command	1
U. S. Army War College	1
U. S. Army Aviation and Surface Materiel Command	2
U. S. Army Airborne, Electronics and Special Warfare Board	1
Chief of Naval Operations	1
Bureau of Ships	1
Bureau of Naval Weapons	1
Bureau of Supplies and Accounts	1
U. S. Naval Supply Research and Development Facility	1
U. S. Naval Postgraduate School	1
U. S. Naval Ordnance Test Station	1
David Taylor Model Basin	1
Marine Corps Landing Force Development Center	1
Marine Corps Educational Center	1
U. S. Coast Guard	1
U. S. Maritime Administration	1
Ames Research Center, NASA	2
NASA-LRC, Langley Station	2
Lewis Research Center, NASA	2
NASA Representative, Scientific and Technical Information Facility	2
Human Resources Research Office	2
U. S. Army Standardization Group, Canada	1
Canadian Liaison Officer, U. S. Army Transportation School	3

British Army Staff, British Embassy	4
U. S. Army Standardization Group, U. K.	1
Defense Documentation Center	10
U. S. Government Printing Office	1